An observational study of Davis Strait transports

Mary Beth Curry

A dissertation
submitted in partial fulfillment of the
requirements for the degree of

Doctor of Philosophy

University of Washington

2013

Reading Committee:

Craig M. Lee, Chair

Susan L. Hautala

Eric A. D'Asaro

Program Authorized to Offer Degree:
School of Oceanography
College of the Environment

University of Washington

Abstract

An observational study of Davis Strait transports

Mary Beth Curry

Chair of the Supervisory Committee:
Craig M. Lee
Applied Physics Laboratory

Davis Strait is one of two main gateways where freshwater from the Arctic enters the North Atlantic. An observing system began operating in Davis Strait in September 2004 with the goal of providing sustained, long-term quantification of Arctic-subarctic exchange west of Greenland. The system, including moorings, Seaglider surveys and autumn hydrographic sections, was designed to quantify volume, freshwater and heat transports and associated uncertainties. The goal of this analysis is to quantify Davis Strait transport variability and identify atmospheric forcing mechanisms driving the variability to help aid in understanding how exchanges between the Arctic and North Atlantic are being modified due to recent changes observed in the Arctic.

Data from six years (2004-10) of continuous measurements give annual volume, liquid freshwater and temperature transports through Davis Strait of -1.6 $\pm$ 0.5 Sv, -93 $\pm$ 6 mSv and 23 $\pm$ 2 TW, respectively (negative sign indicates southward transport). Sea ice export contributes additional 11 mSv of freshwater transport. The array provides the first year-round measurements in the upper 100 m and over the shelves, accounting for 38% (-0.6 Sv) of the net volume and 55% (-51 mSv) of the net freshwater transports. Davis Strait volume and freshwater fluxes are the same order of magnitude as those from Fram Strait, the other Arctic outflow gateway.

Interannual and annual variability of the net transports are large, with average an-

nual volume, freshwater and heat transport standard deviations of 0.7 Sv, 17 mSv and 12 TW and interannual standard deviations of 0.3 Sv, 15 mSv and 2 TW. Although there are no clear trends in the current transports, reanalysis of Davis Strait mooring data from 1987-90 reveals that less Arctic outflow and more warm, salty North Atlantic inflow occurred in 2004-10 as compared to the earlier period. A change in Arctic freshwater storage may have also caused a freshening event observed between September 2009 to August 2010.

Lagged correlation analysis between Davis Strait transport and regional sea level pressure (SLP) and winds reveals that atmospheric variability within Baffin Bay significantly influences circulation and transport through Davis Strait. A seasonal SLP trough, related to high SLP over the Arctic and low SLP over the subpolar North Atlantic around Greenland and Iceland, establishes in Baffin Bay beginning around October and weakens rapidly around March and April. The SLP trough is an important mechanism driving Davis Strait transport and forms in response to seasonal temperature changes, seasonal ice variability, the rough ice covered topography of Greenland and the presence of strong low pressure systems that move across the subpolar seas.

TABLE OF CONTENTS

LIST OF FIGURES

Figure Number Page

LIST OF TABLES

ACKNOWLEDGMENTS

This study is part of U.S. National Science Foundation Freshwater Initiative (2004-2007) and the International Polar Year and Arctic Observing Network (2007-2010) programs under grants OPP0230381 and OPP0632231. Additional support was provided by the Department of Fisheries and Oceans, Canada. Knut Aagaard, Jérôme Cuny, Humfrey Melling, Peter Rhines, and Charles Tang contributed information that informed the array design. Jason Gobat, Geoff Schlling, Eric Boget, James Johnson, Keith VanThiel, Murray Scotney, Victor Soukhovstev, Adam Huxtable and James Abriel were essential to the measurement program. Craig Lee, Brian Petrie, Ron Kwok and Dick Moritz were valuable coauthors on the submitted and published versions of the dissertation chapters.

I want to acknowledge and thank my advisor, Craig Lee, for allowing me to be a part of this project, funding my graduate education and accommodating and being supportive of life beyond graduate school. I also want to thank my committee: Craig Lee, Brian Petrie, Susan Hautala, Eric D'Asaro, Jamie Morison, Al Devol and Steve Warren for guiding me along the way. A special thanks to Eric and Susan who have been with me from the beginning of my graduate experience and have seen me transform from a small scale laboratory scientist to a large scale observationalist.

I want to acknowledge my fellow oceanography and atmospheric sciences cohort that made graduate school a great experience and contributed to my understanding of oceanography and atmospheric sciences. Thank you Kim Martini, Zoli Szuts, Steven Cavallo, Mark Carson, Cecilia Peralta Ferriz, Lia Slemons, Ana Ver, John Kirkpatrick, Deb Glickson, Sally Warner, Bonnie Chang and Alison Rogers.

I also can't go without thanking my friends not associated with planetary sciences that helped make sure graduate school never took my sanity and are some of the best friends a person can have. Thank you Jon Butterworth, Brian Lee, Arthur Gyldenege, Kenny Minogue, Mike Tamplin, Traci Underwood, George Perantatos, Scottland Jacobson and Oma McLaughlin.

DEDICATION

I dedicate my dissertation to my wife and son who continually help me keep my perspective on what is most important in this world and to Bryan P. Hutton, my best man and best friend that left this life way too early.

Chapter 1

INTRODUCTION

The influence of oceanic and atmospheric changes in the Arctic on North Atlantic climate variability is unclear. Some model studies (Holland et al., 2001; Jahn et al., 2010) indicate the amount, method and form that freshwater is delivered to the North Atlantic can affect thermohaline circulation in the North Atlantic. Changes in the Arctic and North Atlantic climate due to variations in heat, freshwater and sea ice also initiate changes in ecosystems on all trophic levels (Greene et al., 2008; Post et al., 2009; Kovacs et al., 2010). Recent changes have been observed in the Arctic, including increased air temperatures (e.g., Overland et al., 2008; Stroeve et al., 2012), enhanced sea ice loss (e.g., Stroeve et al., 2012) and variability in Arctic wind-driven circulation and freshwater distribution (Timmermans et al., 2011). Similar changes such as increased Canadian river discharge (Déry et al., 2009), rapid acceleration of West Greenland and Canadian Arctic Archipelago (CAA) glaciers (Chen et al., 2011; Gardner et al., 2011) and ice free Canadian Arctic Archipelago (CAA) channels (Canadian Ice Service, `http://ice-glaces.ec.gc.ca/`) have been observed west of Greenland and in the Canadian subarctic. These shifts suggest volume, freshwater and heat transport between the Arctic and North Atlantic Oceans may also be changing. Davis Strait is one of two major oceanic gateways for exchange between the Arctic and North Atlantic Oceans (Figure 1.1). Understanding how freshwater is exchanged through the primary pathways between the Arctic and North Atlantic is crucial for understanding how the ocean responds to climate variations. An observing system began operating in Davis Strait in September 2004 with the goal of providing sustained, long-term quantification of Arctic-subarctic exchange west of Greenland.

The system, including moorings, Seaglider surveys and autumn hydrographic sections, was designed to quantify transports and associated uncertainties, with the aim of isolating secular trends associated with environmental change and understanding the mechanisms driving the observed changes.

Exchanges between the Arctic and North Atlantic Oceans occurs via pathways on both sides of Greenland. West of Greenland, exchanges are primarily one way, southward from the Arctic to the North Atlantic via the CAA, Baffin Bay and Davis Strait (Figure 1.2). A small component of CAA outflow bypasses Baffin Bay to flow through Fury and Hecla Strait, (0.1 Sv volume and 38 mSv freshwater, 1 Sv = 10^6 m^3 s^{-1} = 31,536 km^3 yr^{-1}) before entering the Labrador Sea through Hudson Strait (Straneo and Saucier, 2008). On the east side of Greenland, freshwater exits through Fram Strait and flows southward along the eastern shelf of Greenland as the East Greenland Current (EGC) (Cuny et al., 2005).

In order to understand transport variability through Davis Strait, it is also necessary to understood how Arctic outflow and glacial runoff is modified within Baffin Bay. Baffin Bay is a semi-enclosed basin between Greenland and Canada (area $\approx$ 690,000 km^2) with a broad shelf on the Greenland side, narrow shelf on the Canadian side and bottom depths around 2300 km in the deep flat central region (Figure 1.2). Davis Strait lies at the southern boundary of Baffin Bay. Along the moored array Davis Strait is 330 km wide (Figure 1.3), with a 10 km wide western shelf (Baffin Island) and 100 km wide eastern shelf (Greenland). The central sill depth, 640 m, limits deep exchanges between Baffin Bay and the Labrador Sea. Circulation within Baffin Bay is cyclonic and topographically steered (Tang et al., 2004). Mean winds through Baffin Bay are typically southward and strongest in autumn/winter but weaken and often reverse direction in the summer (National Ocean and Atmospheric Administration, `www.esrl.noaa.gov/psd/data/composites/day/`).

Arctic Ocean waters enter Baffin Bay at its northern end through the three main passages of the CAA: Lancaster Sound (sill, 125 m), Jones Sound (sill, 120 m) and

Nares Strait (sill, 250 m) (Tang et al., 2004). Upon entering Baffin Bay via these three passages, Arctic water flows southward along Baffin Island and out through Davis Strait into the Labrador Sea as the broad, shallow Baffin Island Current (BIC) (Tang et al., 2004). Additional inflows enter Baffin Bay along the coast of Greenland, flowing northward through Davis Strait, and include the fresh West Greenland Current (WGC) on the shelf and the warm, salty West Greenland Slope Current (WGSC). The WGC is a combination of the southward flowing EGC from the Arctic via Fram Strait (de Steur et al., 2009) and the East Greenland Coastal Current (EGCC) arising from the addition of East Greenland coastal inflow and glacial runoff (Bacon et al., 2002; Sutherland and Pickart, 2008) that have traveled around the southern tip of Greenland and travel north through Davis Strait. The WGSC is a branch of the North Atlantic Current that enters and circulates cyclonically in the Irminger Sea and continues along the East Greenland slope seaward of the EGC around the southern tip of Greenland, turning north towards Baffin Bay (Cuny et al., 2002; Myers et al., 2007). The warm WGSC has been linked to subsurface glacial erosion off the coast of central West Greenland (Holland et al., 2008; Rignot et al., 2010). Net outflow through Davis Strait to the Labrador Sea includes contributions from the inflows into Baffin Bay as well as any modifications made while in residence in the bay such as: precipitation minus evaporation (P-E), air-sea exchanges and sea ice growth and melt.

Sea ice in Baffin Bay and Davis Strait insulates the water column from surface winds, but also alters water density through sea ice formation and melting. Density increases due to brine rejection during growth and decreases due to the addition of freshwater when melting. In Baffin Bay, sea ice generally begins to form in September, reaching maximum coverage in March and having ice free conditions in late summer (Tang et al., 2004). In Davis Strait sea ice formation generally begins in November. Maximum ice cover typically occurs in March and ice extends across the full width of the strait during this time. The rest of the year, warm WGSC water and strong offshore winds from West Greenland keep the West Greenland slope and shelf, typically as far north as Disko Island, ice-free.

In northern Baffin Bay, a series of polynyas exist between Greenland and the CAA passages (Steffen, 1985). The presence of polynyas and sea ice in Baffin Bay allows for easier water mass transformations due to brine rejection and the release of oceanic heat to the atmosphere. A polynya is an area of low ice concentration or open water which is surrounded by ice in a region where ice would be expected. Polynas are driven by wind (latent heat polynya), atmospheric/ocean heating (sensible heat polynya) or both (Barber et al., 2001). Polynyas in Baffin Bay typically start to form between November and March and remain through ice break up with the spatial extent depending largely on the formation of an ice arch in Nares Strait (Barber et al., 2001; Kwok, 2005). Baffin Bay polynyas are created by the strong northerly winds associated with ageostrophic, orographically channeled flow down the atmospheric pressure gradient through Nares Strait (Samelson and Barbour, 2008). Formation of the ice arch prevents sea ice from entering northern Baffin Bay (Barber et al., 2001). Northerly winds blow ice southward but the ice arch prevents thick Arctic ice from filling in the exposed region and new ice, which is more easily forced by the wind, begins to form. Though the polynyas begin as latent heat polynyas, sensible heat is important, particularly late in the season, off the southern coast of West Greenland. Coastal upwelling due to the strong northernly winds and winds blowing off northwest Greenland elevate the thermocline and bring warm WGSC water to the surface (Steffen, 1985; Barber et al., 2001). Both enhanced brine rejection due to polynyas and the upwelling and mixing of warm, salty water can increase the density of surface water in Baffin Bay.

Current knowledge of transports and circulation in Davis Strait rests on results from year-round moored measurements collected between September 1987−September 1990 (Ross, 1992). The 1987-90 array (Figure 1.3a) consisted of five moorings per year deployed at six positions in the central strait but included neither measurements over the shelves nor in the upper 150 m. Two studies (Tang et al., 2004; Cuny et al., 2005), based on the 1987-1990 measurements, each adopted different approaches for extrapolating across the upper 150 m and either made highly uncertain estimates of shelf contributions or confined their analyses to the central strait. Differences in methods from these three studies produced the same average net volume transport of -2.6 $\pm$ 1.0 Sv (negative sign indicates southward transport) including the West Greenland shelf and shear in the upper 150 m (Cuny et al., 2005) and -2.6 $\pm$ 1.2 Sv excluding the West Greenland shelf and shear in the upper 150 m (Tang et al., 2004). Liquid freshwater transports from the two studies range from -99 $\pm$ 34 mSv (Tang et al., 2004) to -92 $\pm$ 34 mSv (Cuny et al., 2005) with ice contributing an additional -21.3 mSv (-873 km^3 yr^{-1}) to -12.9 mSv (-528 km^3 yr^{-1}). Cuny et al. (2005) also estimate that 18 $\pm$ 17 TW of heat is transported through the strait.

Many model and observational studies have focused on quantifying CAA transports and understanding the dominant forces driving transport variability (Münchow and Melling, 2008; Jahn et al., 2010; Houssais and Herbaut, 2011; McGeehan and Maslowski, 2012; Peterson et al., 2012). Peterson et al. (2012) find that Lancaster Sound volume transport, based on observations from a moored array across Barrow Strait in Lancaster Sound between 1998-2006, is significantly correlated with northeastward winds in the Beaufort Sea, parallel to the western coasts of the CAA at monthly to interannual time scales, consistent with sea surface height (SSH) gradients through the strait. They also note that freshwater transport is driven by variations in volume transport. Münchow and Melling (2008) use bottom pressure sensors, tide gauges and a moored array across Nares Strait between 2003-06 to estimate volume transport and show that both along and across strait sea level pressure (SLP) gradients contribute to the net southward flow through the strait. This is consistent with findings from Samelson and Barbour (2008) showing a connection between northerly winds and SLP gradients with sea ice export through Nares Strait. Model results from Jahn et al. (2010); Houssais and Herbaut (2011); McGeehan and Maslowski (2012) generally agree with the observations noting that SSH and SLP variations through the CAA passages in addition to large-scale climate variations. High resolution (≈ 9 km) model results from McGeehan and Maslowski (2012) suggest that inflows through eastern Davis Strait could regulate CAA and Davis Strait outflow by altering SSH in Baffin Bay and thus the SSH gradients between the ends of the CAA passages and between Baffin Bay and the Labrador Sea.

This dissertation is divided into three main chapters followed by a general conclusion. Chapter 2 uses the first year (2004-05) of data from the moored array to estimate volume, freshwater and heat transports using objective analysis (OA) and put them in context with freshwater and volume budgets for Baffin Bay and Fram Strait. Chapter 3 presents OA estimates of volume, freshwater and heat transport through Davis Strait between 2004-10 using year-round full strait moored measurements and concurrent Seaglider surveys. The complementary combination of high temporal resolution provided by the moored array and fine spatial resolution achieved by Seaglider-based sampling allows for more accurate quantification of transports and uncertainties than previously possible. Additional data from the Advanced Microwave Scanning Radiometer (AMSR-E) and the National Centers for Environmental Prediction and National Center for Atmospheric Research (NCEP-NCAR) reanalysis products assist in estimating the volume and freshwater contributions from sea ice. The 1987-90 moored measurements are reanalyzed using similar OA methodology; transports between the two time series are compared. Chapter 4 uses the OA monthly volume transport estimates from Davis Strait, presented in Chapter 3, between 1987-90 and 2004-10 to identify atmospheric forcing mechanisms driving volume transport variability by investigating linear relationships between Davis Strait transport, Baffin Bay inflows, regional winds and SLP at monthly and longer time scales. Transport variability is also compared to the large-scale Arctic Oscillation (AO) and the North Atlantic Oscillation (NAO) climate indices. Chapter 5 summarizes the results in Chapters 2 - Chapter 4.

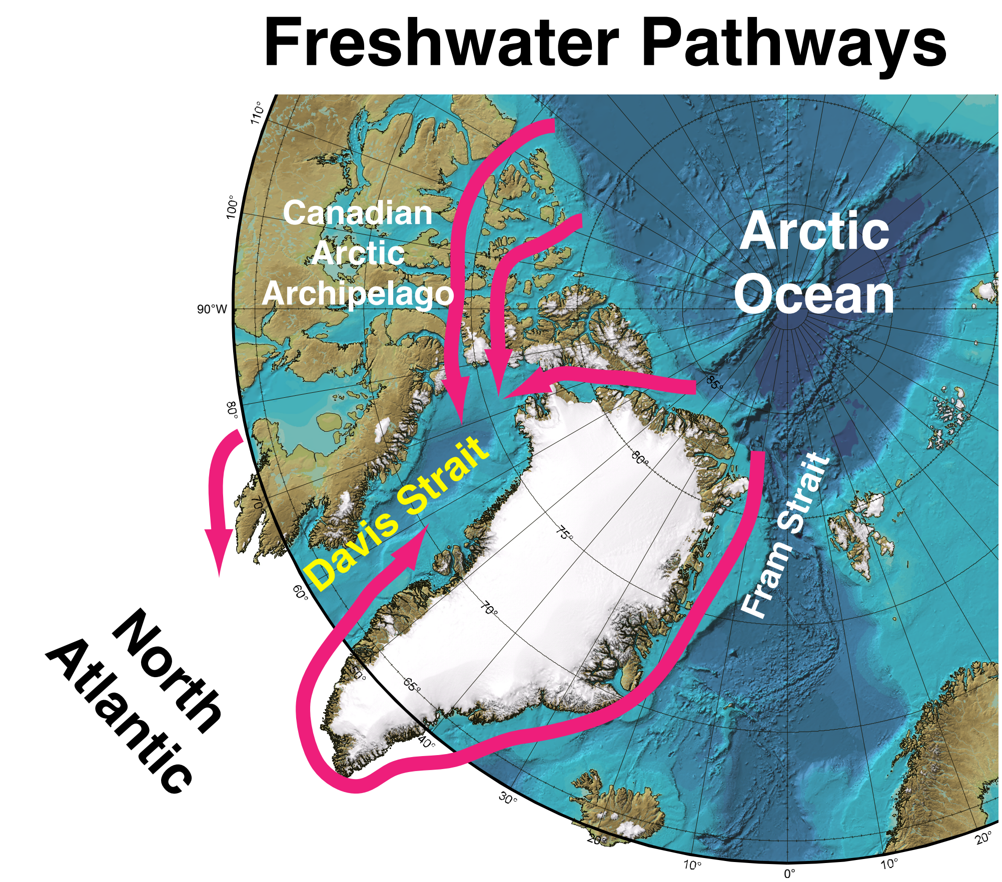

Figure 1.1: Freshwater pathways from the Arctic Ocean to the North Atlantic Ocean via Davis Strait by way of the Canadian Arctic Archipelago and Fram Strait. International Bathymetric Chart of the Arctic Ocean image of the Arctic Ocean courtesy of (Jakobsson et al., 2008).

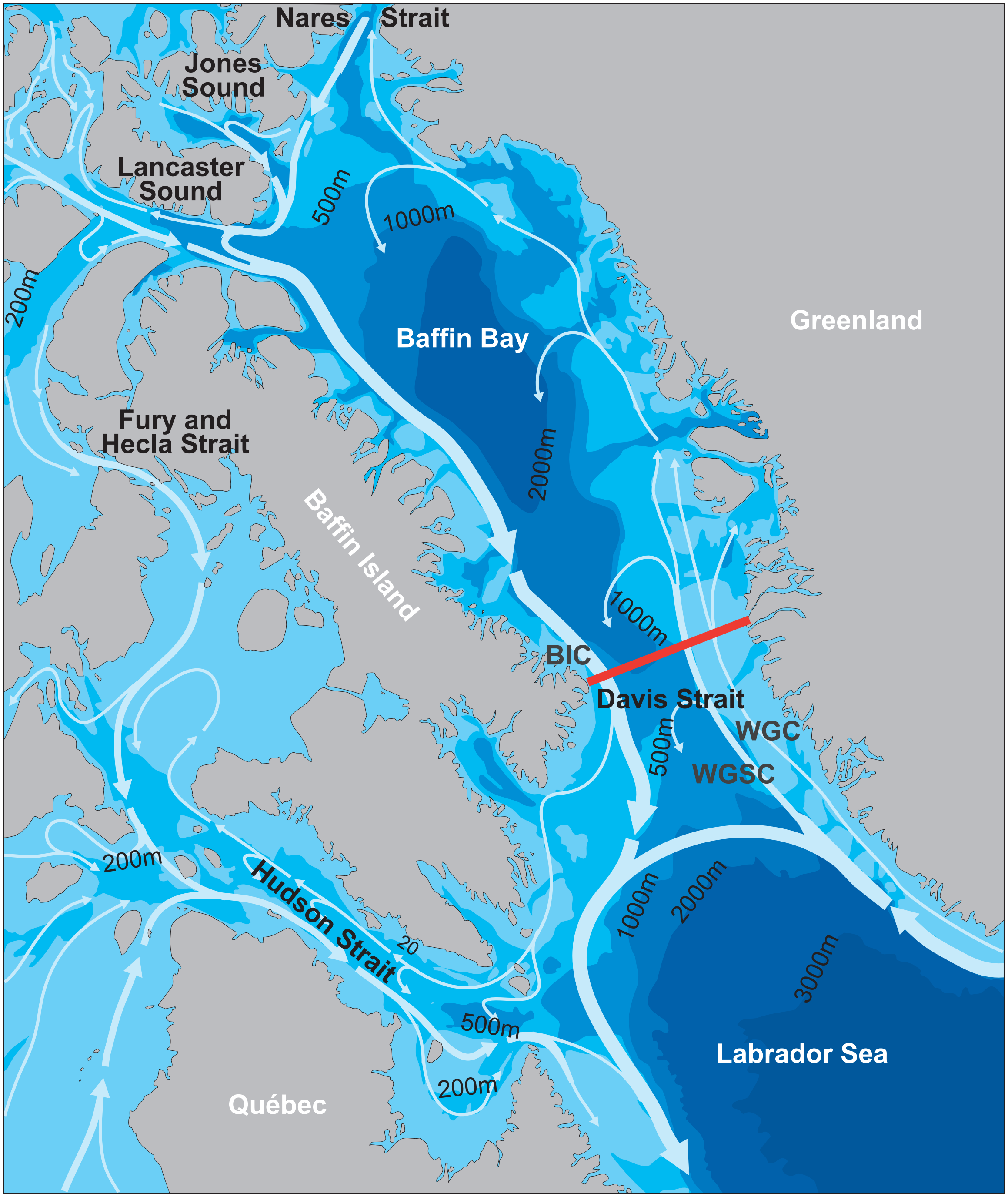

Figure 1.2: General circulation in Baffin Bay and Davis Strait (white arrows) and the location (red line) of the 2004-10 moored array. Arctic water by way of the Canadian Arctic Archipelago leaves Davis Strait as the broad, surface-intensified Baffin Island Current (BIC). Northward flow on the eastern side of Davis Strait consists of the fresh West Greenland Current (WGC) of Arctic origin on the shelf and warm, salty West Greenland Slope Current (WGSC) of North Atlantic origin on the slope.

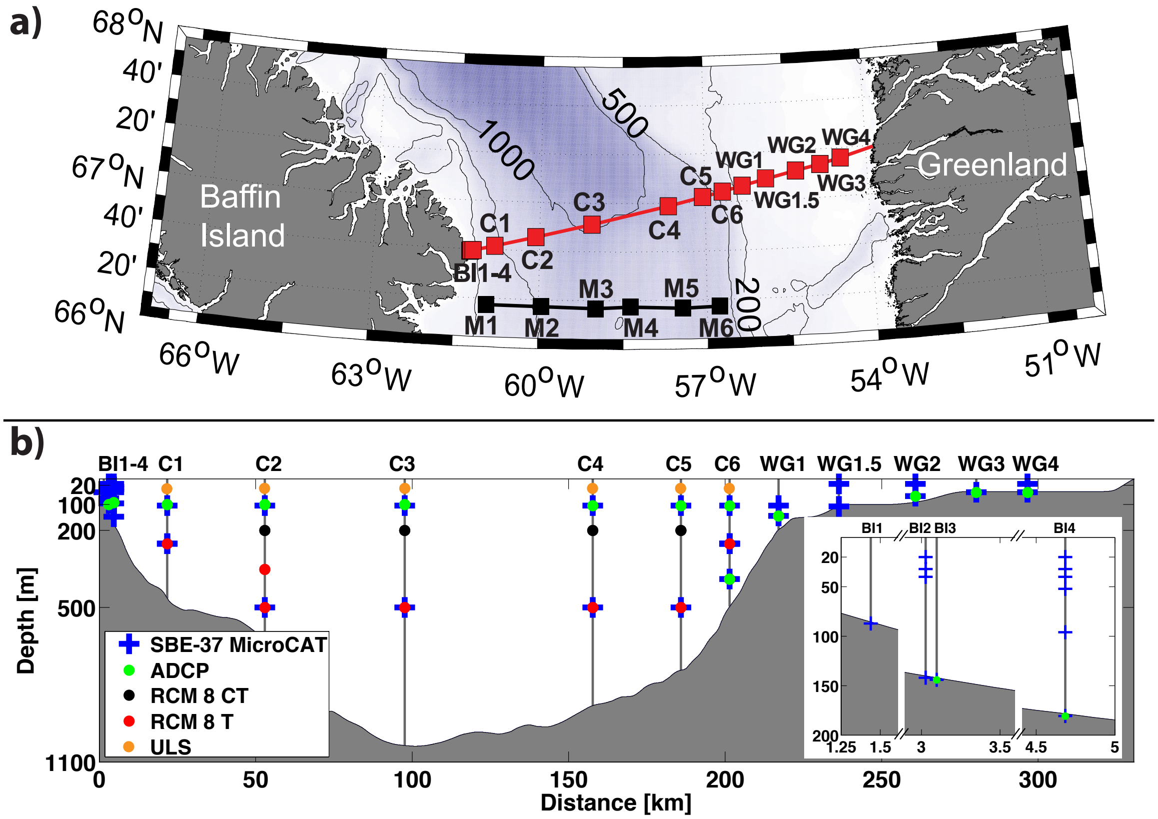

Figure 1.3: (a) Davis Strait 2004-10 (red line) and 1987-90 (black line) moored arrays with squares indicating mooring locations. (b) Summary of Davis Strait 2004-10 moored array instrumentation. Blue crosses indicate SBE37 MicroCAT conductivity, temperature and pressure recorders; green dots represent RDI ADCPs; black dots denote Aanderaa RCM8 velocity, conductivity, and temperature recorders; red dots denote Aanderaa RCM8 velocity and temperature recorders; and orange dots denote ULSs. Inset image shows a close-up of the Baffin Island shelf instruments. Spatial coverage varies from year to year throughout the program.

=========== Chapter 2

Chapter 2

VOLUME, FRESHWATER AND HEAT FLUXES THROUGH DAVIS STRAIT, 2004-05

2.1 Introduction

Arctic waters flow into the North Atlantic through the Canadian Arctic Archipelago (CAA) and Fram Strait (Aagaard and Carmack, 1989). Recent changes in the Arctic including increased air temperatures (e.g., Overland et al., 2008), enhanced sea ice loss (e.g., Wang and Overland, 2009), increased Canadian river discharge (Déry et al., 2009), and ice free CAA channels (Canadian Ice Service, `http://ice-glaces.ec.gc.ca/`), suggest potentially large changes in volume, freshwater, and heat transports between the Arctic and North Atlantic Oceans. Variability in freshwater export through Davis Strait could impact North Atlantic deep convection (e.g., Våge et al., 2009), alter the strength of the Atlantic Meridional Overturning Circulation (Holland et al., 2001), and affect western North Atlantic continental shelf ecosystems (Greene et al., 2008).

Davis Strait captures the CAA outflow after modification during its transit through Baffin Bay to the Labrador Sea (Figure 2.1a). Arctic Ocean waters, entering northern Baffin Bay through Nares Strait, Jones and Lancaster Sounds, flow southward along Baffin Island through Davis Strait as the broad, surface-intensified Baffin Island Current (BIC) (Tang et al., 2004; Cuny et al., 2005). Northward flow on the eastern side of Davis Strait consists of the fresh West Greenland Current (WGC) of Arctic origin on the shelf and warm, salty West Greenland Slope Current (WGSC) of North Atlantic origin on the slope. These inflowing waters, modified during their cyclonic circulation in Baffin Bay, join the BIC and exit western Davis Strait at depths typically > 400 m. The net Baffin Bay outflow combines CAA flows, river runoff, sea ice, and inputs from Greenland and the North Atlantic. The smaller Fury and Hecla Strait component (0.1 Sv volume and 38 mSv freshwater, 1 Sv = 10^6 m^3 s^{-1} = 31 536 km^3 yr^{-1}) of the CAA outflow bypasses Baffin Bay and enters the Labrador Sea through Hudson Strait (Straneo and Saucier, 2008).

2.2 Data and Methods

2.2.1 Data

A long-term monitoring program in Davis Strait began in September 2004. The 2004-05 program included 14 moorings (4 per shelf and 6 central moorings; Figure 2.1b,c) north of the sill (640 m) at a maximum depth of 1040 m. Instrumentation measured velocity, temperature, and conductivity at 30 minute and hourly intervals. On the Baffin Island shelf, a prototype iceberg-resistant mooring (IceCAT), consisting of a float and SBE37 MicroCAT inductively coupled to a bottom-mounted data logger measured temperature and conductivity at 5-minute intervals.

Currents were resolved parallel and orthogonal to the array line (77.3°); tidal variability was removed with a 34-hour low-pass Butterworth filter and sub-sampled to obtain daily values; missing data were filled by interpolation and extrapolation using archived data to produce full-depth temperature (T) and salinity (S) (BIO, http://www.mar.dfo-mpo.gc.ca/science/ocean/), and along-strait velocity (V) profiles at each mooring. See Online Appendix A.

2.2.2 Objective Mapping

Objective analysis (OA) (Bretherton et al., 1976) was used to construct daily variable (= observed value - mean value) maps of V, T, and S fields using a Gaussian covariance function. Correlations calculated from hydrographic sections and mooring time series yielded horizontal decorrelation length scales of 20 km (V) and 40 km (T and S). Slowly varying daily mean fields were created using further low-passed data (10-day cutoff to reduce tidal and meteorological variability) and spatially averaged into domains defined by depth (0-150, 200-250, and 500 m) and location (e.g. the shelves and WGSC-BIC frontal zone). The mean and variable fields were mapped onto a regular, two-dimensional grid with 4 m cells at depths < 150 m, 10 m cells at depths > 150 m at a horizontal resolution of 5 km. See Online Appendix B.

2.2.3 Flux Calculations

Daily volume, freshwater, and heat fluxes were averaged to compute monthly and annual fluxes. The reference salinity (34.8, mean Arctic Ocean salinity; Aagaard and Carmack, 1989), sea ice salinity (5), and temperature (0°C) were chosen to maintain consistency with Cuny et al. (2005). Mooring deployment and recovery provided $<$ 10 days of data in September, insufficient to compute reliable flux estimates for that month. Monthly fluxes for September 2005 were estimated as the average of October 2004 and August 2005 values.

2.2.4 Uncertainties

Flux uncertainties were estimated as the sum of OA random error, standard error of the mean calculated using the Students t-distribution with 95% confidence limits, and maximum range of flux estimates obtained using different approaches to compute the mean field. Additional uncertainties associated with the ice flux and estimation of the shelf and 0-100 m salinities were added to the freshwater flux uncertainty estimate. Sensitivity tests were performed to estimate flux variability associated with differences in mean field and sea ice flux.

2.3 Results and Discussion

2.3.1 Current and Water Mass Structure

Circulation during 2004-05 was dominated by northward flow on the West Greenland (WG) shelf and slope and southward flow over the remaining Strait with weaker currents below 200 m (Figure 2.2a). The surface-intensified (upper 200 m) southward flow extended eastward ∼150 km from Baffin Island with a bi-modal structure featuring strong flows over the slope, weaker currents approximately 100 km offshore, and maximum velocities at the BIC-WGSC front. The narrow (∼50 km) WG slope current had an average a velocity magnitude seven times greater than the WG shelf current. Opposing currents in the BIC-WGSC front were strongest in autumn and winter and present in all months except April. A weak northward flow over the Baffin slope in December and January was also noted by Tang et al. (2004) and Cuny et al. (2005).

Following the definitions of Tang et al. (2004), four water masses are identified in Davis Strait and defined in Figure 2.3. Arctic Water dominated the upper layers to depths approaching 200 m and extending to ∼200 km from Baffin Island (Figure 2.2b,c). Salinity increased ∼0.4 from December to March in the upper 200 m with local ice formation (∼1.25 m) accounting for only ∼0.1 of the increase, the remaining due to salt advection. The strong BIC-WGSC frontal zone, separating AW and TrW from WGIW, is evident over the slope. Maximum temperatures and salinities of the WGIW occurred in autumn, decreased until April and remained nearly constant until August, consistent with advection from the south (Manfred Stein, pers. comm.). Recirculated WGIW influenced the temperature of TrW but their temperature variations were not well correlated, possibly due to variations in recirculation and mixing time scales in Baffin Bay. The WGSW temperature had an annual cycle of ∼6°C with a late summer maximum and March minimum. Salinity variations on the WGSW (autumn minimum, May maximum, typically freshest at the coast) reflect melting Arctic sea ice advected from Fram Strait, local and advected runoff, and interactions with WGIW. Ice was present from November 2004 to July 2005 with peak coverage in February.

2.3.2 Annual and Monthly Fluxes

Mean volume, freshwater (including sea ice), and heat fluxes through Davis Strait, October 2004 to September 2005, were -2.3 $\pm$ 0.7 Sv, -116 $\pm$ 41 mSv and 20 $\pm$ 9 TW respectively. As autumn CTD data suggest that waters below the sill did not cross the Strait, flux calculations were extended only to 640 m. Transport from 0 to 100 m was 39% (-0.9 Sv) of the net volume and 59% (-69 mSv) of the net freshwater fluxes. Shelf contributions were small: for WG, 0.4 Sv of volume, 15 mSv of liquid freshwater, and 3 TW of heat; the Baffin Island shelf accounted for -0.1 Sv, -7 mSv, and 1 TW. The heat flux estimates must be viewed with caution since the net volume flux is not zero (Schauer et al., 2008).

Net monthly volume and freshwater fluxes were southward year round with weak peaks in December-January and June (Figure 2.4). Though not statistically significant, the peaks suggest transport may have be driven by advection (December-January) from the Arctic Ocean via the CAA and local (June) forcing related to the spring-summer Baffin Bay ice melt. A reasonable advection speed of 0.08-0.12 m s^{-1} is required for the broad June-August transport peak in Lancaster Sound (Prinsenberg et al., 2009) to have triggered the December-January transport peak at Davis Strait. Heat flux was strongest between October and December, due to increased southward transport of cold BIC water and northward transport of warm WGSC water: it was nearly constant between January and August.

The September linearly interpolated volume and freshwater fluxes, -1.7 Sv and -99 mSv, agreed well with the geostrophic estimates from the hydrographic sections for 2004, -1.9 Sv and -96 mSv, and 2005, -2.6 Sv and -107 mSv, particularly for freshwater. The geostrophic transports were based on a $\sim$1 day transect of the Strait and neglect barotropic contributions, particularly large for the northward WG slope current, which could account for the larger difference in volume transport.

Sea ice contributes significantly only to the freshwater flux. Kwok (2007) estimated that 360x10^3 km^2 of sea ice with an average thickness of 1-1.5 m was exported between November 2004 and May 2005. Assuming a thickness of 1.25 m, this implies 450 km^3 of sea ice export which, when combined with the estimate from Jordan and Neu (1982) of 17 km^3 for June and July, yields 467 km^3 yr^{-1} or 11 mSv of freshwater export through Davis Strait.

2.3.3 Water Mass Fluxes

Particular water masses dominate the heat and freshwater fluxes. The annual negative liquid volume flux (-4.2 Sv) consists of 50% (-2.1 Sv) AW and 40% (-1.7 Sv) TrW. The fresher AW makes up 72% (-103 mSv) of the annual negative liquid freshwater flux (-143 mSv) whereas TrW contributes only 23% (-33 mSv). The annual positive heat flux (+30 TW) shows 37% (+11 TW) from AW, 37% (+11 TW) from WGIW and 10% (+3 TW) from WGSW.

2.3.4 Comparisons to Previous Studies

These results extend the Davis Strait flux estimates beyond 1987-90 (Ross, 1992) and are more robust. The 1987-90 estimates, based on six central strait moorings, lacked measurements shallower than 150 m and over both shelves, where the 2004-05 results indicate that 55% (73%) of the volume (liquid freshwater) transport occurs. Three studies using the 1987-90 data adopted different approaches for extrapolating across the upper 150 m and either made highly uncertain estimates of shelf contributions (Cuny et al., 2005) or confined their analyses to the central Strait (Loder et al., 1998; Tang et al., 2004). Differences in upper-layer extrapolation methods produced volume fluxes ranging -3.3 to -2.6 ($\pm$ 1.2) Sv, liquid freshwater fluxes ranging from -120 to -92 ($\pm$ 34) mSv, and a heat flux (Cuny et al. (2005) only) of 18 $\pm$ 17 TW. The freshwater transport from ice ranged from -21.3 mSv (873 km^3 yr^{-1}; Tang et al. (2004)) to -12.9 mSv (528 km^3 yr^{-1}; Cuny et al. (2005)).

The 2004-05 volume, liquid freshwater and heat flux estimates (-2.3 $\pm$ 0.7 Sv, -105 $\pm$ 41 mSv, and 20 $\pm$ 9 TW) are within the uncertainties of the 1987-90 estimates (-2.6 $\pm$ 1 Sv, -92 $\pm$ 34 mSv, and 18 $\pm$ 17 TW; Cuny et al. (2005)) but the WG shelf contributions differ substantially. The 2004-05 volume, freshwater and heat flux estimates for the WG shelf (0.4 Sv, 15 mSv, and 3 TW) are less than half the 1987-90 estimates (0.8 Sv, 38 mSv and 7 TW). Neglecting the fluxes over the WG shelf where Cuny et al. (2005) had no measurements, net southward volume and liquid freshwater fluxes have decreased between 1987-90 (-3.4 Sv and -130 mSv) and 2004-05 (-2.7 Sv and -120 mSv), not a statistically significant margin, but nonetheless intriguing and contrary to expectations. The solid (ice) component of freshwater flux between 2004-05 (-11 mSv) nearly matches the estimate from 1987-90 (-12.9 mSv).

2.3.5 Baffin Bay Budgets

Contemporaneous measurements across the primary pathways of Baffin Bay, combined with estimates of ice contributions, precipitation less evaporation (P-E) and historical data from Jones Sound, allow assessment of Baffin Bay volume and freshwater budgets (Table 2.4, see Appendix C). Budgets close to within 0.6 Sv for volume and 5 mSv for freshwater, both within the uncertainties of the estimates. These imbalances represent 26% and 4% of the net annual volume and freshwater transports through Davis Strait and provide a rough gauge of the arrays' ability to monitor the fluxes. The larger volume flux imbalance may reflect decreased resolution below 200 m in Davis Strait (a larger fraction of the volume, relative to freshwater, flux is in the deeper layer) or interannual variability.

2.3.6 Comparison to Fram Strait

Net volume and freshwater transports through Davis Strait are similar in magnitude to those estimated for Fram Strait, the other major pathway connecting the Arctic and North Atlantic. Davis Strait net volume and freshwater fluxes are within the uncertainty of the Fram Strait estimates (-2.3 $\pm$ 4.3 Sv, Schauer et al. (2008); Rudels et al. (2008) and -119 $\pm$ 40 mSv, Rudels et al. (2008); Kwok et al. (2004), see Appendix D). Estimates of volume and freshwater outflows for the Barents Sea (Skagseth et al., 2008; Ingvaldsen et al., 2004; Aagaard and Carmack, 1989) and Hudson Strait (Straneo and Saucier, 2008) indicate that Davis and Fram Straits combined account for 98% of the total volume and 84% of the total freshwater Arctic outflows.

2.4 Conclusion

Davis Strait, along with Fram Strait, represents a critical component of Arctic volume and freshwater budgets and an important input of freshwater for the subpolar North Atlantic. The 2004-05 fluxes are statistically similar to those calculated for 1987-1990, though comparisons suggest a decrease of the volume transport for the central Strait. Varying methodologies, observational coverage and record length along with interannual variability create a somewhat disparate comparison, suggesting a re-analysis using common methodologies. Larger differences might have been expected given recent changes seen in the Arctic and CAA. Continued measurements are needed to monitor and understand any variability of the CAA outflow in response to Arctic change

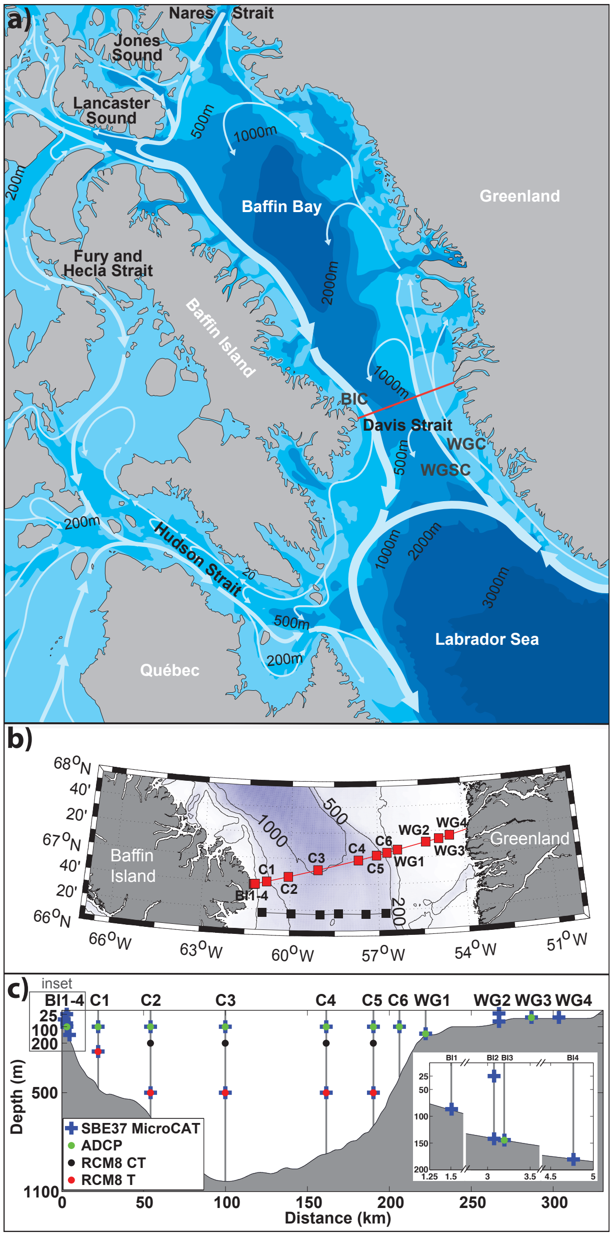

Figure 2.1: (a) General circulation in Baffin Bay and Davis Strait (white arrows) noting the Baffin Island Current (BIC), West Greenland Current (WGC), West Greenland Slope Current (WGSC), and moored array (red line). (b) Zoom panel of Davis Strait and 2004-05 (red squares) and 1987-90 (black squares) mooring sites. (c) Moored array instruments, depths, and locations. Blue crosses indicate SBE37 MicroCAT conductivity, temperature, and pressure recorders, green dots represent RDI ADCPs, black dots denote Aanderaa RCM8 velocity, conductivity, and temperature recorders, and red dots denote Aanderaa RCM8 velocity and temperature recorders. Inset image shows a close-up of the Baffin Island shelf instruments.

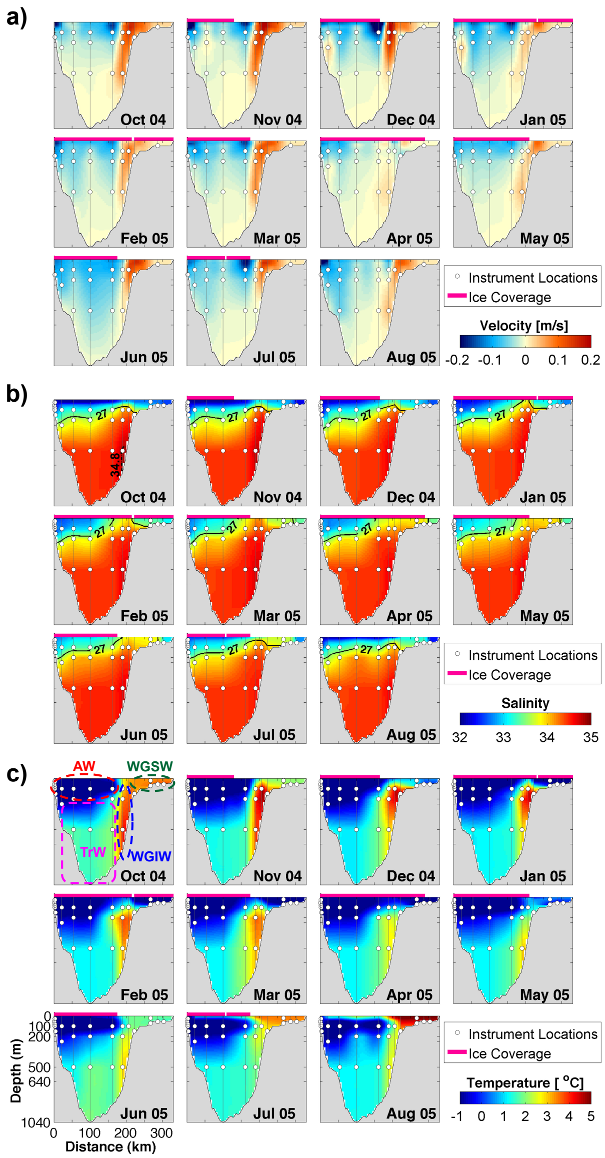

Figure 2.2: Objectively analyzed monthly mean (a) along-strait velocity, (b) salinity, and (c) temperature. Gray lines indicate moorings, white dots instrument locations for each property, and the pink bars areas along the moored array that are covered by sea ice 60% of the month. The 34.8 salinity contour (dashed black line) and the 27 kg m^{-3} isopycnal (black line) are noted in panel (b). Mean salinities $\geq$ 34.8 were seen only in October. The boundaries of the four dominant water masses (AW: Arctic Water, WGIW: West Greenland Irminger Water, WGSW: West Greenland Shelf Water, and TrW: Transitional Water; see Figure 2.3 for θ-S characteristics) are shown for October in panel (c).

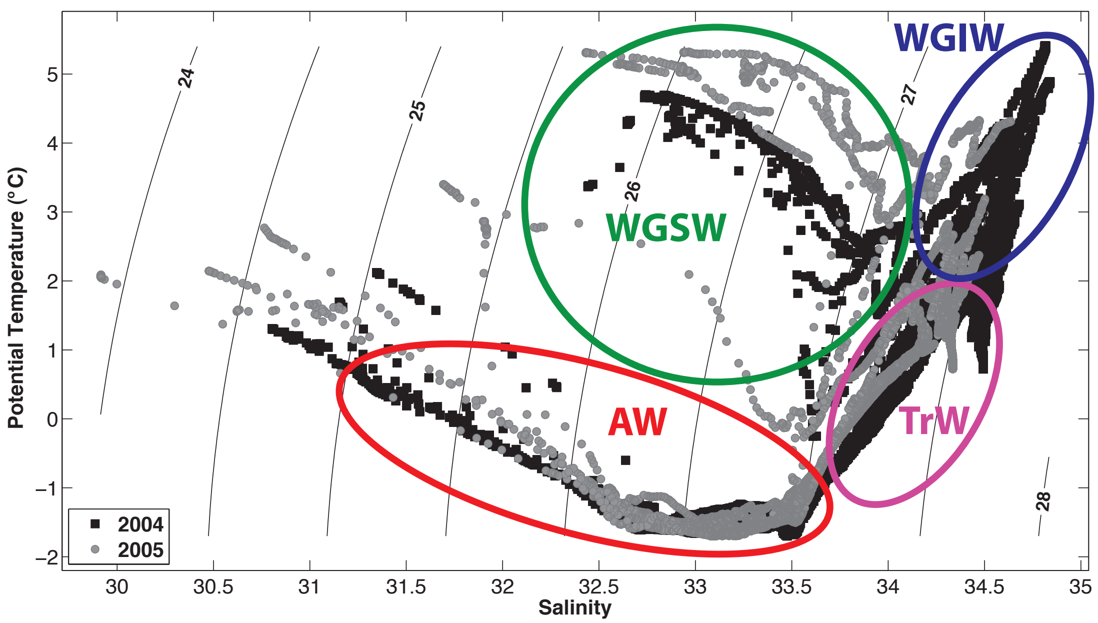

Figure 2.3: Davis Strait water masses defined using potential temperature (θ) and S: Arctic Water (AW (red ellipse), $\theta \leq 1$°C; S $\leq$ 33.7) present in the western Strait at depths < 300 m, West Greenland Irminger Water (WGIW (blue ellipse), $\theta > 2$°C; S > 34.1) along the West Greenland slope, West Greenland Shelf Water (WGSW (green ellipse), $\theta < 7$°C; S < 34.1), and Transitional Water (TrW (magenta ellipse), $\theta \leq 2$ °C; S > 33.7) usually at depths > 300 m. Water masses illustrated using September 2004 (black squares) and September 2005 (gray circles) hydrographic data along the mooring line.

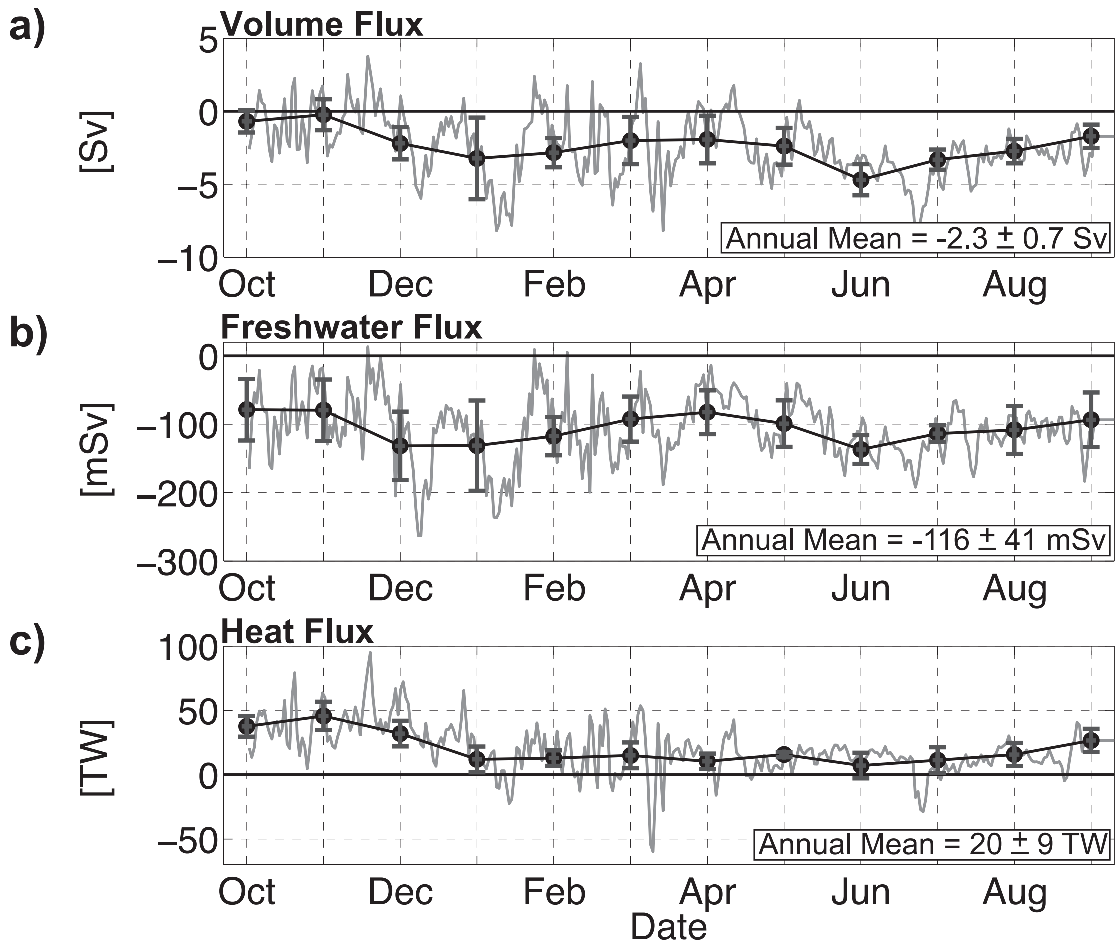

Figure 2.4: Monthly mean fluxes, including uncertainties, for (a) volume, (b) liquid freshwater (reference 34.8), and (c) heat (reference 0°C). Daily fluxes are shown in gray and annual mean fluxes, including uncertainties, are noted in the bottom right of each panel. The annual freshwater flux estimate includes the contribution from sea ice, -15 mSv. All fluxes are estimated from the surface to the sill depth, 640 m.

Table 2.1: Baffin Bay volume and freshwater (referenced to 34.8) budgets.

Baffin Bay Passages	**Volume Transport (Sv)** Inflow	Outflow	**Freshwater Transport (mSv)** Inflow	Outflow
Nares Strait[a,b] 2003-2006	0.72 ± 0.11		28 ± 3	
Lancaster Sound[c] 1998-2006	0.7 ± 0.2		48 ± 15	
Jones Sound[d] 1998-2002	0.3 ± 0.1		12 ± 4	
CAA Ice[e,f] 1996-2007	< 0.1		5.7 ± 1	
Greenland Ice Sheet[g] 1995-2007	< 0.1		7.2 ± 1	
P-E[h,i,j,k,l] 1961-2001	< 0.1		7.0 ± 4	
Baffin Island Runoff [h,m] 1971-2000	< 0.1		2.8 ± 1	
Davis Strait 2004-2005		-2.3 ± 0.7		-116 ± 41
Total	**1.7 ± 0.2**	**-2.3 ± 0.7**	**111 ± 16**	**-116 ± 41**
Difference	**-0.6**		**-5**	

[a]Münchow and Melling (2008); [b]Rabe et al. (2009); [c]Prinsenberg et al. (2009); [d]Melling et al. (2008); [e]Agnew et al. (2008); [f]Kwok (2005); [g]Mernild et al. (2009); [h]Canadian Climate and Data Information Archive (available online at www.climate.weatheroffice.ec.gc.ca); [i]Jensen and Rasch (2008); [j]National Climate Data Center (available online at www.ncdc.noaa.gov/oa/ncdc.html); [k]Kållberg et al. (2005); [l]Danish Meteorological Institute (available online at `www.dmi.dk/dmi/index/gronland/klimanormaler-gl.htm`); [m]Water Survey of Canada (available online at `geogratis.cgdi.gc.ca/geogratis/en/index.html`)

Chapter 3

MULTI-YEAR VOLUME, FRESHWATER AND HEAT TRANSPORTS THROUGH DAVIS STRAIT, 2004-10

3.1 Introduction

Quantifying and understanding how and in what form freshwater is delivered from the Arctic to the North Atlantic in response to oceanic and atmospheric variability is necessary for understanding changes in North Atlantic thermohaline circulation (Holland et al., 2001; Jahn et al., 2010). Recent changes have been observed in the Arctic, including increased air temperatures (e.g., Overland et al., 2008; Stroeve et al., 2012), decreased sea ice extent and volume (e.g., Stroeve et al., 2012; Kwok and Untersteiner, 2011) and increased variability in Arctic wind-driven circulation and freshwater distribution (Timmermans et al., 2011). Changes have also been observed west of Greenland and in the Canadian subarctic, such as increased river discharge (Déry et al., 2009), rapid acceleration of West Greenland and Canadian Arctic Archipelago (CAA) glaciers (Chen et al., 2011; Gardner et al., 2011) and ice-free channels in the CAA (Canadian Ice Service, `http://ice-glaces.ec.gc.ca/`). These shifts suggest that volume, freshwater and heat transports between the Arctic and North Atlantic Oceans may also be changing. Davis Strait is one of two major oceanic gateways for exchange between the Arctic and North Atlantic Oceans (Figure 3.1). Since September 2004, a comprehensive observational program in Davis Strait, including a year-round full strait moored array and concurrent Seaglider surveys, has been focused on quantifying volume, freshwater and heat transport variability to aid in understanding how exchanges between the Arctic and North Atlantic are being modified due to recent changes observed in the Arctic.

Outflow from the Arctic Ocean enters the North Atlantic through two major pathways, to the east and west of Greenland. On the west side of Greenland, Arctic outflow exits though the narrow, shallow channels of the CAA (Nares Strait, Jones Sound and Lancaster Sound) and circulates cyclonically within Baffin Bay before continuing southward to the Labrador Sea via Davis and Hudson Straits (Figure 3.1). Outflow from Baffin Bay through Davis Strait captures freshwater inputs from: integrated CAA outflows; the West Greenland Current (WGC); glacial runoff from West Greenland and the CAA; and sea ice, precipitation and river contributions from Baffin Bay. A small component of CAA outflow bypasses Baffin Bay to flow through Fury and Hecla Strait, (0.1 Sv volume and 38 mSv freshwater, 1 Sv = 10^6 m^3 s^{-1} = 31,536 km^3 yr^{-1}) before entering the Labrador Sea through Hudson Strait (Straneo and Saucier, 2008). On the east side of Greenland, freshwater exits through Fram Strait and flows along the eastern shelf of Greenland as the East Greenland Current (EGC), continues around the southern tip of Greenland and travels northward through Davis Strait along the West Greenland shelf as the WGC (Cuny et al., 2005).

Davis Strait, along the moored array line (Figure 4.2a), extends 330 km between Baffin Island, Canada and Greenland, with a 5 km wide western shelf (Baffin Island) and a 113 km wide eastern shelf (Greenland). A sill (640 m maximum depth) south of the array limits deep exchanges between Baffin Bay and the Labrador Sea. Circulation within the strait is predominately two-way and topographically steered (Tang et al., 2004). Arctic Ocean water travels southward via Nares Strait, Jones Sound and Lancaster Sound along Baffin Island through Davis Strait as the broad, surface-intensified Baffin Island Current (BIC) (Tang et al., 2004; Cuny et al., 2005) (Figure 3.1). Northward flow on the eastern side of Davis Strait consists of the low-salinity WGC of Arctic and Greenland origin on the shelf and the warm, salty West Greenland Slope Current (WGSC) of North Atlantic origin. The WGC is a combination of the EGC flowing southward from the Arctic through Fram Strait (de Steur et al., 2009) and the East Greenland Coastal Current (EGCC) arising from the addition of

East Greenland coastal inflow and glacial runoff (Bacon et al., 2002; Sutherland and Pickart, 2008). The WGSC is a branch of the North Atlantic Current that enters and circulates cyclonically in the Irminger Sea and continues along the East Greenland slope seaward of the EGC around Greenland (Cuny et al., 2002; Myers et al., 2007). Both the WGC and WGSC flow around the southern tip of Greenland before turning north towards Baffin Bay. Sea ice is generally present in western and central Davis Strait between November and July, reaching a maximum in March, (Canadian Ice Service, `http://ice-glaces.ec.gc.ca/`) but warm WGSC water and strong offshore winds from West Greenland keep the West Greenland slope and shelf free of ice as far north as Disko Island, for most of the year.

Warm North Atlantic water can enhance glacial erosion of Greenland outlet glaciers causing fresh meltwater to be released into the ocean and therefore decreasing the salinity of the WGC and ECG (Straneo et al., 2010; Holland et al., 2008; Rignot et al., 2010). While the volume of meltwater might not be significant, the addition of very fresh water might generate shallow buoyancy driven boundary currents around Greenland. Straneo et al. (2010) observed subsurface glacial melting off the coast of East Greenland, in Sermilik Fjord, associated with warm, subtropical waters brought from the shelf into the fjord through wind-driven exchange. Warm WGSC water traveling northwards through Davis Strait have been linked to subsurface glacial erosion off the coast of central West Greenland (Holland et al., 2008; Rignot et al., 2010). Fresh glacial meltwater from eroding West Greenland glaciers within Baffin Bay contributes to the net freshwater outflow through Davis Strait.

Changes in Arctic outflow through Davis Strait may affect deep convection in the Labrador Sea which influences the strength of the Atlantic Meridional Overturning Circulation (Holland et al., 2001; Jahn et al., 2010). However, views differ on the nature of these linkages. Våge et al. (2009) proposed that the freshwater export through Davis Strait enhanced deep convection in 2007 by increasing the northwestern Labrador Sea ice cover, allowing the cold winds from the Canadian landmass to reach the deep convective regions largely unaltered, leading to enhanced heat transport from the ocean to the atmosphere. Model studies suggest two possible outcomes of enhanced freshwater flow from the CAA into the Labrador Sea. Goosse et al. (1997) conclude that an increase in freshwater discharge into the Labrador Sea leads to pronounced surface salinity and density decreases, increased stratification and reduced deep water formation. In contrast, model results from Myers (2005) indicate that CAA outflow is confined to the western Labrador Sea shelf and slope and has little impact on the offshore, deep convection area. Similarly, Schmidt and Send (2007) use observations to suggest that freshwater from the WGC has a stronger impact on stratification in the central Labrador Sea than the BIC does. It has been suggested that downstream of the Labrador Sea, increases in southward freshwater transport along the western North Atlantic continental shelf initiate dramatic regime shifts in the shelf ecosystems and alter the abundances and annual cycles of phytoplankton, zooplankton and higher trophic-level consumers populations (Greene et al., 2008).

Current knowledge of transports and circulation in Davis Strait rests on results from the first year of this monitoring program, excluding Seaglider surveys (Curry et al., 2011), and year-round moored measurements collected between September 1987−September 1990 (Ross, 1992). The 1987-90 array (Figure 4.2a) consisted of five moorings per year deployed at six positions in the central strait but included neither measurements over the shelves nor in the upper 150 m. Two studies (Tang et al., 2004; Cuny et al., 2005), based on the 1987-1990 measurements, each adopted different approaches for extrapolating across the upper 150 m and either made highly uncertain estimates of shelf contributions or confined their analyses to the central strait. Differences in methods from these three studies produced the same average net volume transport of -2.6 $\pm$ 1.0 Sv (negative sign indicates southward transport) including the West Greenland shelf and shear in the upper 150 m (Cuny et al., 2005) and -2.6 $\pm$ 1.2 Sv excluding the West Greenland shelf and shear in the upper 150 m (Tang et al., 2004). Liquid freshwater transports from the two studies range from -99

$\pm$ 34 mSv (Tang et al., 2004) to -92 $\pm$ 34 mSv (Cuny et al., 2005) with ice contributing an additional -21.3 mSv (-873 km^3 yr^{-1}) to -12.9 mSv (-528 km^3 yr^{-1}). Cuny et al. (2005) also estimate that 18 $\pm$ 17 TW of heat is transported through the strait.

This paper presents objectively analyzed (OA) estimates of volume, freshwater and heat transport through Davis Strait between 2004-10 using year-round full strait moored measurements and concurrent Seaglider surveys. The complementary combination of high temporal resolution provided by the moored array and fine spatial resolution achieved by Seaglider surveys allows for more accurate quantification of transports and uncertainties than previously possible. Seaglider surveys began in September 2005 with occupations during the ice-free months, and extended to provide cross-strait sections during the ice-covered periods starting in 2008. Volume and freshwater transports by sea ice are estimated using sea ice velocity and concentration data derived from passive microwave measurements by the Advanced Microwave Scanning Radiometer (AMSR-E), National Centers for Environmental Prediction and National Center for Atmospheric Research (NCEP-NCAR) reanalysis products and sea ice thickness estimated from upward looking sonar (ULS) measurements. Section 4.2 introduces the data used in this study and Section 4.3 describes the methods employed for estimating transports and corresponding uncertainties. Results are presented and discussed in Section 3.4 in terms of along-strait velocity, temperature and salinity variability, water mass component transports, net transports and sea ice transports. Section 3.5 describes and investigates the causes behind a freshening event observed, starting in September 2009, in the upper 250 m between Baffin Island and mid-strait. The 1987-90 moored measurements are reanalyzed using similar OA methodology; transports between the two time series are compared in Section 3.6. The focus of this paper is to quantify and describe transport variability in Davis Strait. A complementary paper investigating the forces controlling the observed variability is forthcoming and only briefly addressed in this paper.

3.2 Data and Data Processing

The Davis Strait observing system began operating in 2004 with the goal of providing sustained, long-term quantification of Arctic-subarctic exchange west of Greenland. The system was designed to quantify transports and associated uncertainties, with the aim of isolating secular trends associated with environmental change and understanding the mechanisms driving observed changes. The observing system consists of year-round moorings (eight-nine shelf and six central moorings (Figure 4.2); continuous, year-round Seaglider-based sections in the central strait, roughly between the 500-m isobaths; and annual autumn hydrographic sections with chemical sampling. The array was positioned north of the sill, at a maximum depth of 1040 m, in an attempt to avoid bathymetrically-induced flow complications and allow for concurrent Seaglider surveys. Seaglider surveys are conducted in both ice-covered and ice-free conditions, with at least two complete central strait surveys for each calendar month.

3.2.1 2004-10 Moored Array

RDI Acoustic Doppler Current Profilers (ADCP), Aanderraa Recording Current Meters (RCM8) and SeaBird SBE37 MicroCATs measure velocity, temperature and conductivity at 30 minute (ADCP and MicroCAT) and hourly (RCM8) intervals. On the shelves, iceberg-resistant packages (IceCAT), consisting of floats and SBE37 MicroCATs inductively coupled via a weak link to bottom-mounted data loggers, measured conductivity and temperature in the upper 20-50 m at 5-minute intervals. IceCATs mitigate risk of data loss due to interaction with overhead ice by preserving all measurements in a bottom-mounted data logger that is isolated from the near-surface elements by a weak link. Salinity is computed using the 1978 Practical Salinity Scale equations and constants (Perkin and Lewis, 1980). Spatial coverage varied during the program due to changes in instrumentation and losses from instrument failure and unrecovered moorings. Appendix D Table 1 summarizes the locations, depths, record lengths and type of instruments deployed between September 2004-September 2010.

For analysis, currents are rotated parallel and orthogonal to the array line (77.3°). Prior to filtering the data to remove high frequency variability, data gaps less than 15 days are filled. Velocity gaps, typically spanning the time between mooring recoveries and deployments, are filled by reconstructing tidal (M2, K1, S2 and O1) velocity using harmonic fits. For temperature and salinity, gaps less than five hours are filled using linear interpolation. Temperature and salinity gaps between five hours and 15 days are filled using a smoothed version of the data that have been linearly interpolated and then low-pass filtered with a 10-day cutoff frequency to reduce tidal and meteorological variability. After the velocity, temperature and salinity gaps are filled in, high frequency variability is removed using a 34-hour low-pass Butterworth filter and the data are sub-sampled at noon each day to obtain daily values of velocity, salinity and temperature. Daily data are then placed on a two-dimensional with vertical spacing every 4 m in the upper 372 m and 10 m spacing between 380 m and 1040 m and horizontal spacing every 5 km between 0 km and 330 km. Grid bottom depths are defined using the International Bathymetric Chart of the Arctic Ocean (IBCAO, Jakobsson et al. (2008)). Mooring locations are added to the horizontal grid making it uneven. In the vertical, observations at the mooring sites are placed on the vertical grid as near to their measured depth as possible.

3.2.2 Seagliders

Starting in September 2005, autonomous Seagliders (Eriksen et al., 2001) were added to the monitoring program to resolve temperature, salinity and density variability at scales smaller than the mooring separation distances and to provide consistent measurements in the region near the ice-ocean interface. Seagliders are small, long endurance autonomous underwater vehicles that propel themselves through the water by changing their buoyancy such that they alternately sink and rise. Seagliders change their center of gravity to control their attitude, thus using wings and rudder to project vertical motion into the horizontal. This allows Seagliders to control their course and navigate from waypoint to waypoint as they sawtooth in depth. Seagliders exploit this capability to repeatedly occupy sections across the central strait, roughly following the mooring line. Temperature and conductivity along dive paths are bin-averaged onto a regular depth grid at 5-m intervals. Seagliders profile from the sea surface (or approximately 5 m below the ice-ocean interface, when ice is present) to within 10 m of the bottom depth, as defined by the International Bathymetric Chart of the Arctic Ocean (IBCAO, Jakobsson et al. (2008)) and by soundings from a short-range acoustic altimeter. They surface at 2-6 hour intervals, with approximately 1-4 km horizontal distance between surfacings, depending on dive depth, and take roughly 10 days to complete one central strait section. the typical horizontal speed is 0.25 m s^{-1} (20 km/day). Missions completed between September 2005 and June 2011 yielded 46 full central strait sections with at least two sections within each calendar month. Details of the sections used in this analysis are summarized in Appendix D Table 2.

In ice-free environments, Seagliders rely on GPS for geopositioning and Iridium satellite modems for telemetry of commands and data. Seasonal ice cover complicates Seaglider operations by blocking access to the sea surface, and thus to services that rely on satellites. In the presence of ice, Seagliders use a combination of an ice climatology, an acoustic altimeter and a comparison between in situ near-surface temperature and the freezing point to distinguish overhead ice from open water. When ice prevents surfacing, Seagliders navigate by trilateration from an array of RAFOS sources (Rossby et al., 1986). The moored array includes seven RAFOS sound sources, each broadcasting a 40 second, 5-Hz sweep centered at 780 Hz, six times per day. Seagliders carry Benthos RAFOS-2 hydrophones, Seascan clocks and receiver modules. Source to Seaglider ranges are computed using one-way travel times and in situ depth-averaged sound speed. Ranges are corrected for Doppler shift and multilateration. Navigation solutions are computed using nonlinear least squares, initialized with the previous acoustic navigation solution. Positions are quality filtered using the implied speed over ground. All navigation processing is done in real-time onboard the Seaglider, with position accuracies of roughly 2 km.

Observations collected by Seagliders are projected onto the mooring line to produce a series of standard sections. Currents within the strait cause Seagliders to deviate from their intended track, while position errors associated with RAFOS tracking add uncertainty to recorded positions when operating under ice. The great circle arc length is used to find the shortest horizontal distance between each dive (ascending and descending) and the gridded mooring line. Dives farther than 40 km from the mooring line are excluded. Dive paths are visually inspected to determine the start and end dives for each full or partial section across the central strait and bad data points/dives are eliminated. Only sections spanning more than 75% of the central strait are used in this analysis.

Each dive in a section is assigned to a horizontal grid point on the gridded mooring line by optimizing the minimum horizontal distance and minimum bottom depth difference between the gridded mooring line and the dive. Typically for each dive, the grid point with the minimum horizontal distance is also the grid point with minimum bottom depth difference, but for cases where this is not true the minimum bottom depth difference grid point is chosen unless the horizontal distance difference is greater than 10 km. After all dives in a section are assigned to a horizontal position on the grid, each section is linearly interpolated onto the two-dimensional mooring grid and then smoothed horizontally and vertically using a moving window with five vertical bins (20-50 m) and six horizontal bins (30 km) to reduce high frequency variability. Since Seagliders only sample in the central strait, mooring data are used to fill in over the shelves and slopes for sections completed before September 2010. For the sections completed after the 2009-10 mooring period, multi-year average monthly mooring data are used to fill in over the shelves. The combined data sets are linearly interpolated in the horizontal and then vertical directions and extrapolated to the edges to create full two dimensional sections. The full sections are smoothed horizontally with a moving

20 km window over the interpolated transition where the mooring and Seaglider data sets are merged.

3.2.3 Sea Ice Data

Upward Looking Sonars

Applied Physics Laboratory/University of Washington Mark 2 ULSs collected sea ice draft (d) measurements above the moorings in the central strait at pre-programmed intervals (Figure 4.2b). The ULS emits a 1 ms pulse of high-frequency, narrow-beam, vertically-oriented acoustic energy into the water column, then measures and records the round-trip travel time (τ) between emission of the pulse and detection of the signal coming back from the underside of the ice, or from the sea surface. Simultaneously, the ULS measures and records the in-situ water pressure (P_{uls}). Range (R) to the target is estimated from τ, and depth (D) below sea-level is estimated from P_{uls}. The ice draft is estimated as depth minus range,

$$d = D - R,$$

and ice thickness (h) in meters is estimated as

$$h = 1.14d.$$

Thickness estimates do not take into account snow cover on the ice and the multiplier is less accurate for ridged ice as compared to smooth ice. The specifications, operational parameters, data reduction procedures and ULS accuracy are described in Drucker et al. (2003) who conclude that at D = 34 m, individual ULS measurements of d of smooth ice have a random rms error (rmse) of ≈ ± 0.04 m. Some of the contributions to this estimate of random error are proportional to D and for this analysis it is assumed that

$$rmse(D) = \frac{D}{34} rmse(34m).$$

Errors of measuring ice thickness in rough ice, e.g. pressure ridges, rubble fields and floe edges are larger and less well-known than the smooth ice errors. For instance, typical ULS measurements in rough ice are subject to bias that depends on the ice roughness and the effective footprint of the sonar (e.g., Vinje et al., 1998; Rothrock and Wensnahan, 2007). To address this problem, the ULS applies two different detection criteria to each received sound pulse, and records two different measurements of τ. The first-return (FR) corresponds to the nearest detectable target (and thickest ice) in the effective footprint of the sonar. The last-valid return (LVR) corresponds to the most-distant detectable target (and thinnest ice) in the effective footprint. To qualify as "valid", the ULS receiver voltage must remain above the detection threshold 0.7 ms (i.e. 70% of the pulse duration) after initial detection. Because the FR need not be "valid", at some observation times there is a FR but not an LVR value of τ. At observation times when both FR and LVR are determined the ice roughness on spatial scales smaller than the effective footprint may be analyzed in terms of the difference in thickness hFR - hLVR. Moritz and Ivakin (2012) analyzed ULS data acquired near the North Pole and an LVR was detected at more than 99% of the observations times. They find that, consistent with intuition, within footprint roughness is correlated (r = 0.81) with roughness estimated from the under-ice profile on scales larger than the effective footprint. Following their analysis procedures, the average value of FR and LVR are used as an unbiased estimate of τ at each observation time.

Each ULS samples on two schedules, called low-resolution (LR) and high-resolution (HR). The HR data are acquired at 10-second intervals between 00:00:00 and 00:25:00 each day. Some of the ULS acquire a second set of HR data from 12:00:00 to 12:25:00 each day (Table 3.1). The HR data resolve most of the features in the profile of the underside of the ice, and are useful in calibrating the ULS time series relative to sea-level. Each ULS acquires LR data continuously at a constant interval, but this interval varies among the different ULS, from 2 minutes to 5 minutes (Table 3.1). The LR data have more statistical degrees of freedom per measurement than the HR data, and are useful in estimating sample statistics and confidence limits while making efficient use of the 26 Amp-hour battery energy and 2 megabyte storage capacity of ULS.

The ULS data are averaged over the time series for each calendar month, excluding "open water" data points, defined here as h ¡ 5 cm in winter and h ¡ 10 cm in summer. The resulting sample statistic represents the monthly mean thickness of sea ice at points where there is ice, not open water. Errors in the monthly averages depend on measurement errors and sampling errors. The effect of random measurement errors on the sample mean thickness is negligible when averaging over a month and it is assumed that by averaging the FR and LVR measurements, no adjustment for footprint bias is required. Therefore only the sampling errors need to be considered. These are estimated as standard errors of the mean, using the bootstrap methods of Politis and White (2004) and Kreiss and Paparoditis (2011) to account for effects of dependence in the data. This method automatically accounts for differences in the total number of LR data points per month due to differences in the LR sampling rate Table 3.1.

AMSR-E

Daily sea ice area transports across Davis Strait are computed using daily ice concentration estimates and gridded 89 GHz brightness temperature fields from the AMSR-E radiometer on the NASA Aqua platform (National Snow and Ice Data Center, `http://nsidc.org/data/amsre/`, Cavalieri et al. (2004b), Cavalieri et al. (2004a)).

Canadian Ice Service

Daily ice coverage maps provided by the Canadian Ice Service (`http://ice-glaces.ec.gc.ca/`) are used to define surface ocean temperatures when ice is present over the array line. Ice is considered either present or not and no distinction is given between types of ice.

3.2.4 1987-90 Moored Array

An array of five moorings deployed across central Davis Strait, south of the 2004-2010 array (Figure 4.2a), employed RCM5s to collect hourly measurements of velocity, temperature and salinity at depths of 150, 300 and 500 m from September 1987 to September 1990 (Ross, 1992; Cuny et al., 2005). Quality controlled data were obtained from the Bedford Institute of Oceanography (BIO) data archive, `http://www.mar.dfo-mpo.gc.ca/science/ocean/`. Data were processed in the same manner as the 2004-10 moored array data. Daily data are then placed on a two-dimensional with vertical spacing every 4 m in the upper 372 m and 10 m spacing between 380 m and 690 m and horizontal spacing every 5 km between 0 km and 330 km. Grid bottom depths are defined using the IBCAO (Jakobsson et al., 2008). Mooring locations are added to the horizontal grid making it uneven. In the vertical, observations at the mooring sites are placed on the vertical grid as near to their measured depth as possible.

3.3 Methods

3.3.1 Objective Analysis (OA)

Objective analysis (Bretherton et al., 1976) with some modifications is used to construct daily, full strait, sections of along-strait velocity, temperature and salinity (VTS) for the 2004-10 and 1987-90 data sets. The use of OA allows for the separation of the low frequency background (average) field from the variable (anomaly) field to systematically deal with large spatial and temporal gaps. A Gaussian covariance function:

$$C(x) = \sigma^2 \exp\left[-\left(\frac{\Delta x}{L_x}\right)^2\right],$$

based on horizontal separation (Δx), decorrelation length scale (L_x), and data anomaly variance (σ^2) is used to describe the weight of a given observation on the surrounding grid points. Correlation functions calculated from the moored observations and compared with results from the high-resolution hydrographic and Seaglider sections yield horizontal decorrelation length scales of 20 km (V) and 40 km (T and S).

Formulation of the background fields and creation of the daily full-depth VTS profiles are detailed in Appendix E. Mooring data and Seaglider TS sections are used to calculate average OA large-scale background VTS fields for each year-day; these fields are used with all six years of observations. When spatial gaps between the moorings exceed the decorrelation length scales the OA relaxes to the background fields. Using low frequency background fields to fill spatial gaps reduces the connection between total daily OA VTS results and higher frequency variability present in the daily VTS data due to forcings such as winds. Monthly background field V, T and S profile shapes at the mooring locations are used in combination with the daily moored observations to create daily full depth VTS profiles from moored observations collected at discrete depths.

3.3.2 Transport Calculations

Daily volume, freshwater and heat transports are calculated for each grid cell, summed over the grid domain, and time averaged to compute monthly and annual transports. Annual transports start in October and end in September of the following year. September 2010 transports are an average of September 2005-09 transports due to the lack of September 2010 data. Volume transport is calculated by multiplying the mapped velocity field at each grid cell by the area. Positive values indicate northward transport into Baffin Bay, negative values indicate southward transport into the Labrador Sea. Transports are estimated between the surface and sill depth (640 m). Total area across the strait is 133 km^2 with the West Greenland Shelf contributing 7 km^2. Freshwater transport is calculated as:

$$FW_{transport} = \sum V_i \frac{S_0 - S_i}{S_0} A_i,$$

where V, S and A are the mapped grid cell velocity, salinity and area respectively. The reference salinity ($S_o = 34.8$), considered the average Arctic Ocean salinity (Aagaard and Carmack, 1989), is chosen to maintain consistency with previous studies (Tang et al., 2004; Cuny et al., 2005). Heat transport is calculated as:

$$H_{transport} = \sum \rho_i V_i (T_i - T_0) C_p A_i,$$

where ρ is the water density, T the mapped temperature and C_p the specific heat of water for each grid cell. The reference temperature ($T_o = 0$°C) is chosen to maintain consistency with Cuny et al. (2005).

3.3.3 Sea Ice Transport Calculations

Daily sea ice area transport through Davis Strait between November and May for each year are estimated using AMSR-E satellite data following the methods presented in Kwok (2007) using the latest data available. Sea ice area transport is estimated north of the moored array along a line at ≈ 68°N spanning ≈ 460 km across Baffin Bay (Kwok (2007), Figure 1b). The perpendicular component of the ice motion is integrated across the strait using the trapazpidal rule and the motion is constrained to zero at the coastal endpoints. Area estimates are weighted by the AMSR-E ice concentration to account for open water areas.

Sea ice volume transports are estimated using the monthly time-averaged ice thickness derived from the ULS data. Monthly ice thicknesses from the moored ULSs (Table 3.1) are interpolated or extrapolated to obtain monthly ice thicknesses across the ice area transport line. Monthly ULS ice thicknesses are multiplied by the daily area transports across the strait and averaged to obtain monthly ice volume transports.

Due to low ULS data returns, multi-year averages of the monthly ice thicknesses are used to fill data gaps when no data are available (Table 3.1).

Freshwater export via sea ice is calculated as:

$$FW_{icetransport} = Vol_{ice}\frac{S_0 - S_{ice}}{S_0}\frac{\rho_{ice}}{\rho_{water}},$$

where Vol_{ice} is the annual sea ice volume transport through Davis Strait, S_{ice} = 5 is the sea ice salinity chosen to be consistent with Cuny et al. (2005), ρ_{ice} its density (900 kg m^{-3}) and ρ_{water} the density of fresh water (1000 kg m^{-3}). Monthly ice transports are averaged to obtain annual and the six year average estimates.

3.3.4 Uncertainty Analysis

Details of the uncertainty analysis are discussed in Appendix F. Transport uncertainties for the 2004-10 and 1987-90 data sets are estimated by summing in quadrature three types of errors, those due to: (i) noise (data − large-scale background fields) as estimated by the OA, (ii) assumptions regarding the creation of the large-scale background fields, estimated by altering the background fields, and (iii) biases due to spatial gaps in the moored array, estimated using data variance and the OA covariance function. Monthly errors for all three sources are averaged and divided by the square root of the number of monthly estimates to obtain yearly error estimates. Similarly, yearly error estimates are averaged and divided by the square root of the number of years minus one to obtain the six (2004-10) and three (1987-90) year average errors. The three types of error are summed in quadrature to determine total transport uncertainties.

3.3.5 Trends

Trends in monthly and annual transports are assessed using linear regression. Confidence limits are estimated for the regression lines to determine significance. Confidence bounds are estimated as:

$$CI = \pm t_{(\alpha,df)} S_{yx} \sqrt{\frac{1}{N} + \frac{(x_i - \bar{x})^2}{\sum (x_i - \bar{x})^2}},$$

using

$$S_{yx} = \sqrt{\frac{1}{N-2} \left[\sum (y_i - \bar{y})^2 - \frac{\sum \left[(x_i - \bar{x})(y_i - \bar{y})\right]^2}{\sum (x_i - \bar{x})^2} \right]},$$

where $t_{(\alpha,df)}$ is the critical t-statistic using a Student's t-distribution at the 95% (α) confidence level using the integral time scale to determine the degrees of freedom (df), S_{yx} the standard error of the estimate, x_i time (the independent variable), $\bar{x}$ average time, y_i transport (the dependent variable), $\bar{y}$ average transport and N the number of observations used in the regression analysis. The Corresponding P-value (p) is also computed using a Student's t-distribution at the 95% confidence level using the integral time scale to determine the df.

3.4 Results and Discussion

3.4.1 General Circulation and Water Mass Variability

Circulation within Davis Strait is predominantly two-way and topographically steered (Tang et al., 2004). Only the along-strait component of the velocity will be discussed in this paper and described using north (into Baffin Bay) or south (towards the Labrador Sea), rather than describing the flow direction as north/south perpendicular to the array line, for brevity. Southward flow extends over half the strait from Baffin Island until just off the West Greenland slope (175 km from Baffin Island) and northward flow extends over the West Greenland slope and shelf. Both maximum southward and maximum northward transport occurs between October-December. Sea ice is generally present between November and July with peak coverage January to March.

Objectively analyzed results of along-strait velocity, temperature and salinity are presented in Figure 3.3 as six-year averages of mean monthly sections across the strait. The accuracy and time-space resolution of the data presented in Figure 3.3 are unprecedented in Davis Strait and allows for more accurate, full strait, descriptions of VTS variability and estimates of transports. These data comprise the basis for distinguishing variability on annual and interannual time scales. Data is also grouped into four different water mass classes identified in Davis Strait. Each water mass travels a unique path before crossing Davis Strait and suggests that the water mass properties and transports vary independently. Variability of the individual water masses cannot be distinguished by viewing only the net quantities, therefore the variability and structure of circulation, temperature and salinity in Davis Strait are separated and described in terms of water mass classes. Four primary water masses are identified by salinity and potential temperature (θ) following Tang et al. (2004):

* Arctic Water (AW, $\theta \leq 2°$C; S ≤ 33.7) is cold, low-salinity flowing southward as the BIC, at depths < 300 m. Though of Arctic origin, this water has been modified by glacial runoff, air-sea fluxes, local sea ice melt in Baffin Bay and in the CAA.

* West Greenland Irminger Water (WGIW, $\theta > 2°$C; S > 34.1) is warm, saline water that originates in the North Atlantic and flows cyclonically around the Irminger Sea. It then rounds the southern tip of Greenland and travels northward along the West Greenland slope as part of the WGSC, passing through Davis Strait as a mostly barotropic current.

* West Greenland Shelf Water (WGSW, $\theta < 7°$C; S < 34.1) is of Arctic origin, with contributions from Greenland glacial runoff. The WGSW travels from east Greenland, turns northward at Cape Farewell and flows through Davis Strait as the WGC along the West Greenland shelf.

* Transitional Water (TrW, $\theta \leq 2°$C; S > 33.7), usually found at depths > 300 m. The TrW is the product of water masses that flow into Baffin Bay, mix and

undergo local modifications, and flow south through Davis Strait at depth.

The locations of the cores of the four water masses are indicated in the first panel of Figure 3.3c. The locations of the major current systems (BIC, WGC, WGSC) are indicated in Figure 3.1. The annual variation of the monthly average velocity, potential temperature and salinity, averaged over each water mass class, is shown in Figure 3.5) for each of the six years and for the six-year average (referred to in this paper as the annual cycle). Monthly averages are also presented in Figure 3.6 as TS diagrams where symbols identify the water masses and the color shading quantifies the along-strait velocity.

Arctic Water

Changes in AW properties reflect changes in Arctic outflow. Average AW velocities are southward the entire period, largest (-0.07 m s^{-1}) September-October and smallest (-0.04 m s^{-1}) December-January (Figure 3.5). Velocity increases again between June and July, except during 2007 and 2008. Annual and interannual velocity variability is large, with an average interannual coefficient of variability (ratio of the standard deviation to the absolute value of average) of 0.23 using monthly AW velocity averages for each year and an annual coefficient of variability of 0.15 using yearly averages of AW velocity.

Although AW velocity is southward on average, small wintertime velocities are often accompanied by northward flow along the Baffin Island slope (Figure 3.3). Velocities at C1, both in the upper 100 m and at 250 m, and sometimes at C2 200 m, reverse and are directed northward between December and February (average $\approx$ 0.04 m s^{-1}). Smaller southward velocities on the Baffin shelf and in the upper 100 m at C2 are typically observed during these reversals (Figure 3.4). The timing and magnitude of the reversals vary, but the largest (peak velocities of 0.08 m s^{-1}) occurred in 2007-08 and the smallest (0.01 m s^{-1}) in 2008-09. Cuny et al. (2005) also observed flow reversals in the 1987-90 mooring data at M1 between November and February with peak velocities of 0.12 m s^{-1} and suggested local seasonal eddies as the cause rather than advection from the south. The wintertime reversals during 1987-90 are evident in the monthly along-strait currents at site A (station M1 in Cuny et al. (2005)) presented in Tang et al. (2004) Figure 23a. Shallower and more inshore measurements from 2004-10 confirm the reversals are not accompanied by shifts in TS and are likely caused by eddies.

Salinity varies annually according to the timing of sea ice formation and melt within Baffin Bay as well as the timing of discharge of meltwater from Greenland and CAA glaciers. On average, ice starts to form within Baffin Bay in September, reaching a maximum extent in March, and begins to melt in April with ice-free conditions in August (Canadian Ice Service). Greenland surface melt generally occurs between June and August (Mote, 2007). As sea ice forms in Davis Strait, salt is rejected and stratification weakens as the dense water mixes downward. Arctic Water salinity increases during ice formation, reaching a maximum April-May, with the annual cycle maximum (33.16) occurring in May (Figure 3.5). In 2005-06 the salinity maximum was the highest of all years in April, having a monthly average salinity of 33.28. When sea ice and glaciers begin to melt, the addition of freshwater increases stratification and decreases AW salinity. Salinity reaches a minimum December-January, with the annual cycle minimum (32.92) occurring in January. The observed increase in AW salinity is consistent with a simple estimate of local ice growth using the conservation of mass and salt and annual cycle of AW salinity. The conservation of mass is expressed as:

$$\rho_{w1} H_{w1} A = \rho_{ice} H_{ice} A + \rho_{w2} H_{w2} A,$$

and the conservation of salt is expressed as:

$$\rho_{w1} H_{w1} S_{w1} A = \rho_{ice} H_{ice} S_{ice} A + \rho_{w2} H_{w2} S_{w2} A,$$

where ρ_{ice} is the ice density (900 kg m^{-3}), $\rho_{w1} = \rho_{w2} = 1027$ kg m^{-3} is the density of AW when ice begins to form and when ice begins to melt, S_{ice} is the salinity of ice (5), S_{w1} is the salinity of AW when ice begins to form, S_{w2} is the salinity of AW when ice begins to melt, $H_{w1} = 250$ m is the depth of AW as ice begins to form, H_{w2} is the unknown depth of AW as ice begins to melt, $H_{ice} = 2$ m is the ice thickness and A is the area. The areas are equal when considering a column of water. Ice begins to form in Davis Strait in November ($S_{w1} = 32.95$) and the predicted increase in salinity ($S_{w2} = 33.15$), using the above formulas, agrees well with the annual maximum salinity in May (33.16).

Starting in September 2009 and extending through August 2010, AW salinity was much lower than all other years and is not consistent with local sea ice melting. Using the same equations above, instead estimating the decrease in salinity due to local ice melting using the 2008-09 maximum salinity in May 2009 ($S_{w2} = 33.15$), salinity is estimated to decrease to 32.95 (S_{w1}) due to local melting yet the observed 2009-10 minimum average salinity in November 2009 is 32.79. This freshening event is discussed in more detail in Section 3.5.

The annual variation of AW temperature follows the annual variation of climatological air temperature, with a lag of about 1 month. Average air temperatures are coldest January-March with the minimum in February and warmest June-August with the maximum in July (Environment Canada, National Climate Data and Information Archive, Canadian Climate Normals 1971-2000, `http://www.climate.weatheroffice.gc.ca/`). The annual cycle of AW temperature has a minimum (-1.5°C) in April and maximum (-0.6°C) in August. The average annual range of air temperature is $\approx$ 34°C compared to $\approx$ 0.1°C for AW. November 2006-January 2007 was anomalously warmer (average, $\approx$ 0.2°C) than the annual cycle. This warming also coincides with below average AW salinities October-December 2006.

West Greenland Irminger Water

Monthly average WGIW velocities are northward except between July and August 2010, when it is weakly negative (-0.01 m s^{-1}). Maximum velocity typically occurs between October and December. Velocity generally decreases after December reaching a minimum between June and August (Figure 3.5). While the timing of the yearly maximum is fairly consistent from year to year the timing of the minimum varies. The annual minimum velocity is in August (0.01 m s^{-1}) but the timing of the yearly minimums range from April-August and even December in 2006-07. Interannual velocity variability is large, with an average interannual coefficient of variability of 0.71 using monthly WGIW velocity averages for each year and an annual coefficient of variability of 0.12 using yearly averages of WGIW velocity.

Annual variations in WGIW velocity are connected with variability upstream, in the Irminger and Labrador Seas. During the same time as the velocity yearly maximums, polar cyclones move eastward across the Labrador and Irminger Seas. Polar cyclones cause intense cyclonic wind stress on both sides of Greenland, which in models has been shown to enhance cyclonic circulation in the Irminger and Labrador Seas during autumn and winter (Spall and Pickart, 2003). Observations from de Jong et al. (2012) support the modeling hypothesis and show that there is enhanced circulation in the Irminger Sea during autumn and winter. Baroclinic Rossby waves develop to maintain cyclonic circulation in the summer until the wind increases again the following autumn (Spall and Pickart, 2003).

Annual and interannual WGIW variations in velocity, temperature and salinity prior to this monitoring program were not well resolved. The annual cycle of salinity exhibits two peaks, though these vary interannually in magnitude and timing. The first peak occurs between October and January and the second between March and May. In contrast, temperature has a clear annual signal with maximum values November-December then decreasing until reaching a minimum July-August. The annual maximum occurs in November (3.9°C) and the minimum in July (2.7°C). The mechanisms driving WGIW variability in and upstream of Davis Strait are poorly understood. Eddies shed off the West Greenland coast into the Labrador Sea during autumn likely drive lateral transports of heat and salt, and likely modulate transport of WGIW through Davis Strait (Lilly et al., 2003; Prater, 2002).

West Greenland Shelf Water

At the location of the mooring array, the West Greenland shelf extends 113 km from the coast to the shelf break, 34% of the total cross-strait distance. Monthly variations of WGSW velocity, salinity and temperature and density are the most consistent from year to year compared to the other water masses (Figure 3.5 and Figure 3.6). Velocity is northward in all months, with maximum values September-November and then decreasing until reaching a minimum February-April. The annual maximum occurs in September (0.07 m s^{-1}) and the minimum in April (0.02 m s^{-1}). Interannual velocity variability is large, with an average interannual coefficient of variability of 0.42 using monthly WGIW velocity averages for each year and an annual coefficient of variability of 0.11 using yearly averages of WGIW velocity.

Salinity variability over the shelf is driven by upstream variations in Arctic freshwater and sea ice outflow through Fram Strait and freshwater (both sea ice and glacier runoff) contributions from and around Greenland via the EGC and EGCC (Bacon et al., 2002; Sutherland and Pickart, 2008; de Steur et al., 2009). Yearly maximum salinity occurs April-June with the annual maximum (33.66) occurring in May. The maximum salinity (33.85) in 2005-06 was 0.18 higher than average. Salinity typically remains fairly constant between April and June then starts to decrease, reaching a yearly minimum August-October with the annual minimum (32.75) occurring in October. Shelf salinities are freshest at WG4, 34 km from the coast, between April and September. Using archived hydrographic surveys, Cuny et al. (2005) also noticed a salinity minimum $\approx$ 20 km offshore of West Greenland during the summer. They suggest that this could be a continuation of the East Greenland Coastal Current; an inner branch of the EGC, driven by Greenland ice melt and glacial runoff as described by Bacon et al. (2002); Sutherland and Pickart (2008).

The required ice thickness necessary to account for the annual cycle of WGSW salinity due to local sea ice formation and melt is 1.66 m using the annual cycle of WGSW salinity and conservation of mass and salt presented earlier where, ρ_{ice} is the ice density (900 kg m^{-3}), ρ_{w1} = 1026 is the density of WGSW when ice begins to form in November, ρ_{w2} = 1027 kg m^{-3} is the density of WGSW when ice begins to melt in May, S_{ice} is the salinity of ice (5), S_{w1} = 32.86 is the salinity of WGSW when ice begins to form, S_{w2} = 33.66 is the salinity of WGSW when ice begins to melt, H_{w1} = 50 m is the depth of WGSW as ice begins to form, H_{w2} is the unknown depth of WGSW as ice begins to melt and A is the area. Ice along the West Greenland shelf at the array line is seasonal. Extrapolating ice thickness from the slope (Table 3.1), suggests seasonal ice growth over the shelf is less than 1 m. To achieve the annual maximum salinity, assuming 1 m of ice growth, an initial salinity of 33.16 is needed, 0.3 greater than the observed annual salinity when ice starts to form (32.86). The differences in salinity suggest external sources of freshwater (e.g., glacial melt, runoff, EGC/EGCC) account for roughly 38 % (33.16-32.86/33.66-32.86) of the annual cycle of salinity over the shelf.

Annual atmospheric variations likely drive the strong annual temperature cycle on the shelf. Annual minimum WGSW temperatures occur March-April and continue to rise as air temperatures increase. The shelf reaches a maximum temperature August-September with the average maximum occurring in August (4.2°C). The annual minimum happens a month earlier than for AW, in March (-1.0°C) and is most likely due to the reduced time it takes to cool the shallow shelf water compared to deeper AW.

Transitional Water

Transitional Water is the largest water mass by area in Davis Strait and is composed of water that is modified during its passage through Baffin Bay and then exits through Davis Strait at depths below 250 m. Annual variations in TrW water properties are weaker than the other water masses in Davis Strait. Velocity is weakly southward for all months with minimum velocities March-May and the annual minimum occurring in April (-0.01 m s^{-1}). Even though the maximum southward velocity in the annual cycle occurs in July (-0.02 m s^{-1}), yearly maximums occur in either October or June-July. Interannual velocity variability is large, with an average interannual coefficient of variability of 0.28 using monthly WGIW velocity averages for each year and an annual coefficient of variability of 0.11 using yearly averages of WGIW velocity.

Topographic steering in Baffin Bay creates stronger velocities along the edges and weaker velocities in the interior at depth (Tang et al., 2004). In most months, just west of the northward flowing WGSC, a surface intensified southward current is present off the West Greenland slope (Figure 3.3). This southward current might be an extension of the BIC that has been directed eastward, following the isobaths, and then southward seaward of the West Greenland slope. The current is also present in the 1987-90 M5 mooring time series (Tang et al., 2004; Cuny et al., 2005). Tang et al. (2004) observed the current in model results along the 1000 and 1500 m isobaths off the West Greenland Shelf between 72 and 68°N and then joining the southward flow off Baffin Island around 67°N. Forcing mechanisms driving the deep flow of TrW through Davis Strait are poorly understood. They likely arise from local topographic controls, winter convection and cyclonic circulation within Baffin Bay and large-scale SLP and SSH variations between the Arctic and North Atlantic (Tang et al., 2004; Rudels, 2011).

Salinity variations in TrW are < 0.1 with the annual minimum (34.27) occurring in December then building up to the annual maximum (34.29) in August. Interannual variability is also, < 0.1 with no statistically significant clear annual cycle. In contrast, TrW temperature annual variations are more consistent from year to year. Maximum temperatures occur June-August with the annual maximum occurring in July (1.2°C). Temperature decreases after August and typically reaches a minimum November-December with a annual minimum of 0.9°C in December. Pockets of warm TrW observed in some of the summer Seaglider sections suggest possible advection of warm WGIW into the central strait.

3.4.2 Transports

Daily VTS OA results are combined with the cross-strait area and averaged to obtain annual and monthly volume, freshwater and heat transports (Figure 3.7, Figure 3.8). Yearly transports and corresponding errors are presented in Table 3.2. Volume transport through Davis Strait is defined as negative when directed southward to the Labrador Sea and positive when directed northward into Baffin Bay. Annual transports from the OA background fields are -1.63 Sv, -113 mSv and 29 TW for volume, liquid freshwater and heat (Figure 3.8).

Daily volume, freshwater and heat transports are also computed based on water mass classification and averaged to obtain monthly and annual transports (Figure 3.9). Net transport through Davis Strait is the summation of transport from the four water masses and unclassified waters. Water undefined by the water mass classes are omitted from Figure 3.9 and represent 0.1 Sv, 4 mSv and 2 TW of the total average volume, liquid freshwater and heat transports.

Interannual and annual variability of the net transports are large, with average annual volume, freshwater and heat transport standard deviations of 0.7 Sv, 17 mSv and 12 TW and interannual standard deviations of 0.3 Sv, 15 mSv and 2 TW. For the annual volume, freshwater and heat transports (Figure 3.7, Table 3.2), the interannual coefficients of variability are 0.15, 0.16 and 0.06. Monthly variability is larger with coefficients of variability of 0.43, 0.23, and 0.51 for volume, freshwater and heat transports (Figure 3.8).

Volume Transports

Yearly net volume transport through Davis Strait is southward for all years with an average transport of -1.6 $\pm$ 0.5 Sv (Figure 3.7). Although the net southward transport decreases steadily between 2004-2008, transport increases again between 2008-10 and no significant trend is observed (p values > 0.2) in the yearly or monthly transports (Figures 3.7 and 3.8). Since volume transport depends on velocity and cross-strait area, monthly volume transport variability is very similar to monthly velocity variability (Figures 3.5, 3.9). Maximum net transport occurred in 2004-05 (-2.0 $\pm$ 0.5 Sv), as a result of increased southward TrW transport in the deep central strait (Figure 3.9). Minimum net transport occurred in 2007-08 (-1.3 $\pm$ 0.4 Sv) primarily from reduced southward transport of AW, due to longer periods of flow reversal along the Baffin slope, and increased WGSW northward transport between November-December. Both AW and TrW have monthly average southward transports for all years with average contributions over the six years of -1.8 Sv and -1.1 Sv. Northward contributions come from WGIW and WGSW, with average transports of 0.4 Sv and 0.7 Sv, plus an additional 0.1 Sv from undefined water. Maximum northward transport of WGIW and WGSW occurs at the same time as maximum southward transport of AW and TrW, resulting in a September-November minimum in net monthly transport, consistent with the strength of cyclonic circulation in Baffin Bay and the Labrador Sea (Spall and Pickart, 2003; Tang et al., 2004). In contrast, timing of minimum transport varies for each water mass.

The largest contribution to volume transport is made by AW. Variability in AW transport is driven primarily by variability in outflow though the CAA passages into Baffin Bay (Lancaster Sound, Jones Sound and Nares Strait) in response to regional and large-scale sea level pressure (SLP) and sea surface height (SSH) variations within Baffin Bay and between the Arctic and North Atlantic (Tang et al., 2004; Cuny et al., 2005; Rabe et al., 2012; Peterson et al., 2012; Rudels, 2011). Transports through the CAA passages have been estimated using moorings throughout various periods spanning the last 13 years. The longest time series, through Lancaster Sound, has been monitored year-round since 1998. Results from Lancaster Sound indicate an average transport of -0.46 ± 0.09 Sv over the 13 year record with maximum transport in July-August and minimum transport November-December (Peterson et al., 2012). Minimum AW transport in 2007-08 (-1.3 Sv) through Davis Strait was concurrent with the minimum outflow through Lancaster Sound between 2004-10 (Peterson et al., 2012). Peterson et al. (2012) show that monthly alongshore wind anomalies in the Beaufort Sea account for 43% of the variance of the Lancaster Sound transport anomalies ($p < 0.01$). In 2007 the Beaufort Gyre experienced the largest anticyclonic wind-driven circulation in 60 years (Proshutinsky and Johnson, 2010), which would reduce northeastern winds in the Beaufort Sea, transport through Lancaster Sound and thus Davis Strait. Nares Strait has been monitored year-round between 2003-06 and 2009-12. Results from 2003-06 show maximum southward transport January-June, minimum southward transport July-December with an average full depth transport of -0.72 ± 0.11 Sv (Münchow and Melling, 2008). Moorings in Jones Sound between 1998-2002 indicate that an additional -0.3 ± 0.1 Sv flows through the smallest passage of the CAA (Melling et al., 2008). The sum of the CAA volume transports (-1.48 Sv) represents 82% of the average AW transport (-1.8 Sv) with additional contributions from WGSW, precipitation less evaporation, sea ice and river and glacial runoff. Some fraction of the fresh, low density WGSW (0.4 Sv) that enters Baffin Bay through eastern Davis Strait likely remains as upper water exits Baffin Bay, through Davis Strait, as AW (Figure 3.6). Winter cooling and brine rejection may increase WGSW density, causing it to sink and eventually leave Baffin Bay as TrW.

Estimates of when outflows from the CAA passages should reach Davis Strait can be made assuming average speeds between 0.15 m s^{-1} and 0.2 m s^{-1}, in agreement with speeds in Nares Strait, Barrow Strait and Baffin Bay (Tang et al., 2004; Münchow and Melling, 2008; Peterson et al., 2012). The travel time between Nares and Davis Straits (1900 km) is ~4-5 months, while that between Barrow and Davis Straits (1450 km) is ~3-4 months. With these delays, peak transport through Lancaster Sound and Nares Strait would be expected to arrive in Davis Strait in October-November and May-November respectively. Annual variability in AW on average tends to have two periods of increased southward transport, October-November and June-July, which correspond well to the estimates above.

Transitional Water, the second largest constituent of the net volume transport, is the only other component that exhibits net southward flow.Maximum transport of TrW typically occurs June-September and minimum transport typically occurs March-April. In 2004-05, the year of maximum TrW transport (-1.4 Sv), the annual cycle is unlike any of the others observed, with strong peaks in southward transport January-February and June-July. The southward peak between January-February arises from increased transport in the southward current off West Greenland, but the peak between June and July corresponds to a general increase in southward TrW velocity. Dunlap and Tang (2006) modeled September circulation within Baffin Bay and note the presence of the southward current off West Greenland between $\approx 67.5°$N and 71.1°N. In the model, the northern part of the current, just off the Greenland slope with a core 270 km from Baffin Island, transports -0.65 Sv with increased transport in the upper 400 m and weaker transport below. The current south of the array is located 150-210 km from Baffin Island, is more barotropic and transports -2.4 Sv. Along the current mooring line, the 2004-09 average September southward transport 130-201 km from Baffin Island (the horizontal distance where the southward current is observed) is -0.8 Sv with stronger velocities in the upper 200 m compared to at depth. Dunlap and Tang (2006) do not discuss the dynamics that govern the southward current off West Greenland but mention that it is part of a cyclonic gyre on the West Greenland shelf/slope. Average TrW transport roughly equals the sum of that from the inflows into Baffin Bay through eastern Davis Strait (WGIW, WGSW and unclassified water). The average transport difference between TrW and incoming water is 0.1 Sv and varies between -0.1 Sv and 0.2 Sv over the six years. However, some fraction of WGSW is likely to leave Baffin Bay as AW.

Annual variability of WGSW was unknown prior to this monitoring program. Quantifying the previously unknown annual range of WGSW transport is important for constraining Davis Strait transports and understanding the mechanisms controlling flow around Greenland. Since the 1950s, hydrographic data have been collected annually along the West Greenland shelf and slope typically, between June and July, by the Danish Meteorological Institute on behalf of the Greenland Institute of Natural Resources (Myers et al., 2007, 2009). Annual sections have been occupied between the southern tip of Greenland at Cape Farewell and near the Davis Strait mooring line at Sisimiut (Figure 3.1). Transports of WGSW have been quantified by combining hydrographic sections, climatologies and models (Myers et al., 2009), while WGIW transports have been estimated using a combination of hydrographic sections and climatologies Myers et al. (2007). Caution must be used when attempting to identify multiple-year trends from those seasonal snapshots, but when analyzed together with timeseries from the moored array, the sections can be used to enhance understanding of transport variability along the West Greenland shelf and slope. Results from Myers et al. (2009) show the WGSW and WGIW system weakening as it moves north and water is diverted into the central Labrador Sea. Volume transport of WGSW decreases between Cape Farewell (3.0 $\pm$ 0.8 Sv) and Sisimiut (0.0 $\pm$ 0.2 Sv) with transport reducing to $<$ 0.5 Sv between Fylla Bank (0.8 $\pm$ 0.5 Sv) and Maniitsoq (0.2 $\pm$ 0.2 Sv). Average June-July WGSW transport between 2004-10 from this monitoring program is larger (0.4 Sv) than reported by Myers et al. (2009). Myers et al. (2007) use a slightly different definition of WGIW ($\theta > 3.5$°C; S > 34.88) when estimating WGIW transport between Cape Farewell (4.9 $\pm$ 1.1 Sv) and south of Fylla Bank at Paamiut (0.8 $\pm$ 0.7 Sv) between 1995-2005. Average 2004-10 WGIW June-July volume transport from this monitoring program is 0.3 Sv.

Freshwater Transports

Yearly net freshwater transport through Davis Strait is southward (negative) for all years. There is no clear trend (p value > 0.2) in the annual freshwater transport (average = -93 $\pm$ 6 mSv) and significant interannual variability is present in the monthly transports. Daily net freshwater transport is significantly correlated with volume transport (r = 0.72, p value < 0.001) using a Student's t-distribution at the 95% (α) confidence level using the integral time scale to determine the minimum df. Minimum net transport in 2007-08 (-66 $\pm$ 15 mSv) and maximum net transport in 2008-09 (-110 $\pm$ 14 mSv) reflect variations in AW transport (Figure 3.9). Arctic Water makes up 70% of all freshwater transported into and out of Davis Strait.

Variability in AW freshwater transport drives variability in freshwater transport. Minimum AW freshwater transport in 2007-08 (-73 mSv) is followed by maximum AW transport in 2008-09 (-115 mSv). Maximum annual AW freshwater transport typically occurs September-November but the timing of minimum transport varies from year to year, ranging between December-January, April-May and July. Annual freshwater contributions from WGIW and undefined water are small, both ranging between 2-5 mSv. Freshwater transport contributions from WGSW and TrW are in opposite directions and roughly equal with average contributions of 17 mSv and -19 mSv. Even though WGSW freshwater transport is small, Rudels (2011) suggests that a decrease in WGSW salinity might lead to a reduction in baroclinic transport through the CAA by altering the density difference between Baffin Bay and the CAA passages.

The CAA passages provide most of the AW freshwater transport. Jones Sound transports the least amount of freshwater through the CAA with an average of -12 $\pm$ 3 mSv based on moorings from 1998-2002 (Melling et al., 2008). Lancaster Sound has been monitored year-round with moorings since 1998 and contributes approximately the same amount of freshwater as Nares Strait. An average of -32 $\pm$ 6 mSv of freshwater transport (between 1998-2011) plus an additional 2.1 mSv from sea ice (Peterson et al., 2012) passes through Lancaster Sound. Average 2003-06 freshwater transport through Nares Strait is -28 $\pm$ 3 mSv (Münchow and Melling, 2008; Rabe et al., 2012). Secondary contributions from Baffin Island runoff, precipitation less evaporation, Greenland Ice Sheet runoff, and CAA sea ice is -46 mSv (Curry et al., 2011). Freshwater transport variability in Davis Strait tracks well with Lancaster Sound freshwater transport, with both pathways experiencing maximums and minimums during the same years between 2004 and 2010 (Peterson et al., 2012). The sum of CAA liquid freshwater inflows plus secondary contributions into Baffin Bay, excluding Baffin Bay sea ice, is slightly more than (-118 mSv), but compares well with, the average liquid freshwater transport through Davis Strait (-93 mSv).

Sea Ice Transports Sea ice is generally present across the strait between November and June, with land fast ice sometimes present along the Baffin coast as late as July (Figure 3.10a). Maximum ice cover typically occurs in March when ice extends across the full width of the strait even though the West Greenland shelf and slope is often ice-free due to warmer water near the surface and the prevailing winds coming off Greenland. The average November-May sea ice area exported through Davis Strait between 2004 and 2010 is 585,000 km^2 $\pm$6500 km^2. Sea ice area transport between 2004 and 2010 ranges between 372,000 km^2 in 2004-05 to 833,000 km^2 in 2008-09 (Figure 3.10b). Similarly, sea ice volume transport ranges between 217 km^3 in 2004-05 to 466 km^3 in 2008-09 with an average of 334 km^3 over the six years with no clear trend (Figure 3.10c). Observations of ice thickness were insufficient to establish annual variations across the array (Table 3.1). Therefore all available data were used to derive an average thickness time series across the array for the ice season. These series were combined with the interannual varying ice area observations to estimate ice volume transport. If the average ice thicknesses are used for all years, the difference in average 2004-10 ice volume transport is 1 km^3 (335 km^3). Including an additional 17 km^3 of ice export between June and July from Jordan and Neu (1982), average 2004-10 freshwater export through Davis Strait is 351 km^3 yr^{-1} or 11 mSv (Figure 3.10c).

Heat Transports

Net heat transport through Davis Strait is positive for all years with no clear trends. Positive net heat transport through Davis Strait results from the transport of warm water north and cold water south. Average heat transport between 2004-10 is 23 $\pm$ 2 TW with yearly transport ranging between minimums in 2007-08 and 2009-10 (21 TW) and a maximum in 2008-09 (26 TW). Heat transports are not absolute since the net volume transport is not zero.

Heat transport of WGSW has the most distinct annual cycle and smallest interannual variability among all the water masses (Figure 3.9). Heat transport on the Greenland shelf is coupled strongly with annual air temperature variations, with maximum heat transport occurring between August and October and minimum between February and April. Contributions from WGIW and AW contribute the most towards the net heat transport.

Variability in WGIW and AW heat transports reflect variations in volume transports. The relation is opposite for AW, since increased southward transport of cold water equates to an increase in northward heat transport. Quantifying the northward transport of heat from WGIW is needed to investigate the impact of ocean heat on increased melting of West Greenland glaciers. Yearly WGIW heat transport varies between 11 and 13 TW. Seasonal June-July hydrographic sections along West Greenland indicates that heat transported with the WGSC is diverted into the Labrador Sea and does not enter Baffin Bay (Myers et al., 2007). Results from Myers et al. (2007) indicate heat transport is reduced significantly between Cape Farewell (98 $\pm$ 22 TW) and Paamiut (18 $\pm$ 15 TW).

3.5 2009-10 Arctic Water Freshening

Arctic Water began to freshen in September 2009, with salinity remaining well below average through August 2010 (Figure 3.5). Increased net freshwater outflow is observed September-November 2009 (Figure 3.9, Figure 3.8), but smaller than average southward velocities after November 2009 mask the freshening. Daily salinity records from the Baffin Island slope out to the mid-strait, stations C1-C3 at 100 m (Figures 4.2 and 3.11), indicate that freshening began during the annual salinity minimum in September 2009 and extended across to the central strait, station C3. Salinity records on the Baffin shelf also indicate freshening but instrument placement changes and data record lengths make it harder to compare temporal variability (Appendix D Table 1). Freshening is also observed at 200 m for C2 and C3 but not at 250 m at C1. The salinity minimum in 2009 is lower, and lasts longer and spans over a greater distance than in previous years. The freshening continued through August 2010 at C1 but ended at C2 and C3 in May 2010. Preliminary results from 2010-11 indicate the freshening did not continue and salinity returned to near average values.

A year-round mooring deployed in the Switchyard region (between Ellesmere Island, Canada; North Greenland and the North Pole) between April 2008 and May 2009 observed a similar freshening event starting in January 2009 (Jackson et al., 2013). Timmermans et al. (2011) also observed fresher conditions during 2009 in the Switchyard region using CTD data collected between April and November. The freshening in Switchyard is limited to 2009-10, with more saline conditions returning in April-May 2010 (Timmermans et al. (2011), Jackson et al. (2013)). On the basis of numerical simulations and observations, Timmermans et al. (2011) suggest the observed freshening might be a result of the redistribution of freshwater in the Arctic Ocean forced by changes in the wind-driven circulation. In winter 2009, Arctic wind-driven circulation was cyclonic instead of the more typical anticylonic regime causing the anticyclonic Beaufort Gyre to weaken and release stored freshwater (Timmermans et al., 2011). Timing of the upstream freshening event in the Switchyard region is consistent with an advective pathway between the two regions, allowing 11 months for transit through Nares Strait and into Baffin Bay before crossing Davis Strait. Negative salinity anomalies were observed in Barrow Strait during 2009-10, but the freshwater transport was not anomalously large because the volume transport anomaly was also negative (Peterson et al., 2012).

In addition to freshwater changes in the Arctic propagating through Davis Strait, local changes in northwest Greenland and CAA glacier melting might also contribute to the 2009 freshening event as well as to an earlier, freshening signal observed at C1 starting in late 2008. The mass loss of glaciers in Northwest Greenland increased from 30.9 $\pm$ 8 Gt yr^{-1} between 2002-06 to 128.2 $\pm$ 33 Gt yr^{-1} between 2007-09 (Chen et al., 2011). Similarly, mass loss from CAA glaciers increased sharply from 31 $\pm$ 8 Gt yr^{-1} between 2004-06 to 92 $\pm$ 12 Gt yr^{-1} between 2007-09 (Gardner et al., 2011). A rough calculation illustrates the potential contribution of glacier runoff between 2004-2010, assuming that all of the runoff would stay and is mixed evenly in the upper 250 m of Baffin Bay (area = 607 000 km^2), Northwest Greenland mass loss increased linearly between 2005-07, the salinity of glacial runoff is 2 and the same mass loss rates continued through 2010. By itself, the estimated runoff from Greenland is sufficient to reduce the salinity of the upper 250 m of Baffin Bay (area, 607 000 km^2) by 0.04 between 2004-07 and by 0.16 between 2007-10. These estimates are equal to the observed changes in annual average AW salinity between 2004-07 (-0.04) and between 2007-09 (-0.16). This suggests that glacial melt is likely a significant contributor to freshening observed in Davis Strait. However, preliminary results suggest AW salinity returned to near average values in 2011 which is inconsistent with the idea that increased glacial melt with continue to reduce AW salinity. A more rigorous and careful calculation is needed to better understand the implications of increased freshwater contributions from glaciers into Baffin Bay.

3.6 Comparison with 1987-90 Transports

Data from the 1987-90 moored array are objectively mapped in a similar manner as the current array to facilitate more accurate comparisons between the two periods. Transport comparisons are confined to the central strait due to the absence of shelf measurements in the earlier array. Average 2004-10 transport estimates from the shelves account for volume, freshwater and heat transports of -0.1 Sv, -6 mSv and 0 TW respectively from the Baffin shelf and 0.4 Sv, 18 mSv and 4 TW from the West Greenland shelf. Average central strait net volume, liquid freshwater and heat transports for 1987-90 are -3.5 $\pm$ 0.6 Sv, -142 $\pm$ 23 mSv and 18 $\pm$ 7 TW. Of the three previous studies, Cuny et al. (2005) is the only study that will be compared with the current reanalysis since it is also the only one that includes an estimate of the (unmeasured) velocity shear in the upper 150 m. Cuny et al. (2005) presents only northward and southward estimates of the transports and corresponding uncertainties, excluding both the West Greenland and Baffin Island shelves. Net volume, liquid freshwater and heat transports (northward plus southward, with uncertainties summed in quadrature) from Cuny et al. (2005) are -3.4 $\pm$ 1.3 Sv, -130 $\pm$ 60 mSv and 12 $\pm$ 17 TW, respectively. These estimates are within the transport ranges of the reanalysis presented here, and annual variations in transports and water properties agree well between 2004-2010, the 1987-1990 (both reanalysis and Cuny et al. (2005)).

While annual variability agrees well between the two periods, volume and freshwater transports differ significantly. Average central strait volume, liquid freshwater and heat transports for 2004-10, excluding the shelves, are -2.0 $\pm$ 0.2 Sv, -105 $\pm$ 7 mSv and 19 $\pm$ 2 TW, respectively. Transport differences between 1987-90 and 2004-10 are due to changes in velocity or in the extent of the water mass areas, particularly for AW and WGIW. Average AW volume transport to the Labrador Sea decreased from - 2.2 Sv to -1.7 Sv and average WGIW northward transport into Baffin Bay increased from 0.1 Sv to 0.7 Sv. Similarly, the average areal extent of AW decreased from 33 km^2 to 30 km^2 and the average areal extent of WGIW increased from 24 km^2 to 26 km^2 between 1987-90 and 2004-10. Changes in temperature and salinity between the two periods are insignificant with nearly identical average values for all water masses except a slight decrease in WGIW salinity from an average of 34.67 to 34.59. Changes between the two periods are driven by changes in volume transport and reflect changes in the mechanisms controlling transport both into and out of Davis Strait.

It is unclear if more outflow from the CAA occurred during 1987-90 since transport estimates are unavailable before the late 1990s, but variability in Arctic Ocean circulation agrees with observed transport changes between the two periods. Annual anticyclonic circulation in the Arctic was much stronger in the 1980s relative to the current period (Proshutinsky et al., 2009). Weaker anticyclonic circulation concentrates freshwater in the Beaufort Gyre and directs Arctic outflow towards Fram Strait rather than through the CAA (Proshutinsky and Johnson, 1997). The current increase in WGIW inflow is also consistent with changes observed in the strength of the subpolar gyre, showing recent weakening as compared to the late 1980s (Häkkinen and Rhines, 2004). When the subpolar and subtropical gyres weaken, as observed recently compared to the late 1980s, the subpolar gyre contracts and the subpolar front moves westward as the subtropical gyre expands, allowing more high-salinity waters to move northward and enter the Nordic Seas (Häkkinen et al., 2011).

A more thorough discussion of the forcing mechanisms and corresponding variability controlling Davis Strait transport is beyond the scope of this paper, and will be treated in a separate publication.

3.7 Conclusions

Six years of volume, liquid freshwater and heat transports in Davis Strait (2004-10) show significant interannual variability, small annual cycles and no clear trends with average net transports of of -1.6 $\pm$ 0.5 Sv, -93 $\pm$ 6 mSv and 23 $\pm$ 2 TW, respectively. Annual cycles of net volume and freshwater transports are small because of phase cancellation in the annual cycles of water mass transports. Annual cycles of contributions to total transport by individual water masses are more easily discerned in the data, particularly over the West Greenland shelf and slope. Davis Strait outflow was significantly fresher in 2009-10, likely caused by freshwater release from the Beaufort Gyre. This event was not clearly evident in the net or water mass freshwater transports due to a reduction in southward volume transport and the choice of reference salinity.

A comparison of the 2004-10 results with reanalyzed transports for 1987-90 indicate a 43% decrease of net, southward volume transport (from -3.5 to -2.0 Sv, and significantly different) in the central, deep water area of Davis Strait. This is accompanied by a 26% decrease of freshwater transport (from -142 to -105 mSv, significantly different); during both periods, the heat transports were nearly equal. This change is consistent with changes upstream in the Arctic Ocean, and downstream in the subpolar gyre, as reported elsewhere.

Data from the continental shelves and higher space and time resolution provided by the 2004-10 array result in much narrower confidence limits on the estimated transports, so that variability on annual, interannual and longer time scales is resolved better. Seaglider sections across the central strait provide important high resolution knowledge about annual variations in stratification that were unknown prior to this measurement program. Net volume and freshwater transports through Davis Strait are similar in magnitude to those estimated for Fram Strait, the other major pathway connecting the Arctic and North Atlantic. Davis Strait net volume and freshwater fluxes are within the uncertainty of the Fram Strait estimates (-2.3 $\pm$ 4.3 Sv, Rudels et al. (2008); Schauer et al. (2008); Curry et al. (2011) and -120 $\pm$ 30 mSv, Kwok et al. (2004); de Steur et al. (2009)). It is unclear how freshwater export will vary between these two gateways due to changes in the Arctic. Mechanisms driving Davis Strait transports are a complex and poorly understood combination of local Arctic and subarctic interactions. Continued measurements are needed in Davis Strait to isolate interannual variability from long term trends and to attribute observed changes to driving mechanisms in the Arctic and North Atlantic Oceans.

3.8 Data Distribution

Daily and monthly OA2 results are available for download at `iop.apl.washington.edu/data.html`, with the timeseries also available though ACADIS, the repository for US Arctic Observing Network data. Please contact the author if these data are useful to you or used in publications so that we can inform you of changes to the data, document the usefulness of this program and justify the need to continue monitoring Davis Strait variability.

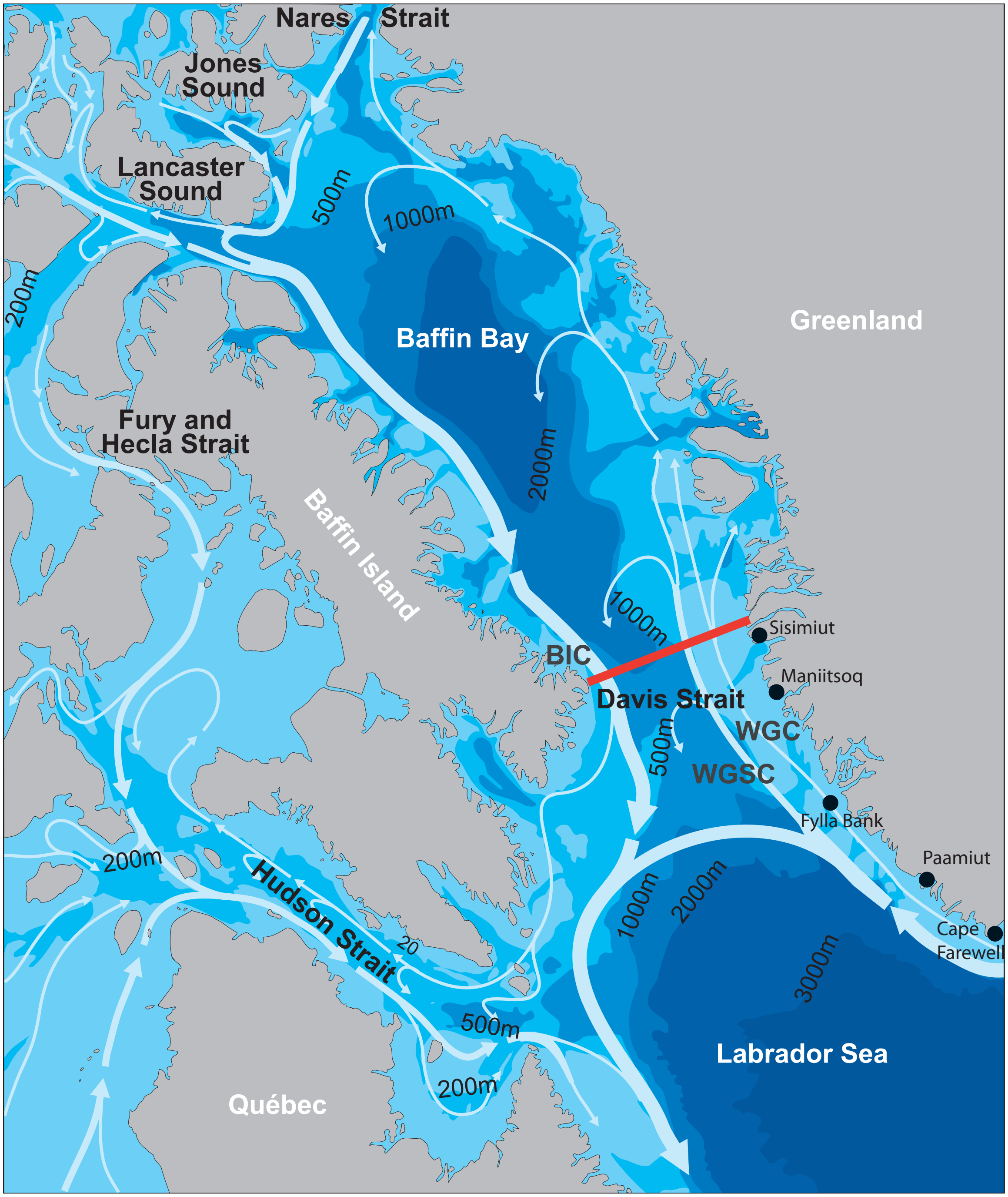

Figure 3.1: General circulation in Baffin Bay and Davis Strait (white arrows) and the location (red line) of the 2004-10 moored array. Arctic water by way of the Canadian Arctic Archipelago leaves Davis Strait as the broad, surface-intensified Baffin Island Current (BIC). Northward flow on the eastern side of Davis Strait consists of the fresh West Greenland Current (WGC) of Arctic origin on the shelf and warm, salty West Greenland Slope Current (WGSC) of North Atlantic origin on the slope.

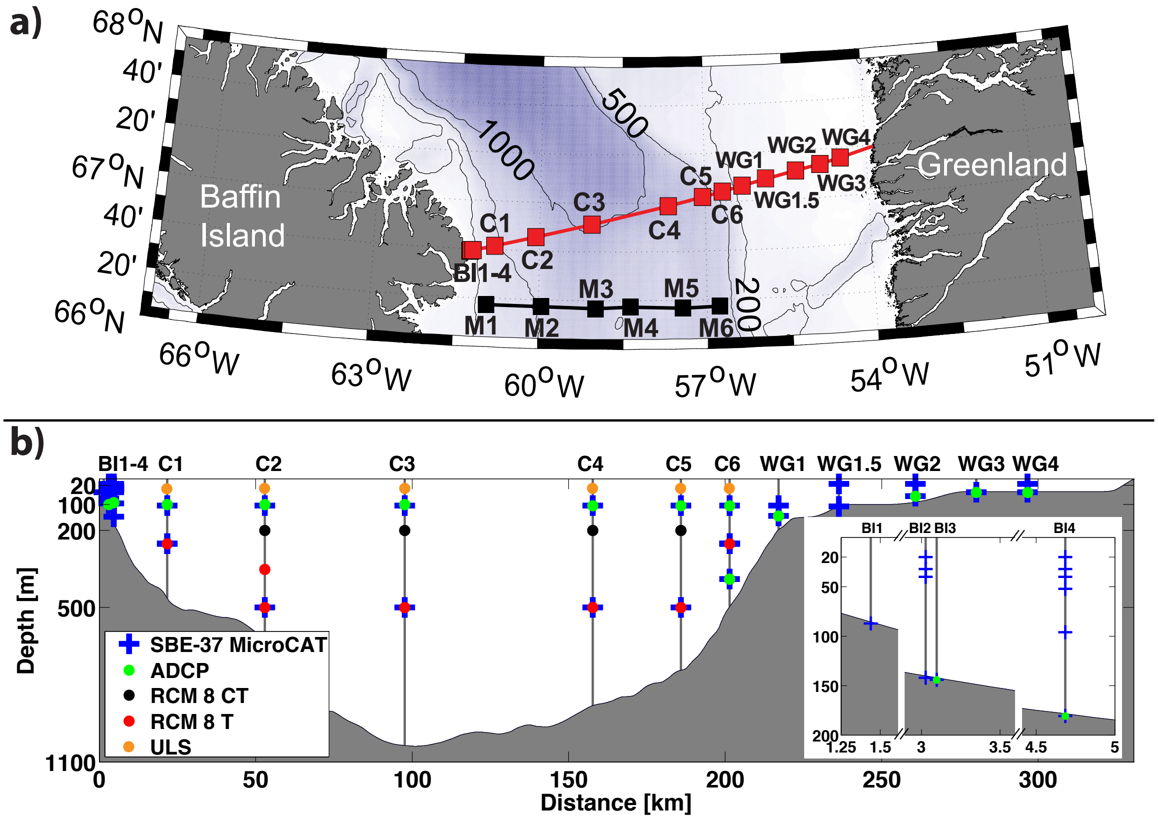

Figure 3.2: (a) Davis Strait 2004-10 (red line) and 1987-90 (black line) moored arrays with squares indicating mooring locations. (b) Summary of Davis Strait 2004-10 moored array instrumentation. Blue crosses indicate SBE37 MicroCAT conductivity, temperature and pressure recorders; green dots represent RDI ADCPs; black dots denote Aanderaa RCM8 velocity, conductivity, and temperature recorders; red dots denote Aanderaa RCM8 velocity and temperature recorders; and orange dots denote ULSs. Inset image shows a close-up of the Baffin Island shelf instruments. Spatial coverage varies from year to year throughout the program.

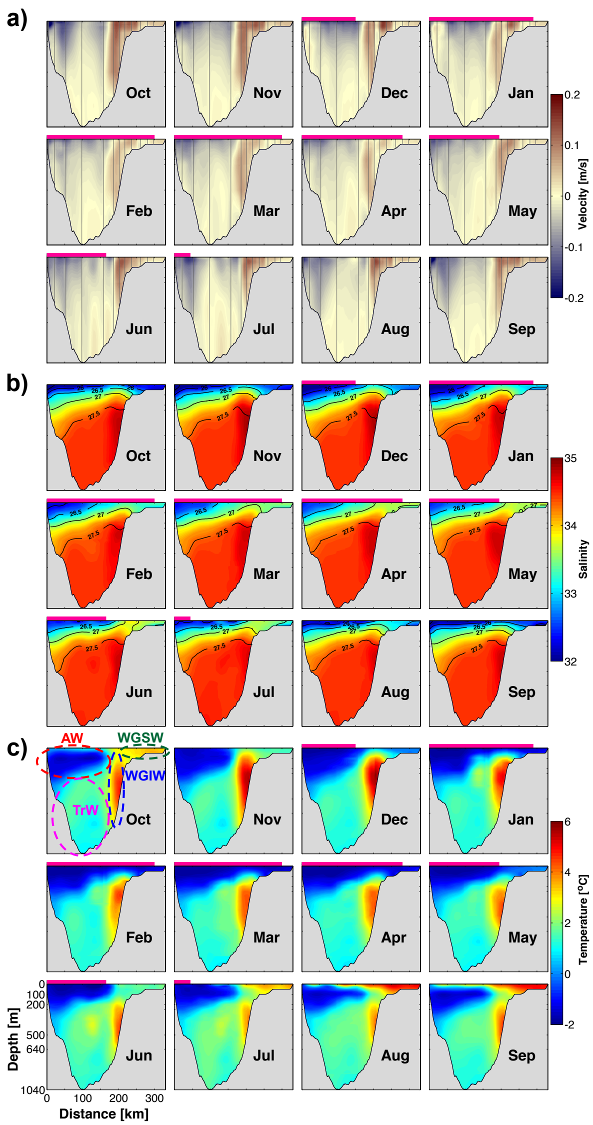

Figure 3.3: Objectively analyzed monthly averages from daily estimates of (a) along-strait velocity, (b) salinity and (c) temperature. Pink bars indicate areas along the moored array that are covered, on average, by sea ice 60% of the month. Gray lines indicate mooring locations in panel (a). Potential density lines (black lines) are noted in panel (b). The boundaries of the four dominant water masses (AW: Arctic Water, WGIW: West Greenland Irminger Water, WGSW: West Greenland Shelf Water, TrW: Transitional Water) are shown for October in panel (c).

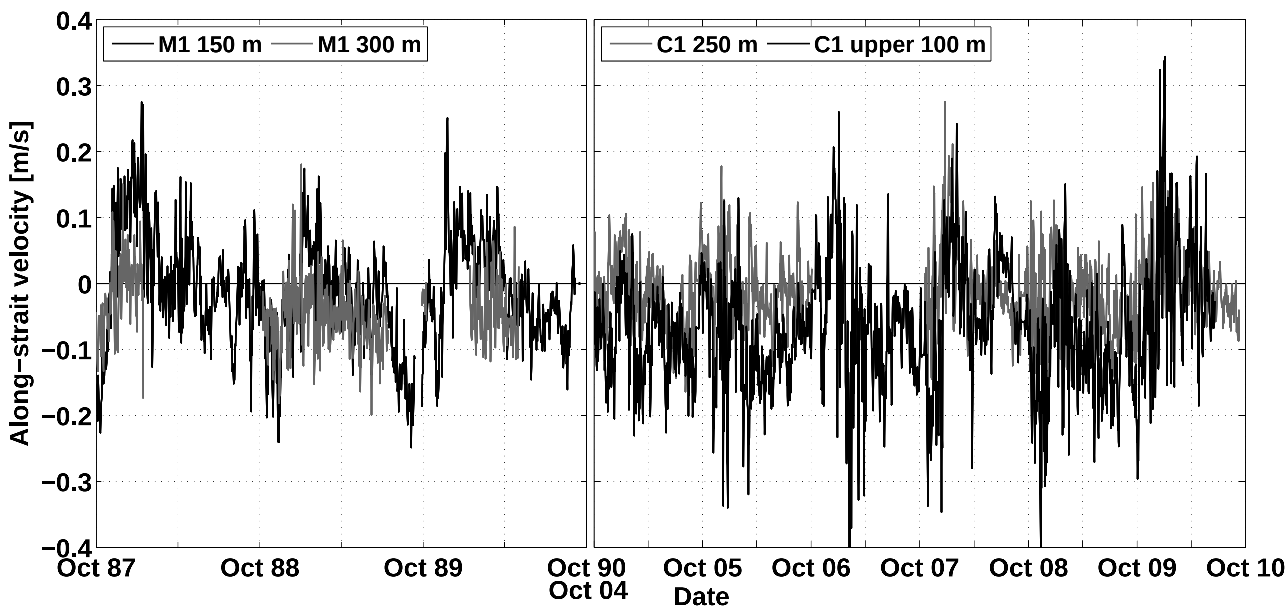

Figure 3.4: Daily along-strait velocities on the Baffin Island slope from October 1987-October 1990 (left panel) at mooring M1 150 m (black) and 300 m (gray) and from October 2004-October 2010 (right panel) at mooring C1 upper 100 m average (gray) and 250 m (black).

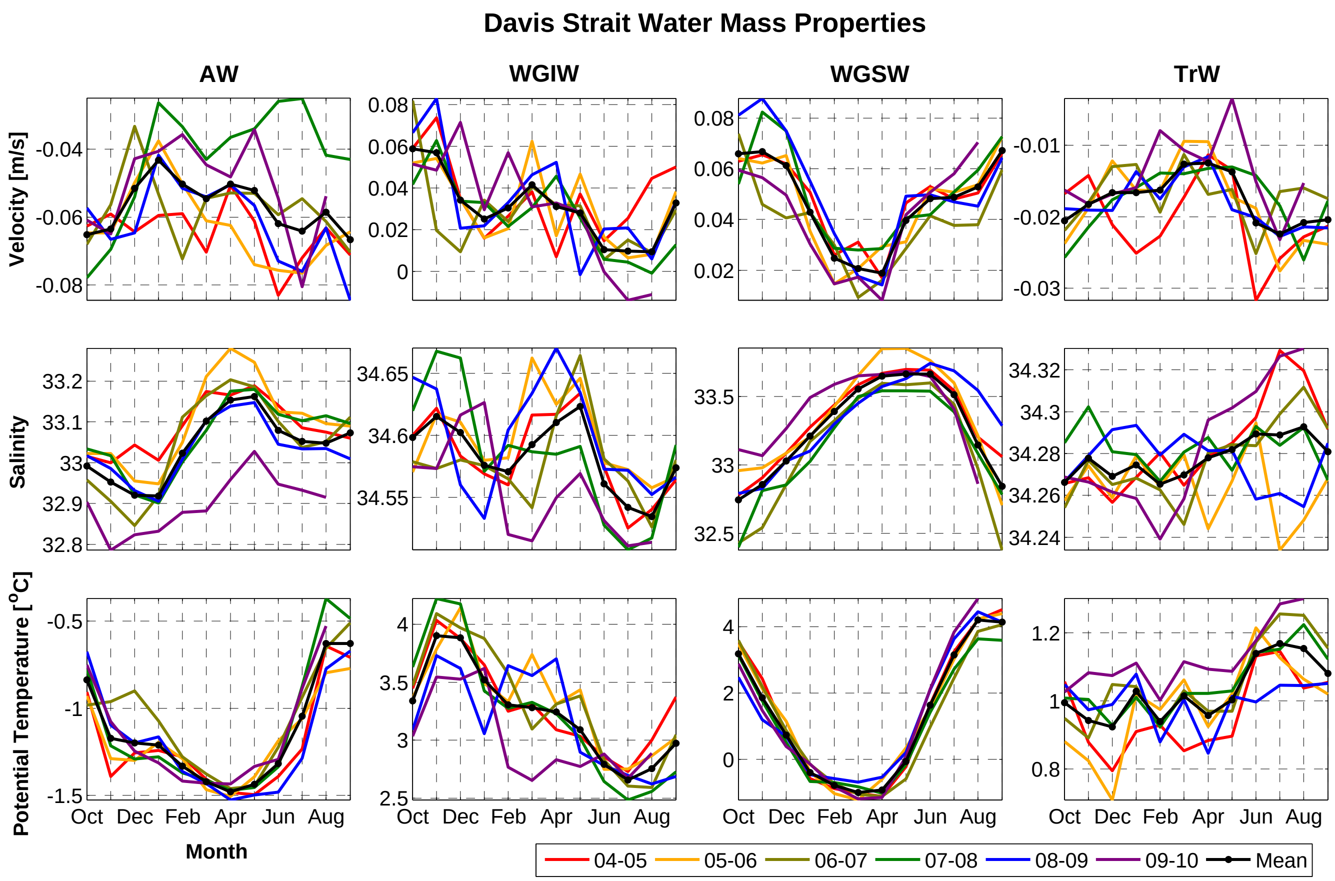

Figure 3.5: Objectively analyzed monthly averages for each year from daily water mass along-strait velocity (negative = southward), salinity and potential temperature estimates with the 2004-10 averages (seasonal cycles) noted by the black lines. Boundaries for the water masses (AW: Arctic Water, WGIW: West Greenland Irminger Water, WGSW: West Greenland Shelf Water, TrW: Transitional Water).

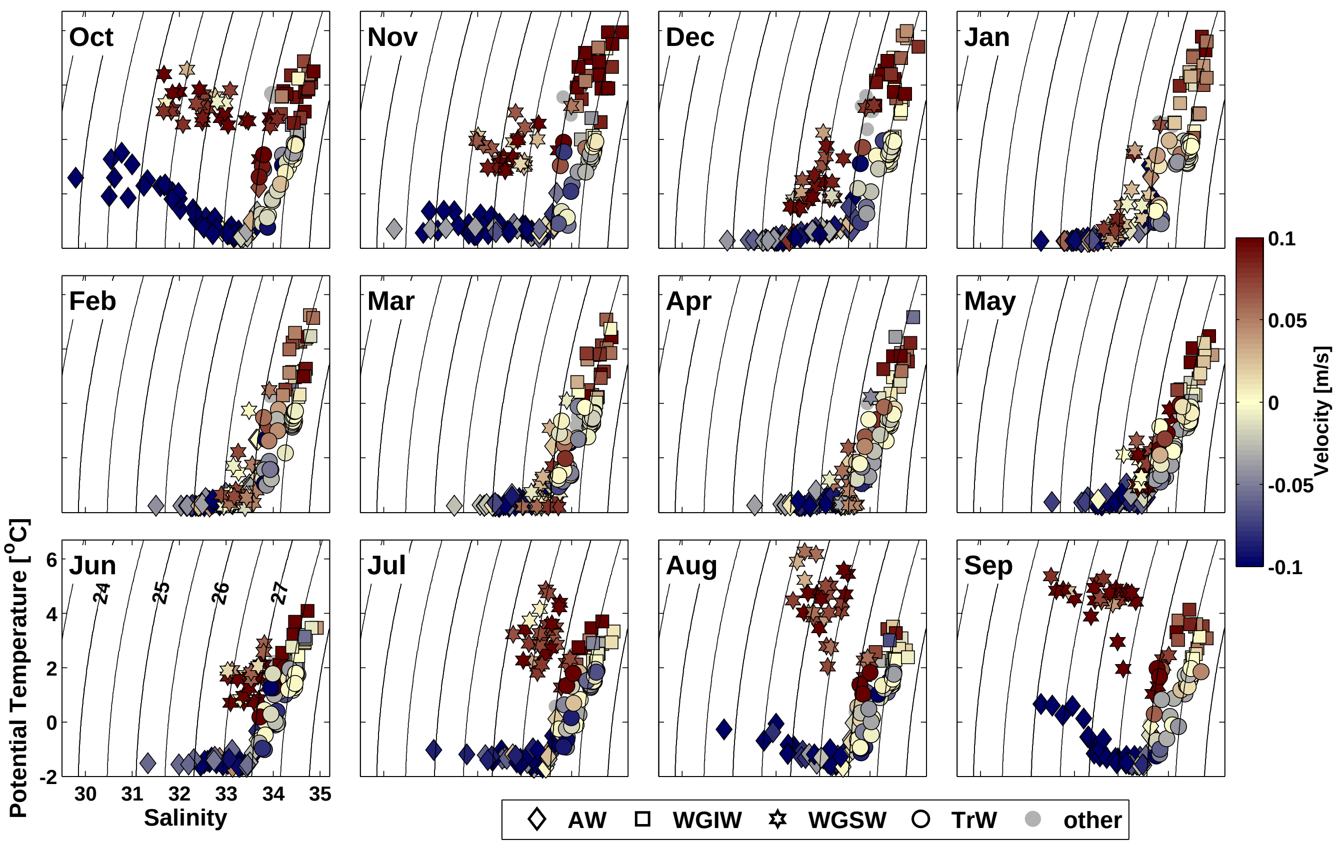

Figure 3.6: Monthly average potential temperature-salinity diagrams noting along-strait velocity and delineated into water mass classes. Boundaries for the water masses (AW: Arctic Water (diamonds), WGIW: West Greenland Irminger Water (squares), WGSW: West Greenland Shelf Water (stars), TrW: Transitional Water (circles)) are defined in Section 4.1. Gray dots indicate unclassified water.

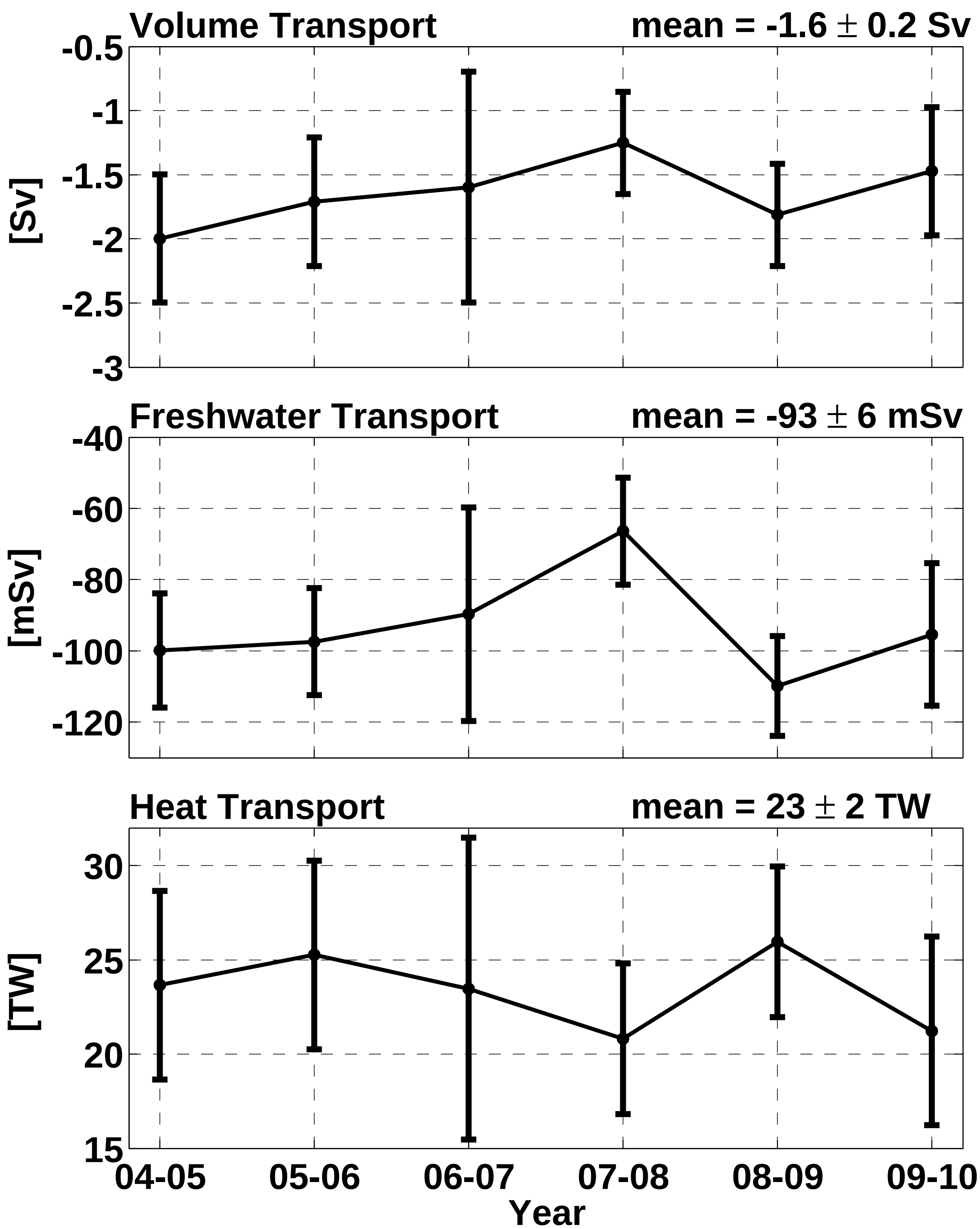

Figure 3.7: Objectively analyzed yearly (October-September) volume, freshwater and heat transports from 2004-2010 (negative = southward transport) including uncertainties. Annual average transports and uncertainties are noted in the top right of each panel. Freshwater transports are referenced to 34.8 and heat transports are referenced to 0°C. All transports are estimated from the surface to the sill depth, 640 m.

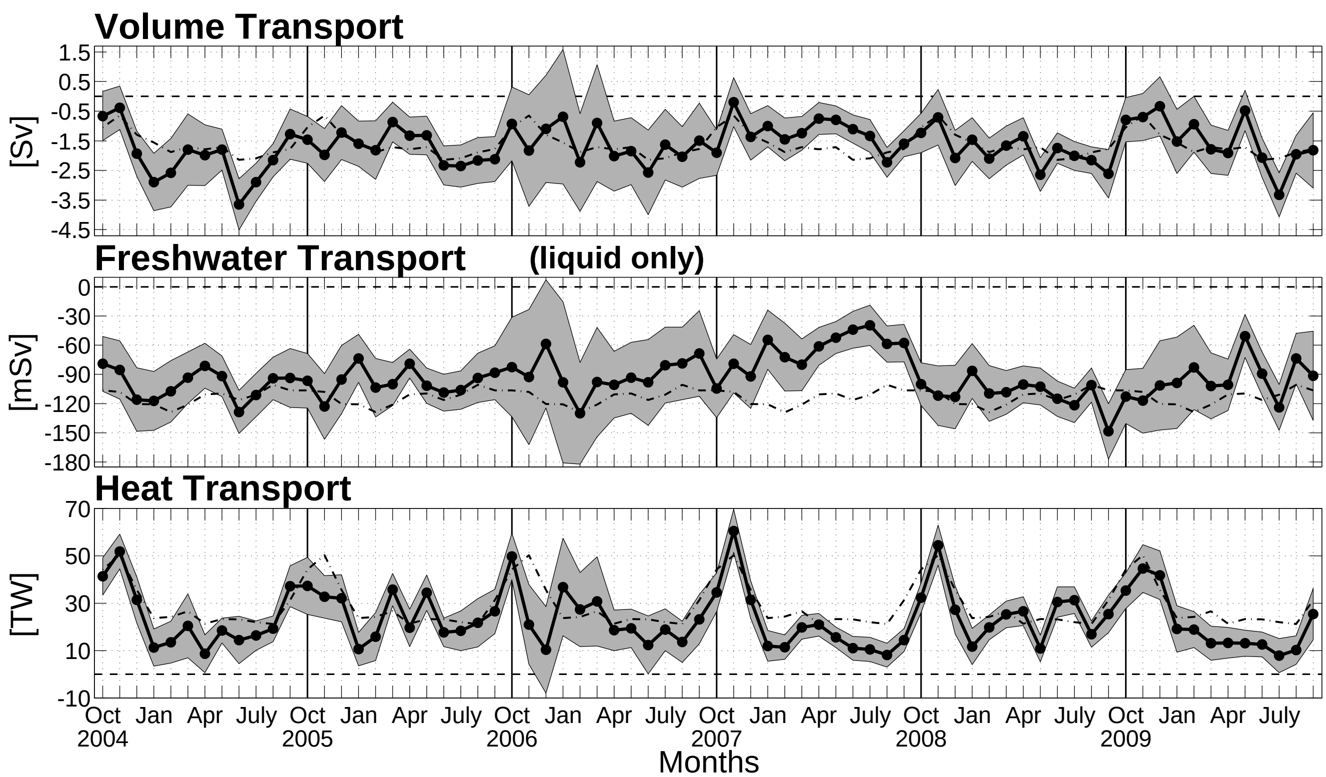

Figure 3.8: Objectively analyzed monthly volume, freshwater and heat transports between October 2004 and September 2010 (negative = southward transport). Shaded areas denote the monthly uncertainty. For comparison, the OA background transports are shown with a dashed line. September 2010 transports are replaced with average September values due to lack of September 2010 data. Freshwater transports are referenced to 34.8 and heat transports are referenced to 0°C. All transports are estimated from the surface to the sill depth, 640 m. Uncertainties are higher in 2006-07 due to the loss of the deepest central strait mooring, C3.

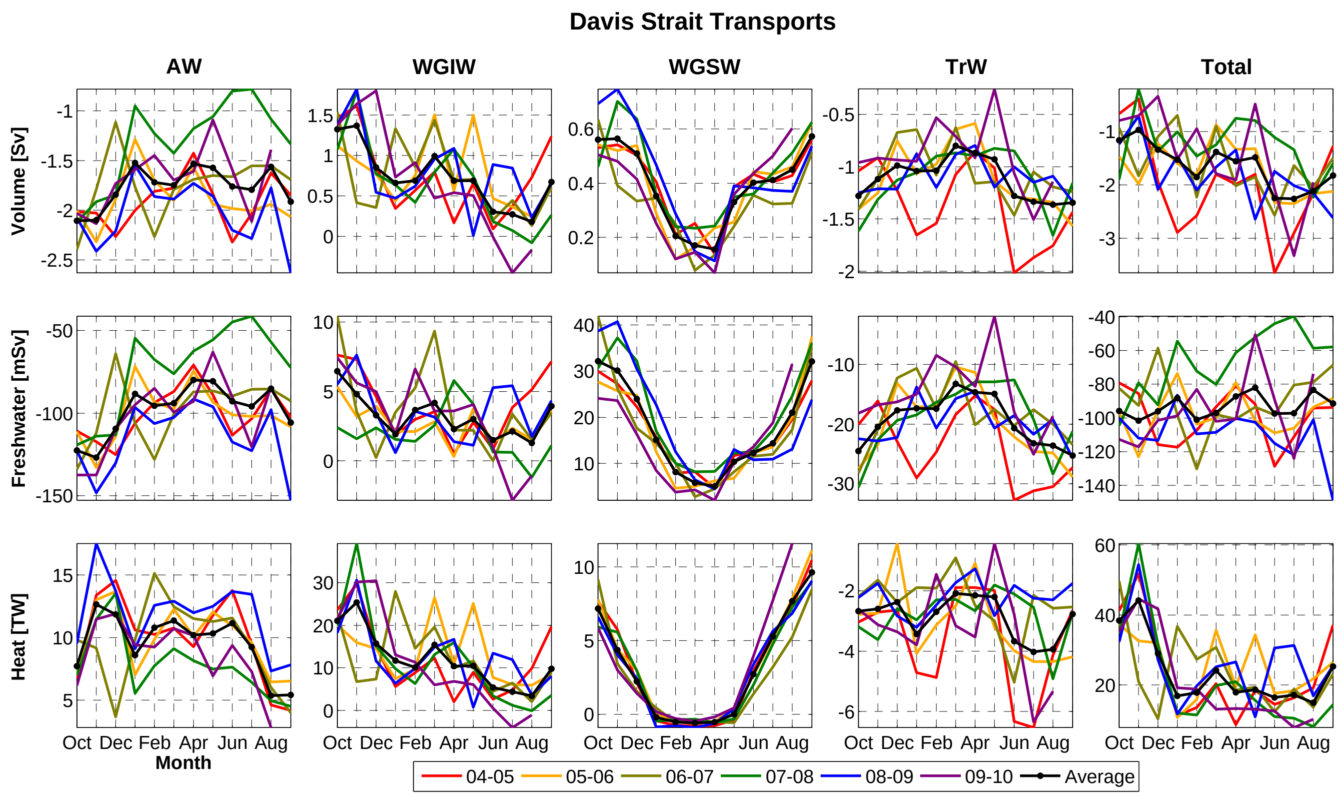

Figure 3.9: Objectively analyzed monthly average water mass volume, freshwater and heat transports for each year (negative = southward transport) with the 2004-10 averages (annual cycles) noted by the black lines. Shaded areas denote the monthly uncertainty. Boundaries for the water masses (AW: Arctic Water, WGIW: West Greenland Irminger Water, WGSW: West Greenland Shelf Water, TrW: Transitional Water). Freshwater transport is referenced to 34.8 and heat transport is referenced to 0°C. All transports are estimated from the surface to the sill depth, 640 m.

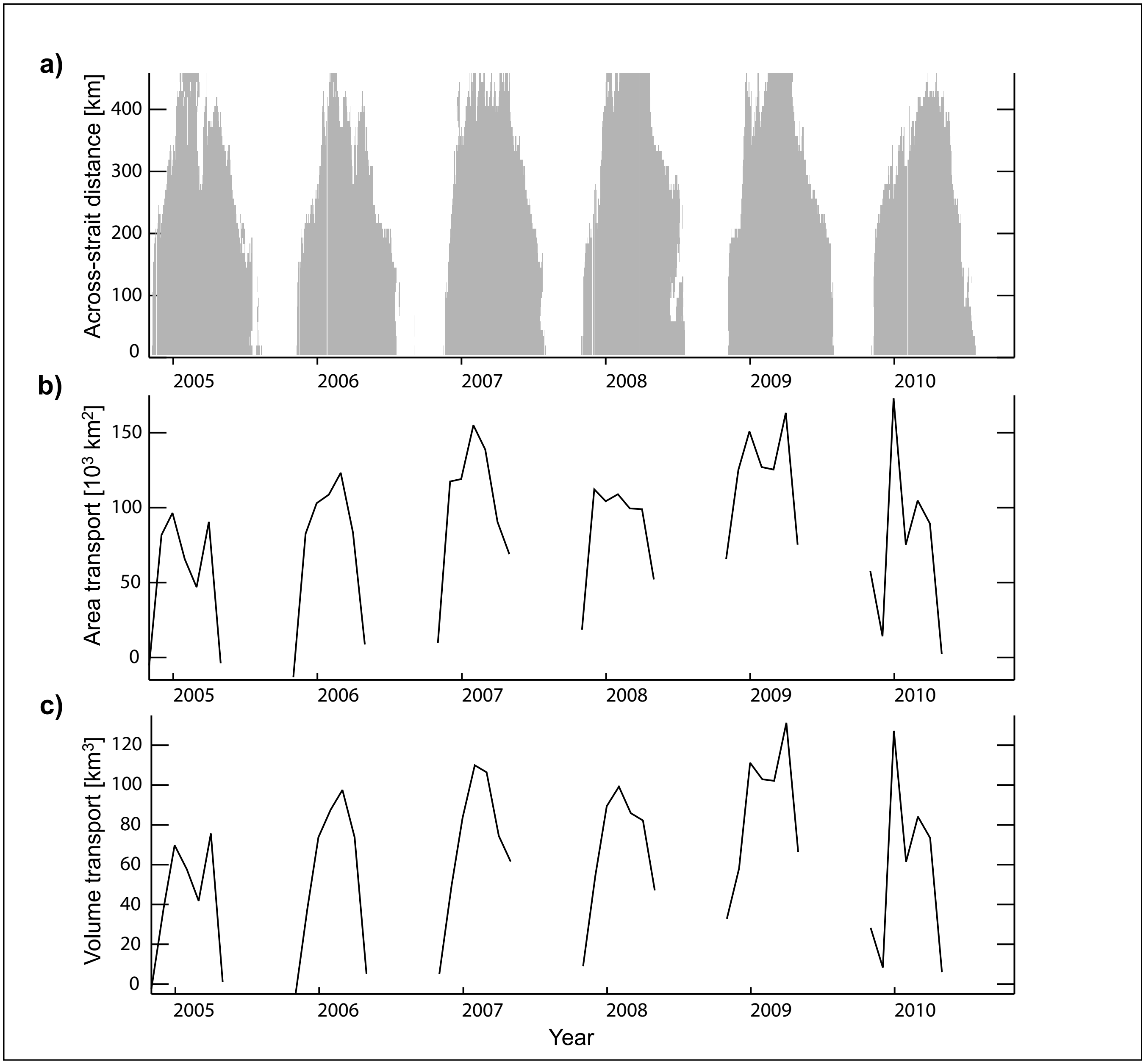

Figure 3.10: (a) Daily (November-May) across-strait sea ice coverage from satellite data (at least 15% coverage) for 2004-2010. Coverage is estimated north of the moored array at $\approx 68°$N and distances noted from Baffin Island. (b) Monthly average sea ice area transports between 2004-2010 using the ice coverage noted in (a). (c) Monthly average sea ice volume transports between 2004-2010 using moored array ULS data.

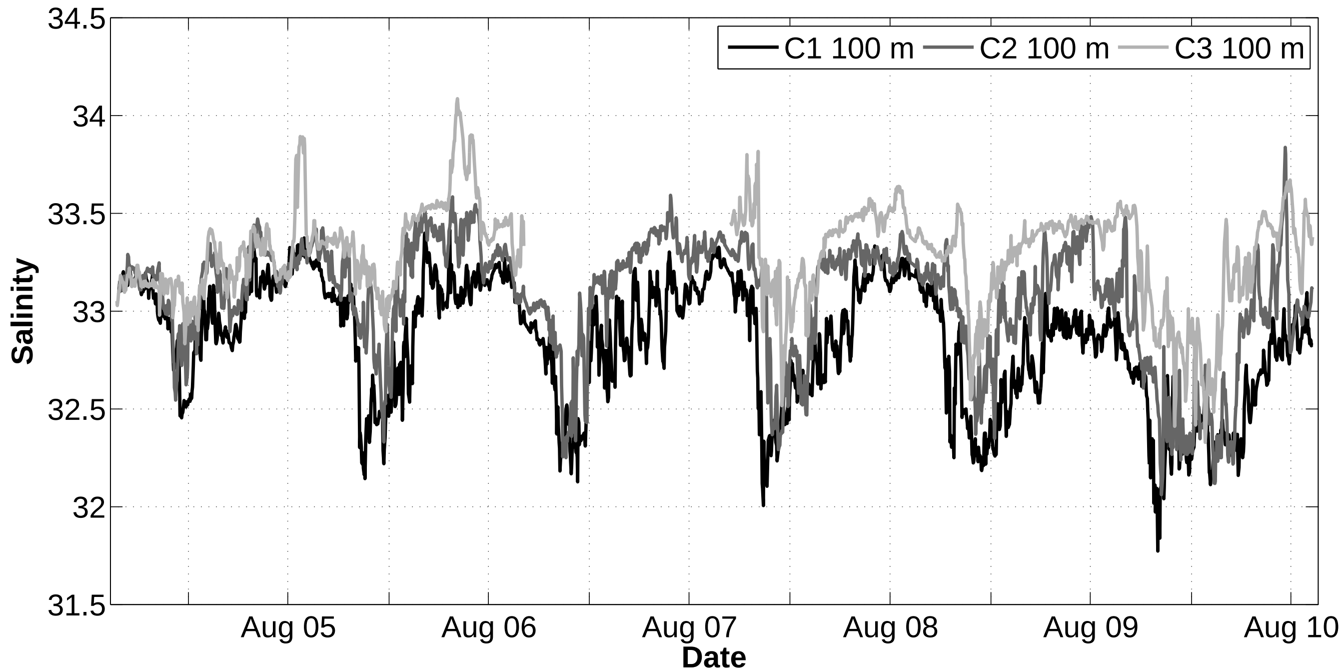

Figure 3.11: Daily Arctic Water salinity between 2004-10 at central strait C1-C3 100 m moorings.

Table 3.1: Davis Strait ULS thicknesses

Instrument	Low-Res.	High-Res.	Monthly Average Thickness (m)									
Year	(min)	(per day)	*Nov.*	*Dec.*	*Jan.*	*Feb.*	*Mar.*	*Apr.*	*May*	*Jun.*	*Jul.*	*Aug.*
C1												
2005 – 06	5	2		0.36	1.48	1.95	2.15	1.84	2.24	1.62	1.61	
2007 – 08	3	1	0.56	1.40	2.61	2.19	2.26	2.75	2.80	1.60		
C2												
2006 – 07	5	2		0.36	0.74	0.88	1.08	1.58	1.68	1.30	1.76	1.86
2007 – 08	3	1	0.54	0.92	1.84	2.18	2.00	2.14	2.44	2.90		
C3												
2007 – 08	3	1	0.44	0.40	0.71	1.02	1.02	0.86	0.76	0.69		
2008 – 09	5	2	0.47	0.53	0.77	0.88	1.14	0.89	1.15	1.07	1.29	
C4												
2006 – 07	5	2				0.66	0.76	0.83	0.84	0.90	0.77	
2007 – 08	5	1	1.35*	0.46	0.66	0.90	0.85	0.89	0.72	0.62		
C6												
2006 – 07	5	2		0.33	0.53	0.57	0.52	0.57	0.48	0.40	0.24	
			Average Monthly Average Thickness (m)									
C1			0.56	0.88	2.05	2.07	2.20	2.30	2.52	1.61	1.61	
C2			0.54	0.64	1.29	1.53	1.54	1.86	2.06	2.10	1.76	1.86
C3			0.46	0.47	0.74	0.95	1.08	0.87	0.96	0.88	1.29	
C4				0.46	0.66	0.78	0.80	0.86	0.78	0.76	0.77	
C6				0.33	0.53	0.57	0.52	0.57	0.48	0.40	0.24	

*Due to low ULS returns and inconsistent results, this value was omitted from the transport estimates.

Table 3.2: Davis Strait uncertainties and transports

	Volume (Sv)				Freshwater (mSv)				Heat (TW)			
Years	*OA*	*Bias*	*Bkgd*	**Total**	*OA*	*Bias*	*Bkgd*	**Total**	*OA*	*Bias*	*Bkgd*	**Total**
$2004-05$	0.2	0.5	0.1	-2.0 ± 0.5	12	10	2	-100 ± 16	3	4	1	24 ± 5
$2005-06$	0.2	0.4	0.1	-1.7 ± 0.5	10	10	3	-97 ± 15	3	4	1	25 ± 5
$2006-07*$	0.3	0.7	0.5	-1.6 ± 0.9	17	19	17	-90 ± 30	5	6	1	23 ± 8
$2007-08$	0.1	0.3	0.1	-1.3 ± 0.4	9	9	7	-66 ± 15	3	2	1	21 ± 4
$2008-09$	0.2	0.4	0.1	-1.8 ± 0.4	9	10	3	-110 ± 14	3	3	1	26 ± 4
$2009-10$	0.2	0.5	0.2	-1.5 ± 0.5	13	14	6	-95 ± 20	4	3	1	21 ± 5
$2004-10$	0.1	0.2	0.1	-1.6 ± 0.2	5	5	3	-93 ± 6	2	2	1	23 ± 2

*Uncertainty is higher because mooring C3 was not recovered.

Chapter 4

ATMOSPHERIC CONTROLS ON DAVIS STRAIT TRANSPORT

4.1 Introduction

The influence of oceanic and atmospheric changes in the Arctic on North Atlantic climate variability is unclear. Some model studies (Holland et al., 2001; Jahn et al., 2010) indicate the amount, method and form that freshwater is delivered to the North Atlantic can affect thermohaline circulation in the North Atlantic. Changes in the Arctic and North Atlantic climate due to variations in heat, freshwater and sea ice also initiate changes in ecosystems on all trophic levels (Greene et al., 2008; Post et al., 2009; Kovacs et al., 2010). Understanding how freshwater is exchanged through the primary pathways between the Arctic and North Atlantic is crucial for understanding how the ocean responds to climate variations.

Exchanges between the Arctic and North Atlantic Oceans occurs via pathways on both sides of Greenland. West of Greenland, exchanges are primarily one way, from the Arctic to the North Atlantic via the Canadian Arctic Archipelago (CAA), Baffin Bay and Davis Strait (Figure 4.1). Inflows into Baffin Bay include: CAA inflows, Baffin Island runoff, glacial meltwater runoff from West Greenland and contributions from East Greenland and the North Atlantic carried northward by the West Greenland shelf and slope currents. The mass loss of glaciers in Northwest Greenland increased from 30.9 $\pm$ 8 Gt yr^{-1} in 2002-06 to 128.2 $\pm$ 33 Gt yr^{-1} in 2007-09 (Chen et al., 2011). Similarly, mass loss from CAA glaciers increased sharply from 31 $\pm$ 8 Gt yr^{-1} in 2004-06 to 92 $\pm$ 12 Gt yr^{-1} in 2007-09 (Gardner et al., 2011). The runoff volume is much lower compared to the volume exported through the CAA but the runoff could significantly alter the density of upper water in Baffin Bay. Outflow through Davis Strait to the Labrador Sea includes contributions from the inflows into Baffin Bay as well as any modifications made while in residence in the bay such as: precipitation minus evaporation (P-E), air-sea exchanges and sea ice growth and melt. Changes in freshwater outflow through Davis Strait may modulate the strength of the Atlantic Meridional Overturning Circulation by impacting Labrador Sea deep convection, but differing views still exist on the strength of the impact (Goosse et al., 1997; Myers, 2005; Våge et al., 2009). Both observations (**?**) and model results (Jahn et al., 2010; **?**) have indicated that Davis Strait freshwater transport variability is controlled primarily by perturbations in volume transport. In order to improve circulation models, understand how water is modified within Baffin Bay, and resolve how freshwater transport impacts Labrador Sea convection, it is necessary to understand the controlling mechanisms driving Davis Strait transport variability.

Recent observations (2004-10) in Davis Strait from a full strait moored array and Seaglider surveys yielded the longest concurrent time series of volume, freshwater and heat transports through the strait, with annual transport averages of -1.6 $\pm$ 0.5 Sv, -93 $\pm$ 6 mSv and 23 $\pm$ 2 TW, respectively (1 Sv = 10^6 m^3 s^{-1}, negative sign indicates southward transport, **?**). Freshwater transports were estimated relative to a reference salinity of 34.8, considered the average Arctic Ocean salinity (Aagaard and Carmack, 1989), to maintain consistency with previous studies (Tang et al., 2004; Cuny et al., 2005). The observation system combines high temporal resolution from the moored array with the high spatial resolution of temperature and salinity from the Seagliders profiling the central strait from the surface to near bottom. Prior to the current observation program, year-round moored measurements were collected in Davis Strait between September 1987 - September 1990 (Ross, 1992; Tang et al., 2004; Cuny et al., 2005). The 1987-90 array (Figure 4.2a) consisted of five moorings per year deployed at six positions in the central strait, south of the 2004-10 array, but included neither measurements over the shelves nor measurements in the upper 150 m. Three studies (Tang et al., 2004; Cuny et al., 2005; **?**), based on the 1987-90 measurements, each adopted different approaches for extrapolating across the upper 150 m and either made highly uncertain estimates of shelf contributions or confined their analyses to the central strait. Differences in methods from these three studies produced average net volume transports of -2.6 $\pm$ 1.0 Sv including the West Greenland shelf and shear in the upper 150 m (Cuny et al., 2005), -2.6 $\pm$ 1.2 Sv excluding the West Greenland shelf and shear in the upper 150 m (Tang et al., 2004) and -3.5 $\pm$ 0.6 Sv excluding the West Greenland shelf and including shear in the full depth velocity profiles (**?**). Liquid freshwater transports from the three studies are: -142 $\pm$ 23 mSv (**?**), -99 $\pm$ 34 mSv (Tang et al., 2004) and -92 $\pm$ 34 mSv (Cuny et al., 2005).

Understanding how Arctic outflow, via the CAA, and glacial runoff is modified within Baffin Bay is important for understanding the variability in transports through Davis Strait. Baffin Bay is a semi-enclosed basin between Greenland and Canada (area $\approx$ 690,000 km^2) with a broad shelf on the Greenland side, narrow shelf on the Canadian side and bottom depths around 2300 m in the deep flat central region (Figure 4.1). Davis Strait lies at the southern boundary of Baffin Bay. Along the moored array Davis Strait is 330 km wide (Figure 4.2), with a 10 km wide western shelf (Baffin Island) and 100 km wide eastern shelf (Greenland). The central sill depth, 640 m, limits deep exchanges between Baffin Bay and the Labrador Sea. Circulation within Baffin Bay is cyclonic and topographically steered (Tang et al., 2004). The three main passages of the CAA enter Baffin Bay at the northern end: Lancaster Sound (sill, 125 m), Jones Sound (sill, 120 m) and Nares Strait (sill, 250 m) (Tang et al., 2004). Arctic Ocean waters, via the CAA, flow southward along Baffin Island and through Davis Strait as the broad, shallow Baffin Island Current (BIC) (Tang et al., 2004). Inflows from the south through Davis Strait, along the coast of Greenland, include the fresh West Greenland Current (WGC) of Arctic and Greenland origin on the shelf and the warm, salty West Greenland Slope Current (WGSC) of North Atlantic origin (Figure 4.3). The WGC is a combination of the southward flowing

East Greenland Current (EGC) from the Arctic via Fram Strait (de Steur et al., 2009) and the East Greenland Coastal Current (EGCC) arising from the addition of East Greenland coastal inflow and glacial runoff (Bacon et al., 2002; Sutherland and Pickart, 2008) that have traveled around the southern tip of Greenland and travel north through Davis Strait. The WGSC is a branch of the North Atlantic Current that enters and circulates cyclonically in the Irminger Sea and continues along the East Greenland slope seaward of the EGC around the southern tip of Greenland, turning north towards Baffin Bay (Cuny et al., 2002; Myers et al., 2007). The warm WGSC has been linked to subsurface glacial erosion off the coast of central West Greenland (Holland et al., 2008; Rignot et al., 2010). Mean winds through Baffin Bay are typically southward and strongest in autumn/winter but weaken and often reverse direction in the summer (National Ocean and Atmospheric Administration, `www.esrl.noaa.gov/psd/data/composites/day/`). The warm inflowing slope current and strong offshore winds from West Greenland keep the West Greenland slope and shelf ice-free most of the year.

The presence of sea ice in Baffin Bay and Davis Strait influences the water column by insulating the water surface from the wind and altering the density of the water column through sea ice formation, causing brine rejection, and sea ice melt, adding freshwater to the ocean. Sea ice generally begins to form in Baffin Bay in September, reaching maximum coverage in March and having ice free conditions in late summer (Tang et al., 2004). Sea ice growth generally begins in November in Davis Strait. Maximum ice cover typically occurs in March and extends across the full width of the strait even though the West Greenland shelf and slope is often ice free due to warmer water near the surface and the prevailing winds coming off Greenland (**?**).

The temperature and salinity of Baffin Bay inflows are likely modified by polynya related brine rejection and heat loss before leaving Baffin Bay through Davis Strait. In northern Baffin Bay, a series of polynyas exist between Greenland and the CAA passages (Steffen, 1985). A polynya is an area of low ice concentration or open water which is surrounded by ice in a region where ice would be expected and are either wind-driven (latent heat polynya), driven by heat from the atmosphere and/or ocean (sensible heat polynya) or both (Barber et al., 2001). Polynyas in Baffin Bay typically start to form between November and March and remain through ice break up with the spatial extent depending largely on the formation of an ice arch in Nares Strait (Barber et al., 2001; Kwok, 2005). Polynyas in Baffin Bay are created by the strong northerly winds associated with ageostrophic, orographically channeled flow down the atmospheric pressure gradient through Nares Strait (Samelson and Barbour, 2008). Formation of the ice arch prevents sea ice from entering northern Baffin Bay (Barber et al., 2001). Northerly winds blow ice southward but the ice arch prevents thick Arctic ice from filling in the exposed region and new ice, which is more easily forced by the wind, begins to form. Though the polynyas begin as latent heat polynyas, sensible heat is important, particularly late in the season, off the southern coast of West Greenland. Coastal upwelling due to the strong northernly winds and winds blowing off northwest Greenland elevate the thermocline and bring warm WGSC water to the surface (Steffen, 1985; Barber et al., 2001).

Observational studies have focused on quantifying CAA transports and understanding the dominant forces driving transport variability (Münchow and Melling, 2008; Peterson et al., 2012). Peterson et al. (2012) show that monthly alongshore wind anomalies in the Beaufort Sea account for 43% of the variance of the Barrow Strait (Lancaster Sound) transport anomalies ($p < 0.01$) at monthly to interannual time scales and is consistent with sea surface height (SSH) gradients through the strait. They also note that freshwater transport is driven by variations in volume transport. Münchow and Melling (2008) show that both along and across strait sea level pressure (SLP) gradients contribute to the net southward flow through Nares Strait. They find that the along-channel pressure gradient explains 70% of the velocity variance at a 33-day period and the cross-channel pressure gradient explains 70% of the velocity variance at a periods between 3-14 days. This is consistent with findings from Samelson and Barbour (2008) showing a connection between northerly winds and SLP gradients with sea ice export through Nares Strait.

Model results from Jahn et al. (2010); Houssais and Herbaut (2011); McGeehan and Maslowski (2012) generally agree with the observations and suggest that SSH and SLP variations through the CAA passages in addition to large-scale climate variations drive CAA transport variability. High resolution (≈ 9 km) model results from McGeehan and Maslowski (2012) suggest that inflows through eastern Davis Strait could regulate CAA and Davis Strait outflow by altering SSH in Baffin Bay and thus the SSH gradients between the ends of the CAA passages and between Baffin Bay and the Labrador Sea. They find that Baffin Bay volume anomalies proceed both Lancaster Sound and Nares Strait volume transport anomalies by one month, having correlations of -0.73 for each, and suggest that volume decreases in Baffin Bay drives CAA transport. The decrease in Baffin Bay volume and SSH, typically occurring between February and April, also coincides with a decrease in northward WGC and WGSC transport into Baffin Bay further suggesting that northward transport into Baffin Bay drives Baffin Bay SSH variability. Although variations in SSH are important for understanding transport variability though Davis Strait, this work only investigates forcings from the atmosphere. Analysis of SSH variability will be incorporated into this analysis in a future publication utilizing modeled SSH due to a lack of good satellite altimetry data and sparse tide gauges.

The goal of this work is to identify atmospheric forcing mechanisms controlling Davis Strait transport. This paper uses objectively analyzed (OA) monthly volume transport estimates from Davis Strait, presented in **?**, between 1987-90 and 2004-10 to investigate linear relationships between Davis Strait transport, Baffin Bay inflows, regional winds and SLP at monthly and longer time scales. Transport variability will also be compared to the large-scale Arctic Oscillation (AO) and the North Atlantic Oscillation (NAO) climate indices. This work is important for evaluating whether numerical models exhibit the same behavior as the observed Davis Strait transports.

Section 4.2 and Section 4.3 introduces the data and methods used in this analysis. The results are presented and discussed in Section 4.4.

4.2 Data

4.2.1 2004-10 Observing System

The Davis Strait observing system has been operational since 2004 and consists of eight or nine shelf and six central strait year-round moorings (Figure 4.2); continuous, year-round Seaglider-based sections in the central strait, roughly between the 500-m isobaths; and annual autumn hydrographic sections with chemical sampling. RDI Acoustic Doppler Current Profilers (ADCP), Aanderraa Recording Current Meters (RCM8) and SeaBird SBE37 MicroCATs measure velocity, temperature and conductivity at 30 minute (ADCP and MicroCAT) and hourly (RCM8) intervals. On the shelves, iceberg-resistant packages (IceCAT), consisting of floats and SBE37 MicroCATs inductively coupled via a weak link to bottom-mounted data loggers, measured conductivity and temperature in the upper 20-50 m at 5-minute intervals. The array was positioned north of the sill (depth, 640 m), at a maximum depth of 1040 m, in an attempt to avoid bathymetrically-induced flow complications and allow for concurrent Seaglider surveys. Seaglider surveys are conducted in both ice covered and ice free conditions, with at least two complete central strait surveys for each calendar month. Monthly along-strait velocity data and monthly volume transports estimated by optimal interpolation between October 2004 - August 2010 and September 1987 - September 1990 are used in this analysis (**?**). Details regarding the data processing and estimation of the volume transports are described in (**?**).

4.2.2 1987-90 Moored Array

A previous year-round moored array was deployed across Davis Strait between September 1987 and August 1990 (Ross, 1992; Tang et al., 2004; Cuny et al., 2005). The array was located south of the current array line (maximum depth, 689 m), and consisted of six central strait moorings (Figure 4.2). Unlike the current array, there were no moorings on the shelves. Each mooring measured velocity, temperature, and conductivity hourly at 150, 300, and 500 m using Aanderaa RCM5s. Monthly velocity data and monthly volume transports estimated by optimal interpolation in a similar manner to the 2004-10 volume transports are used in this analysis. Details regarding the data processing and estimation of volume transports are discussed in detail in (?). Details about the 1987-90 moored array and estimates of transports are described in Cuny et al. (2005).

4.2.3 Atmospheric Model Parameters

National Oceanic and Atmospheric Administration (NOAA) National Centers for Environmental Predictions (NCEP) North American Regional Reanalysis (NARR) outputs meteorological data every three hours, since 1979, on a Northern Hemisphere Lambert Conformal conic grid with $\approx 0.3°$ resolution (32 km) at the lowest latitude. NARR is an extension of the NCEP Global Reanalysis run over the North American Region. NCEP NARR data provided by the NOAA/OAR/ESRL PSD, Boulder, Colorado, USA, from their Web site at `www.esrl.noaa.gov/psd/`. Monthly 10 m winds (meridional and zonal) and mean sea level pressures are used for this analysis.

4.2.4 Atmospheric Indices

The NOAA Climate Prediction Center (CPC) computes monthly Arctic Oscillation (AO) and North Atlantic Oscillation (NAO) indices since 1950 (`www.cgd.ucar.edu/cas/jhurrell/indices.html`). The AO indices are constructed by projecting the monthly 1000 mb height anomalies over the Northern Hemisphere poleward of 20°N onto the loading pattern. The loading pattern of AO is defined as the first Empirical Orthogonal Function (EOF) of monthly mean height anomalies at 1000 mb during 1979-2000. The NAO pattern and indices are identified by applying the Rotated

Principal Component Analysis (RPCA) technique to the monthly mean standardized 500 mb height anomalies over the Atlantic Ocean region 20°N - 90°N between 1950 and 2000. The anomalies are standardized by the 1950-2000 base period monthly means and standard deviations. Monthly and winter time (January-March) AO and NAO indices are used in this analysis.

4.3 Methods

Lagged correlation analysis is used to investigate the linear relationships between Davis Strait volume transports and regional winds and SLP. Monthly NARR gridded SLP and wind fields are correlated with monthly objectively analyzed Davis Strait transports. Davis Strait monthly transports between September 1987-September 1990 and between October 2004-August 2010 are used in this analysis. There is significant interannual variability and no clear annual cycle observed in the net transports and for most water masses (**?**) so correlations are performed by removing only the time average from both the transports and atmospheric variables before computing the correlations unless noted otherwise. Pearson's linear correlation coefficients (r) and P-values (p), using a Student's t-distribution, are used to determine if the correlations are significant at the 95% confidence level. P-values were estimated two different ways based on the method for determining the number of degrees of freedom (dof), the lowest dof was used to determine significance. The number of dof is either two less than the number of months used to calculate the correlation (N-2) or the integral time scale using the autocovariance. Typical values for the integral time scale range between 42 and 63 as compared to N-2 (69) for the period between October 2004 and August 2010. The integral time scale was greater than N-2 only for a couple cases. Correlations are computed between all grid points of SLP/winds and Davis Strait transport but the results are presented and discussed in terms of regional averages. The regions discussed in this analysis are shown in Figure 4.4.

4.4 Results and Discussion

4.4.1 Baffin Bay seasonal SLP and wind variability

Seasonal SLP and wind variability in Baffin Bay is driven primarily by seasonal variations in the Arctic and subpolar North Atlantic due to unequal heating over the Earth and the Earth's rotation. Pressure gradients between the Arctic and North Atlantic drive the winds in Baffin Bay. As winter approaches, the Arctic cools, becomes ice covered and SLP increases. At the same time, the semi-permanent low SLP over the subpolar North Atlantic, near Iceland, is typically lower due to wintertime cyclones moving across the region. This causes a large pressure gradient between the Arctic and the North Atlantic (Figures 4.5). In the summer, when temperatures are warmer and sea ice is at a minimum, SLP differences between the Arctic and subpolar North Atlantic are reduced. Greenland, ice-covered with high topography, acts as a barrier between the Arctic and North Atlantic and distorts the atmospheric flow (**?**). Since the surface of Greenland is ice-covered and far from the surface of the ocean, SLP is typically higher over Greenland compared to the surrounding open water. Atmospheric distortion, from winds flowing around and over Greenland, strengthen the low pressure region in eastern Baffin Bay by bringing cold air from the surface of Greenland down along the coast of Greenland (Barber et al., 2001; Samelson and Barbour, 2008).

In the autumn and winter, when SLP is lower over the North Atlantic, low pressure extends up along the eastern side of Baffin Bay but does not extend across western Baffin Bay due to the presence of sea ice and colder water and air temperatures. The variation in SLP in Baffin Bay creates a SLP trough with a maximum gradient between western Baffin Bay and off the southern coast of West Greenland, south of the current array (between the regions labeled BBw and WGS in Figure 4.4). The trough typically starts to deepen in October and through the winter, then rapidly weakens April-May and remains weak throughout the summer (Barber et al., 2001; Kwok, 2007). The trough is observed in seasonal SLP and wind variability in Baffin Bay between 2004-10 (Figure 4.5) and between 1987-90 (Figure 4.6). Between October and March, strong winds occur over Baffin Bay, Greenland and the Labrador and Irminger Seas with the strongest winds occurring over Greenland. During this time there is an increase in positive wind stress curl along the coast of Greenland and in the Irminger Sea. Positive wind stress curl suggests that upwelling along the Greenland coast is likely (Steffen, 1985; Barber et al., 2001). SLP in this region is lower throughout all seasons between 1987-90 as compared to 2004-10 but winds are stronger in the recent period.

Seasonal variations in SLP and winds shown in Figures 4.5 and 4.6 suggest that cyclonic circulation and thus transport through Davis Strait increases as the trough in Baffin Bay deepens and the pressure gradient between western Baffin Bay and off the southern coast of West Greenland increases. Northward and southward transports through Davis Strait typically increase between September and January (Figure 4.7), consistent with the strength of the trough. However, correlations between Davis Strait transport and the SLP gradient are insignificant. If transport is separated into northward and southward components only the northward component is significantly correlated with the SLP gradient, but weakly ($r = 0.24$, $p = 0.04$). Since Davis Strait is composed of three distinct currents (BIC, WGC and WGSC, Figure 4.1) which arrive via three different pathways, it is likely that each pathway would be driven by different forcings.

4.4.2 Davis Strait water masses

Transport through Davis Strait is two-way and composed of four primary water masses. The water masses originate from different sources and/or are modified differently so correlations are made between water mass transports and the atmospheric variables in addition to the net transports (total, northward and southward).Each water mass is spatially delineated in the yearly averaged OA velocity, temperature and salinity fields shown in Figure 4.3. Net transport through Davis Strait is the summation of transport from the four water masses and unclassified waters. Water undefined by the water mass classes are omitted from from this analysis and represent 0.1 Sv of the net average in both the 2004-10 and 1987-90 transports. Water masses are identified following Tang et al. (2004):

* Arctic Water (AW, $\theta \leq 2$°C; S ≤ 33.7) is cold, fresh water in the western strait, part of the southward flowing BIC, at depths < 300 m. Though of Arctic origin, this water has been modified by glacial runoff, air-sea fluxes, local sea ice melt in Baffin Bay and in the CAA.

* West Greenland Shelf Water (WGSW, $\theta < 7$°C; S < 34.1) is of Arctic origin, with contributions from Greenland glacial runoff. The WGSW travels from east Greenland, turns northward at Cape Farewell and flows through Davis Strait as the WGC along the West Greenland shelf.

* West Greenland Irminger Water (WGIW, $\theta > 2$°C; S > 34.1) is warm, saline water that originates in the North Atlantic and flows cyclonically around the Irminger Sea. It then rounds the southern tip of Greenland and travels northward along the West Greenland slope as part of the WGSC, passing through Davis Strait as a mostly barotropic current.

* Transitional Water (TrW, $\theta \leq 2$°C; S > 33.7), usually found at depths > 300 m. The TrW is the product of water masses that flow into Baffin Bay, mix and undergo local modifications, and flow south through Davis Strait at depth.

Typically correlations are higher and more significant when water mass transports are used instead of the net transports. Though the correlations between net northward inflows and southward outflows are weak and/or insignificant, net southward outflow correlates significantly with WGSW transport when southward transport is lagged one month (r = -0.44, p = 0.002). In comparison, the other inflow, WGIW, has the strongest correlation with southward transport when southward transport is lagged five months (r = 0.28, p = 0.02). Correlations between water mass transports and atmospheric variables are discussed below in relation to each water mass and the most important ones are summarized in Table **??**.

4.4.3 Arctic Water

Arctic Water transport is southward for all months with an average annual transport of -1.8 Sv. There is a weak annual cycle but maximum southward transport occurs between September and December, when the SLP gradient between western Baffin Bay (high pressure) and off the southern coast of West Greenland (low pressure), south of the current array (between the regions labeled BBw and WGS in Figure 4.4) is present in Baffin Bay. Though the timing of maximum AW transport and presence of the SLP gradient in Baffin Bay coincide, the strongest correlation between the 2004-10 AW transport and atmospheric variables is with the predominately northerly winds in western Baffin Bay (r = 0.24, p = 0.07, Figure 4.8 and Figure 4.9). The meridional component of the wind (v) is averaged over the region labeled BBw in Figure 4.4 before computing the correlation. Since the Ekman depth is typically less than the mixed layer depth, it is not surprising that the correlation improves when transport is averaged over the upper 100 m (r = 0.42, p = 4E-4). Correlations with the 1987-90 data set are much lower and not significant, likely caused by the sparse measurements in the near surface water. The 2004-10 array had ADCP velocity measurements every 4 m in the upper 100 m as compared to the point measurements at 150 m in the 1987-90 array.

Northerly winds in Baffin Bay are driven partly by the SLP gradient in Baffin Bay, in particular, the west to east component of the SLP gradient across Baffin Bay. The SLP gradient is estimated between regions, BBw and BBe, in Figure 4.4. Zonal winds driven by the pressure gradient are deflected to the south due to the Coriolis force caused by the Earth's rotation. The v component of the winds is significantly correlated with the SLP gradient across Baffin Bay (r = -0.55, p = 6E-6, Figure 4.9). However, the winds in western Baffin Bay also have a strong west to east (u) component and correlate more strongly with the SLP gradient (r = 0.88, p = 3E-16). Correlation with v winds is weaker than the u winds because there are typically northerly winds in Baffin Bay due to large-scale variability not associated with the local SLP gradient. If the winds obey geostrophy, the horizontal pressure gradient force (PGF) should be equal to the Coriolis force (COR) and the ratio of PGF/COR should be close to 1. The PGF and COR forces are defined as:

$$PGF = \frac{1}{\rho_{air}} \frac{\partial p}{\partial x},$$

$$COR = vf,$$

where ρ_{air} is the air density (1.29 kg m^{-3}), $\frac{\partial p}{\partial x}$ the horizontal SLP gradient across Baffin Bay, v the north/south component of the wind and f the Coriolis parameter estimated using 73°N as the latitude. If the gradient distance (∂x) used for the SLP gradient is taken as the distance between the center of the two regions (301 km), the PGF/COR is -2. If the distance is taken as the width of Baffin Bay (584 km) the ratio is -1.03. The COR is smaller than the PGF partly because the gradient acts over a small area but frictional forces are likely significant. The balance is probably between the PGF, COR and frictional forces.

Inflows into Baffin Bay either exit Davis Strait as AW or TrW. Of the two water masses that travel north across Davis Strait into Baffin Bay, WGIW and WGSW, the surface, low density, WGSW would be the only one most likely to remain classified as AW when exiting Davis Strait. Transport variability between AW and WGSW are significantly correlated (r = -0.35, p = 0.01) with no lag and likely reflects the fact that both water masses are partly controlled by similar forcing mechanisms affecting the shelves around Baffin Bay.

Though the wind is important, AW is controlled primarily by the CAA inflows and could account for up to 82% of the total AW outflow. Lancaster Sound transports an average of 0.46 ± 0.09 Sv between 1998-2011 (Peterson et al., 2012) and represents 25% of the average total AW transport. Average transport through Jones Sound, estimated from moorings deployed between 1998-2002 (Melling et al., 2008), is 0.3 Sv and is less than half the average transport estimate though Nares Strait, 0.72 ± 0.11 Sv, estimated from moorings in place between 2003-06 (Münchow and Melling, 2008). Combined, Nares Strait and Jones Sound represents 57% of the average total AW transport. Even though Nares Strait and Jones Sound transport could represent 57% of AW transport, brine rejection from sea ice growth in Baffin Bay, particularly in the polynya regions, and upwelling of warm WGIW off the slope of Greenland likely modify a portion of the outflow through both pathways enough to be classified as TrW.

Arctic Water transport correlates significantly when Davis Strait lags Lancaster Sound transport by two months (r = 0.57, p = 1E-4). The lag of two months, assuming the distance from Barrow Strait and Davis Strait is 1450 km, yields an average advective speed of 0.28 m s^{-1}. This is faster than the 3-4 month estimate by **?** and larger than average AW speeds (0.1 m s^{-1}) but this simplified calculation does not take into account Kelvin waves or coastal trapped waves that can propagate SSH variations between the two straits. Maximum transport through Barrow Strait occurs between July and August (Peterson et al., 2012), consistent with a two month lag and the timing of maximum AW transport. Even though average AW velocities are lower than the estimated advection speed, southward velocities are stronger over the Baffin Island shelf and slope and typically range between 0.18 m s^{-1} and 0.25 m s^{-1} between September and November.

4.4.4 West Greenland Shelf Water

West Greenland Shelf Water (WGSW) transport is northward for all months with an annual average transport of 0.4 Sv. Maximum transport occurs between September and November and minimum transport between March and April. West Greenland Shelf Water transport is correlated ($r = 0.40$, $p = 0.003$, Figure 4.10) with the v component of the winds averaged off the southern coast of West Greenland (region WGS in Figure 4.4). West Greenland Shelf Water transport has an annual cycle, with an amplitude (0.2 Sv) larger than the average standard deviation of transport (0.2 Sv). Correlation between WGSW transport and WGS v winds is slightly more significant if the annual cycle is removed from both ($r = 0.43$, $p = 2E\text{-}4$). Since the shelf is shallow and the surface and bottom Ekman layers overlap, transport aligns more closely with the direction of the wind instead of being direct at 90° to the wind.

Correlation between the monthly WGSW mooring velocity and v component winds off West Greenland is slightly stronger ($r = 0.53$, $p = 8E\text{-}5$, Figure 4.11) than with WGSW OA transport but reduces to ($r = 0.41$, $p = 0.005$) when the annual cycle is removed from both but the annual cycle is not as strong and the amplitude of WGSW velocity (0.02 m $s{-1}$) is not larger than the standard deviation of WGSW velocity (0.03 m $s{-1}$). The 2004-10 objectively analyzed transport estimates are comprised of large-scale (mean) and variable components as a way to deal with spatial gaps in the moored arrays (**?**). Seaglider surveys across the central strait and moored velocity data are used to estimate the low frequency geostrophic velocity fields used for the OA large-scale velocity fields. There is either a 63 km or 93 km gap in the moored array between the velocity data across the shelf (between WG1 and WG3 or WG4) that is partially filled assuming geostrophy in the OA transport estimates. The reduced correlation with the OA transport might be caused by filling in spatial gaps with low frequency geostrophic velocity instead of nearby observations. No data was collected over the shelf between 1987-90 so no comparisons can be made.

Variability in the v component of the winds is partly in response to the SLP gradient between western Baffin Bay (high pressure) and off the southern coast of West Greenland (low pressure), south of the current array (between the regions labeled BBw and WGS in Figure 4.4) and correlates strongly at no lag (r = -0.67, p = 5E-8, Figure 4.12). The SLP gradient has an annual cycle, with an amplitude (3.5E-4 N m−3) larger than the average standard deviation (3.1E-4 N m−3) but the correlation between the SLP gradient and wind is still significant if the annual cycle is removed from both, though slightly smaller (r = -0.52, p = 3E-6, Figure 4.13). Winds along West Greenland are typically from the north but when the SLP gradient between western Baffin Bay and West Greenland relaxes or reverses, the winds reverse and WGSW transport into Baffin Bay increases.

4.4.5 West Greenland Irminger Water

Monthly average West Greenland Irminger transport is northward for all months with an annual average transport of 0.7 Sv. Though variability is high between years, maximum transport typically occurs October-December and decreases until the annual minimum between June and August. Correlations with atmospheric variables and SLP gradients are weak. The strongest correlation using the 2004-10 data set is obtained when WGIW transport is correlated with the west to east SLP gradient across Davis Strait (r = 0.32, p = 0.009, regions DSw and DSe in Figure 4.4, Figure 4.14); the same connection is not found in the 1987-90 WGIW transport. The SLP gradient across Davis Strait has an annual cycle amplitude (7.6E-4 N m−4) larger than the standard deviation of SLP gradient (6.6E-4 N m−4) and the SLP gradient across Davis Strait is not significantly correlated with WGIW transport if the annual cycle is removed from both.

Before WGIW reaches Davis Strait it is passes through the Irminger and Labrador Seas. Maximum WGIW transport occurs right before and at the beginning of the time of minimum SLP over both regions (December-February). Correlations between

WGIW transport and SLP over the Irminger and Labrador Seas are significant but weak. The largest correlation occurs between October and January with SLP in the Irminger Sea. The correlation between the 2004-10 WGIW transport and Irminger Sea SLP (region Irm in Figure 4.4) is significant ($r = 0.74$, $p = 4E\text{-}5$, Figure 4.15) between October-January but not for the other months of the year. This is also true for the 1987-90 transports ($r = 0.75$, $p = 0.005$, Figure 4.15) and the combined 1987-2010 transports ($r = 0.69$, $p = 4E\text{-}6$).

West Greenland Irminger Water transport correlates with AW transport ($r = -0.38$, $p = 0.008$) and might reflect the balance of inflows with outflows through Davis Strait. The deeper outflow of TrW, however, is not significantly correlated with WGIW transport. West Greenland Irminger Water transport between 1987-90 is not correlated significantly with AW or TrW transport. Transport of WGIW is much lower during 1987-90 (average 0.1 Sv) than during 2004-10 (average 0.7 Sv). The recent increase in WGIW inflow is consistent with changes observed in the strength of the subpolar gyre, showing recent weakening as compared to the late 1980s (Häkkinen and Rhines, 2004). When the subpolar and subtropical gyres weaken, the subpolar gyre contracts and the subpolar front moves westward as the subtropical gyre expands, allowing more high-salinity waters to move northward and enter the Nordic Seas (Häkkinen et al., 2011). The first empirical orthogonal function of satellite altimetry based SSH (from1992-present) is used as a proxy for subpolar gyre upper ocean transport (Häkkinen and Rhines, 2004). The first empirical orthogonal mode is centered over the Gulf Stream and North Atlantic Current with opposite sign SSH anomalies in the subpolar gyre. Transport of WGIW correlates significantly, when lagged by two months, with the first principal component of SSH ($r = 0.39$, $p = 0.02$) and supports a direct connection between variations in the strength of the subpolar gyre and WGIW transport. Monthly subpolar gyre indices courtesy of Häkkinen and Rhines (2004). However, a positive correlation indicates that WGIW transport increases as the subpolar gyre strength increases and is opposite of the transport observations between 1987-90 and 2004-10. Perhaps WGIW transport is influenced predominately by low frequency variability in the subpolar gyre index and not at monthly and higher frequencies.

4.4.6 Transitional Water

Transitional Water transport is southward for all months with an annual average transport of -1.1 Sv. Maximum transport of TrW typically occurs June-September and minimum transport typically occurs March-April. The 2004-10 TrW transport correlates with the SLP gradient between western Baffin Bay and off the southern coast of West Greenland (between the regions labeled BBw and WGS in Figure 4.4) and increases when TrW transport lags the SLP gradient by one month ($r = 0.52$, $p = 5E\text{-}5$, Figure 4.17). Correlation is even stronger for the 1987-90 period and also increases by lagging TrW transport by one month ($r = 0.64$, $p = 0.004$, Figure 4.17). The annual cycle of the SLP gradient is larger than the variability of the SLP gradient. If the annual cycle is removed from both the SLP gradient (amplitude = 3.5E-4 N $m-3$) and TrW transport (amplitude = 0.3 Sv) for the 2004-10 period, the correlation is not significant when TrW is lagged one month ($r = 0.19$, $p > 0.1$). With both annual cycles removed, the strongest correlation occurs when TrW is lagged four months with the SLP gradient ($r = 0.33$, $p = 0.01$). If the annual cycle is removed for both the SLP gradient (amplitude = 3.4E-4 N $m-3$) and TrW transport (amplitude = 0.4 Sv) for the 1987-90 period, the correlation is significant at no lag ($r = 0.40$, $p = 0.02$) but not when TrW transport is lagged one month. Transitional Water transport variability might be indirectly controlled by the SLP gradient and directly controlled by intermediate adjustment processes.

Both outflows across Davis Strait, AW and TrW, correlate significantly with each other both between 2004-10 ($r = 0.40$, $p = 0.006$, Figure 4.18) and even more strongly between 1987-90 ($r = 0.60$, $p = 0.006$). If the annual cycle is removed from both AW transport (amplitude = 0.2 Sv) and TrW transport (amplitude =) the correlation drops slightly between 2004-10 ($r = 0.36$, $p = 0.002$) but increases between 1987-90 ($r = 0.81$, $p = 0.003$). The difference in correlations between the two periods might be influenced by the sampling depths in the 1987-90 array (150, 300 and 500 m) as compared to the current array (upper 100 m, 200/250 and 500 m). Variability of AW and TrW might also be similar if some fraction of the CAA inflows are modified by wintertime convection in Baffin Bay and converted to TrW.

Transitional Water also correlates with one of the inflows through Davis Strait. Transitional Water and WGSW correlate significantly ($r = -0.45$, $p = 0.001$, Figure **??**) but the correlation is weak and not significant if the annual cycles are removed from both. If TrW transport is lagged five months with WGSW transport the annual cycles occur at the same time but the correlation reverses sign and the correlation is slightly higher then at no lag ($r = 0.54$, $p = 2E\text{-}4$, Figure 4.20). If WGSW and AW transport are directly forced or modified by the SLP gradient via the winds and TrW transport is indirectly forced by the SLP gradient that might explain the difference between the correlations with and without an annual cycle, especially for WGSW, and is consistent with the idea that the inflows and outflows are forced together. Average TrW transport roughly equals the sum of that from the inflows into Baffin Bay through eastern Davis Strait (WGIW, WGSW and unclassified water). The average transport difference between TrW and incoming water is 0.1 Sv and varies between -0.1 Sv and 0.2 Sv over the six years. However, some fraction of WGSW is likely to leave Baffin Bay as AW.

Variability of WGSW and TrW transports might be similar if some fraction of WGSW transport is modified by wintertime convection in Baffin Bay and converted to TrW. The lagged response could be caused by modified WGSW exiting Davis Strait at depth or indicate that an increase in WGSW reduces the amount of upper water transformed to TrW in Baffin Bay. If WGSW interacts with WGIW along the West Greenland shelf and slope as it moves northward or is modified by sea ice formation and winter convection in Baffin Bay it could pick up enough heat and salt to be classified as TrW. Northerly winds in Baffin Bay create positive wind stress curl along the coast of West Greenland that would promote upwelling of the salty, warm WGIW on the slope. The time it would take to modify WGSW and leave Davis Strait as TrW probably varies over a wide range, including five months, since WGSW is likely pulled offshore and recirculates as it moves up the coast of West Greenland (Tang et al., 2004; Dunlap and Tang, 2006). Rudels (2011) suggests, using historical data and theoretical analysis, that WGSW and AW transform in Baffin Bay due to ice formation/brine rejection, become denser, and leave Davis Strait at a deeper depth.

4.4.7 AO and NAO

Variations in SLP gradients across and along Baffin Bay, while exhibiting distinct variability from the surrounding region, are connected with large-scale variations in both the Arctic and North Atlantic atmosphere. The AO index describes the large-scale variability between the Arctic and northern mid-latitudes. When the AO is in a warm (positive) phase there is lower SLP over the Arctic and higher SLP over the mid-latitudes. Conversely, when the AO is in a cool (negative) phase there is higher SLP over the Arctic and lower SLP over the mid-latitudes (**?**). The NAO index describes the large-scale variability in the North Atlantic between the semi-permanent low, centered near Iceland, and the semi-permanent high, centered near the Azores. When the NAO is in a positive phase, both the semi-permanent low near Iceland and the semi-permanent high near the Azores are stronger, creating a large SLP gradient in the North Atlantic (**?**). The reverse is true for the negative phase of the NAO. Both the NAO and AO have maximum variability during winter months (January-March); combined indices from January, February and March (JFM) are often used when comparing the NAO and AO with other forms of variability.

When the AO is in a warm (positive) phase, SLP is lower over the Arctic and Baffin Bay with typically colder winters and stronger northerly winds in Baffin Bay. When the NAO is positive, the SLP is lower in eastern Baffin Bay, the Labrador Sea and near Iceland. When the AO and NAO indices are negative the conditions are reversed. Positive AO and NAO indices suggest increased transport through Davis Strait and negative indices, reduced transport. The JFM AO and NAO indices are very different between 1987-90 and 2004-10. Between 1987-90 the AO (-0.33, 2.64, 2.46) was weak the first year and then strongly positive the last two years; the NAO varied similarly but always had positive values (0.54, 1.67, 1.3). Between 2004-10 the AO (-0.75, -0.64, 0.64, 0.78, 0.08, -2.43) was fairly weak until 2009-10 when it turned strongly negative; the NAO (-0.12, -0.17, 0.40, 0.57, 0.21, -1.32) varied similarly. Seasonal SLP between 1987-90 (Figure 4.6) and 2004-10 (Figure 4.5) vary as expected with lower SLP over the Arctic and Baffin Bay region and deeper low pressure around Iceland between 1987-90 and higher Arctic and Baffin Bay SLP with a weaker low near Iceland between 2004-10. Davis Strait transports agree with the variation in indices, with increased southward transport between 1987-90 and weaker transports between 2004-10 (**?**). Net transport through Davis Strait increases during the years with strong positive AO/NAO JFM indices (1988-90 corresponding to -3.4 Sv and -3.7 Sv of transport) and decreases during the year with the lowest AO/NAO JFM indices (2009-10 corresponding to -1.5 Sv of transport).

The monthly NAO and AO indices between September 1987-August 2010 correlate strongly with each other ($r = 0.65$, $p =$ 3E-8). When net monthly 2004-10 Davis Strait transport is lagged with the AO and NAO, correlations are weak and the maximum correlation does not occur at the same lag with the AO (lag 16, $r = 0.28$, $p = 0.04$) and NAO (lag 30, $r = -0.32$, $p = 0.05$). If the net transport is divided into northward and southward components, correlations improve. Northward transport through Davis Strait correlates the highest when transport is lagged five months ($r = -0.43$, $p =$ 4E-4) for the NAO and is not strong or significant for the AO. Since the origins of northward transport come from the North Atlantic, a stronger correlation between northward transport and the NAO is expected. Southward transport correlates the highest when transport is lagged 16 months for the AO ($r = 0.40$, $p = 0.003$) and 10 months for the NAO (r = -0.34, p = 7E-4). The 16 month lag for both the net and southward transport is the same for the AO but not the NAO. Transport correlation with the AO is higher for the southward component of transport and is expected since the majority of southward transport originates in the Arctic. Outflow from the CAA predominately leaves Davis Strait as AW. If only AW is correlated with the AO, the correlation is largest when AW transport is lagged 30 months (r = -0.46, p = 0.002). Model results by Jahn et al. (2010) found that CAA freshwater export is influenced predominately by low frequency variability in the AO. They noted a maximum correlation between the AO and CAA outflow when transport is lagged one year ($r = 0.54$ $p < 0.01$). The correlation increases to 0.71 and 0.75 ($p < 0.01$) for the three- and five- year running means. A 51-year model study from Samelson and Barbour (2008) found similar results, showing that the correlation between the AO and SLP differences in Nares Strait is -0.34 for the annual means but strengthens to -0.57 for the three-year running averages of the annual means. The time series of Davis Strait transport is not long enough to have significant correlations using similar running means.

The variation in correlation and lag time between the transport and the atmospheric indices does not yield strong confidence in the ability of either the AO or NAO to serve as a proxy for Davis Strait transport variability, at least at low frequencies. If the JFM AO and NAO are correlated with annual Davis Strait transports between 2004-10 the results are insignificant. If the 1987-90 JFM transports are added, the correlation is high for both the AO (r = -0.71, p = 0.03) and NAO (r = -0.74, p = 0.02). The time series between 1987-90 is too short to have significant correlations over the three year period alone but the correlations are high. The NAO and AO were much stronger in the late 1980s as compared to the recent period. Davis Strait transport likely correlates better when the AO and NAO indices are strong and large-scale atmospheric variability is strong but regional variability is probably a better indicator for transport variability when the indices are weaker. In a rapidly changing climate, large-scale indices might have to be reevaluated in terms of their significance.

4.5 Conclusion

Lagged correlation analysis between Davis Strait water mass transports and regional SLP and winds reveals that atmospheric variability within Baffin Bay significantly influences circulation and transport through Davis Strait. The SLP trough that forms within Baffin Bay, between western Baffin Bay and off the southern coast of West Greenland, influences the observed variability in Davis Strait transports either directly or indirectly. The trough forms in response to seasonal temperature changes, seasonal ice variability, the rough ice covered topography of Greenland and the presence of strong low pressure systems that move across the subpolar seas. The SLP trough starts to form in October and strengthens through the winter before weakening between April-May. Transport both northward and southward through Davis Strait is enhanced when the SLP trough is present and transport is reduced when SLP variability throughout Baffin Bay and Davis Strait is weak.

Of the four dominant water masses, AW, WGSW, WGIW and TrW, the SLP trough in Baffin Bay partially explains transport variability for all but WGIW. Arctic outflow via the CAA is advected into Baffin Bay could account for up to 82% of AW transport. Local northerly winds in Baffin Bay, driven partly by the west-east SLP gradient across the Baffin Bay, are also important for advecting CAA outflow through Davis Strait. The deeper outflow of TrW correlates with AW but AW is primarily controlled by the CAA inflows so another mechanism might be controlling Baffin Bay inflows and outflows that is related to the SLP gradient or other mechanisms not explored here such as density variations. Variability of AW and TrW might also be similar if some fraction of the CAA inflows are modified by wintertime convection in Baffin Bay.

Since both TrW and WGSW transport relate either directly or indirectly to the SLP trough in Baffin Bay, correlation at no or small lag is expected. However the cause for the lagged correlation at five months is unclear. The delayed signal might be from the modification of WGSW as it moves through Baffin Bay and becomes denser by picking up heat and salt from upwelled WGIW water and sea ice formation. Northerly winds in Baffin Bay create positive wind stress curl along the coast of West Greenland that would promote upwelling of the salty, warm WGIW on the slope. Transport of WGSW has the highest correlation with v component of the winds off of southern West Greenland associated with SLP gradient. When the pressure gradient weakens or reverses it helps set up northward transport over the West Greenland shelf. When the winds, predominately from the north, weaken or reverse, WGSW transport northward increases. Freshwater from Nares Strait, Jones Sound and WGC (carrying WGSW) have the potential for water mass modification due to interactions with WGIW and sea ice formation, particularly when these waters encounter the polynyas in northern Baffin Bay. Lancaster Sound outflow enters Baffin Bay south of the polynya region and likely transits to Davis Strait with little to no modification.

The observations used in this analysis (**?**), other observations in the region (Münchow and Melling, 2008; Peterson et al., 2012) and model results (Jahn et al., 2010; Houssais and Herbaut, 2011; McGeehan and Maslowski, 2012) from the CAA and Baffin Bay as well as theoretical investigations into the dynamics of Baffin Bay (Rudels, 2011) all point to variations in SLP and SSH in Baffin Bay being critical to CAA and Davis Strait transport variability. Variations in winds and SLP in Baffin Bay are associated with variations observed in the Arctic and North Atlantic but they are modified and altered due to the inflows and adjustment caused by the presence of Greenland. Atmospheric variability, both locally within Baffin Bay as well as regionally, are important, but density variations in Baffin Bay can also affect CAA and Davis Strait transports. Rudels (2011) emphasized that variations in Baffin Bay density are important to monitor because additional freshwater from the WGC and glacial runoff could reduce CAA outflow by reducing the density in Baffin Bay and thus impacting the baroclinic exchanges between the Arctic and Baffin Bay. Model re-

)
).
er
r-
d
n

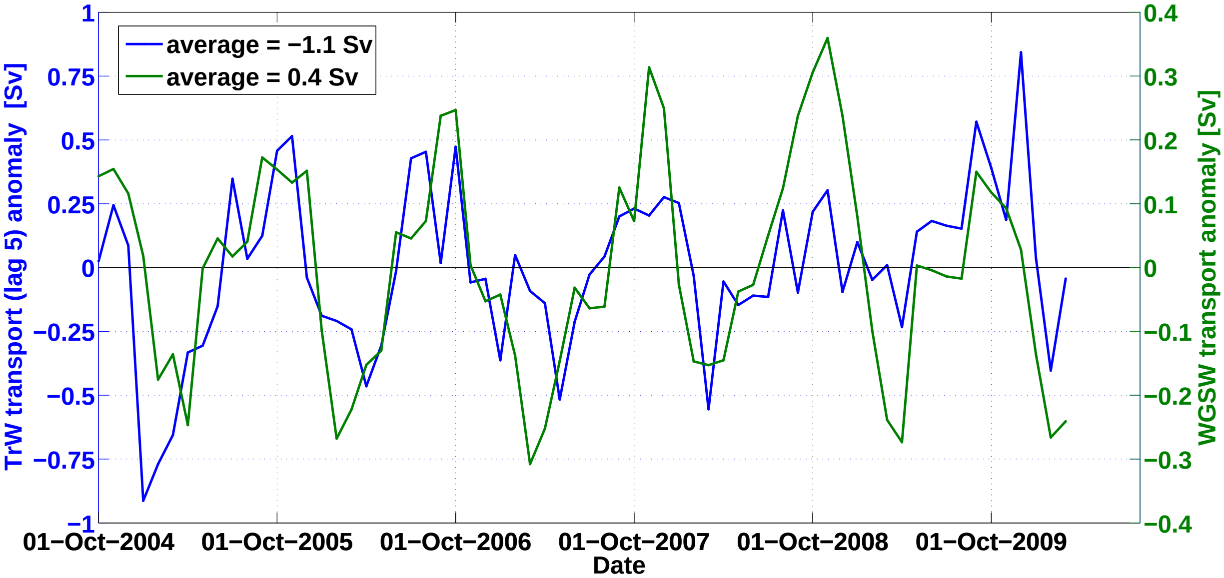

igure 4.20: Monthly TrW transport anomalies (lagged at five months) plotted gainst WGSW transport anomalies for the period between October 2004- August 010.

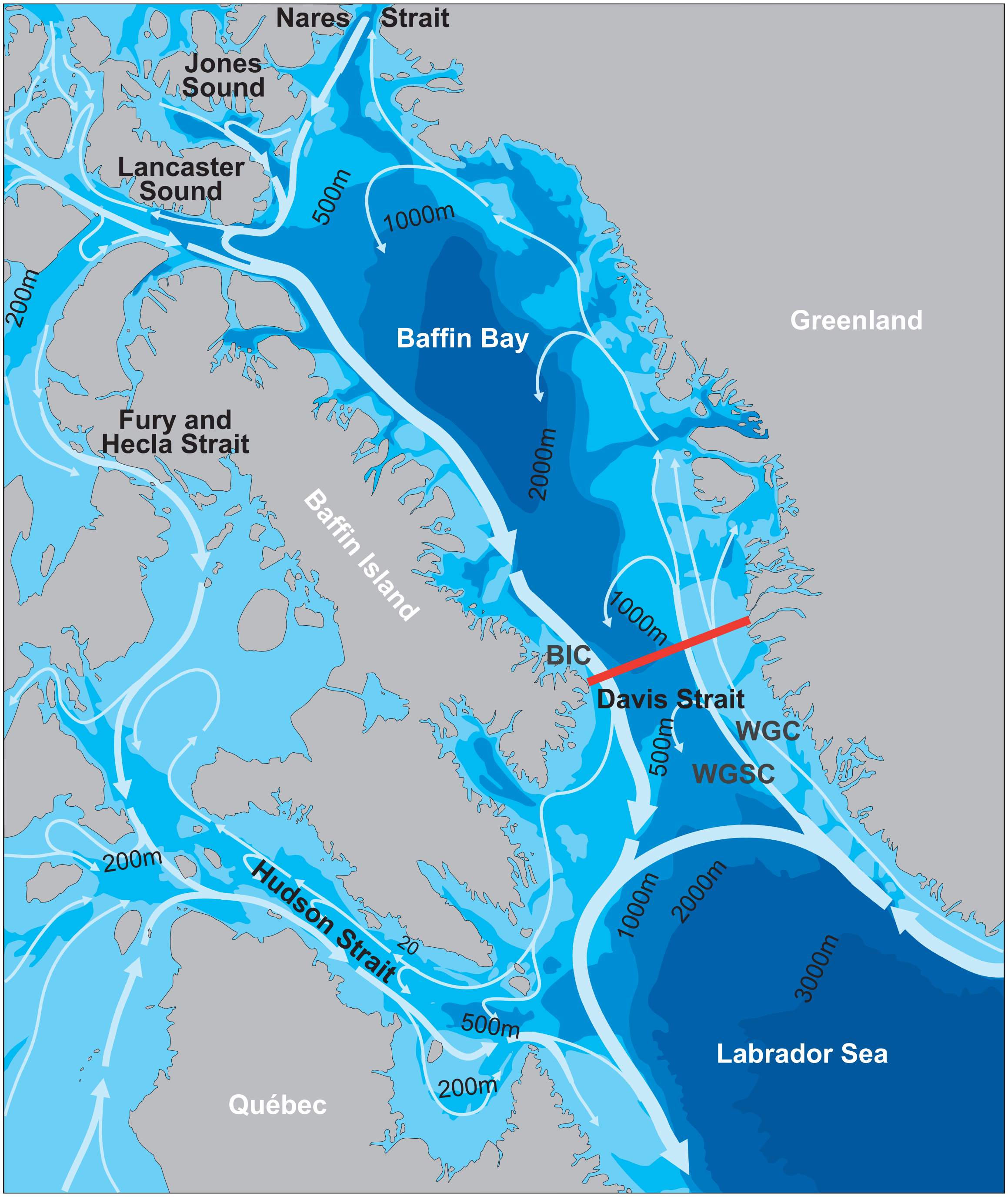

Figure 4.1: General circulation in Baffin Bay and Davis Strait (white arrows) and the location (red line) of the 2004-10 moored array. Arctic water by way of the Canadian Arctic Archipelago leaves Davis Strait as the broad, surface-intensified Baffin Island Current (BIC). Northward flow on the eastern side of Davis Strait consists of the fresh West Greenland Current (WGC) of Arctic origin on the shelf and warm, salty West Greenland Slope Current (WGSC) of North Atlantic origin on the slope.

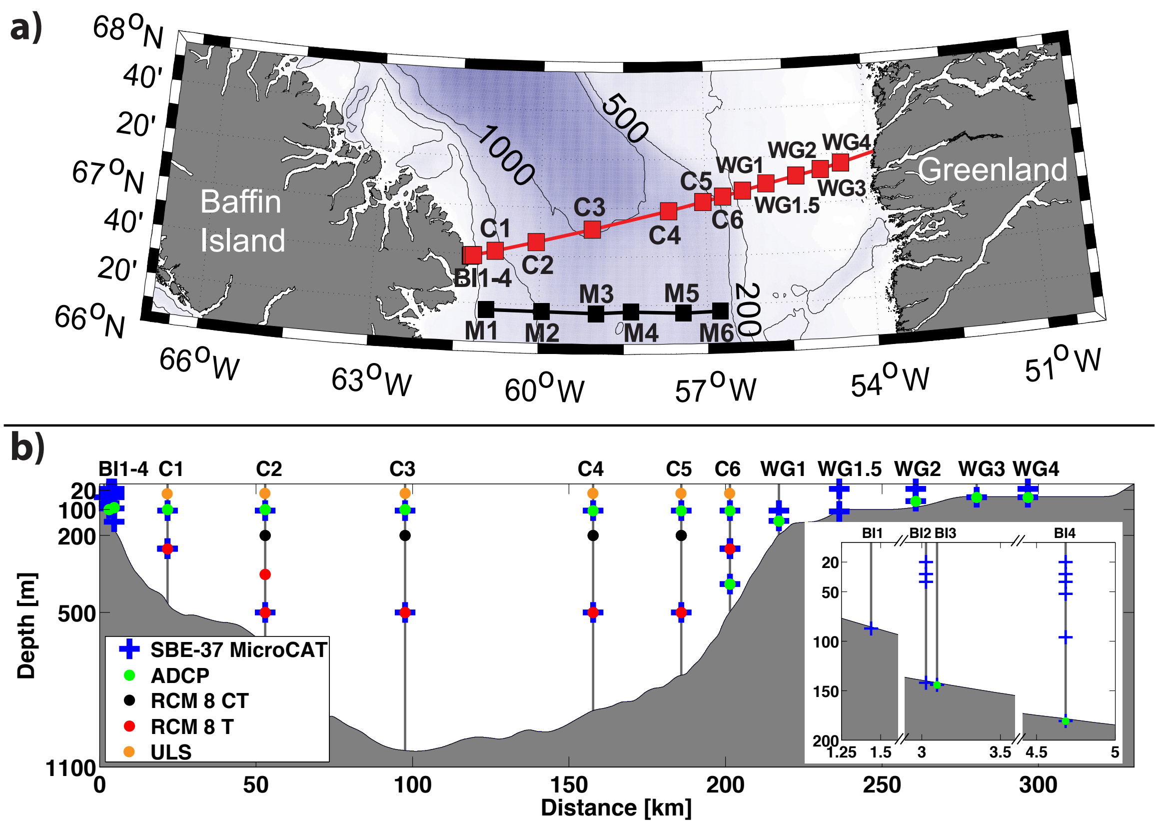

Figure 4.2: (a) Davis Strait 2004-10 (red line) and 1987-90 (black line) moored arrays with squares indicating mooring locations. (b) Summary of Davis Strait 2004-10 moored array instrumentation. Blue crosses indicate SBE37 MicroCAT conductivity, temperature and pressure recorders; green dots represent RDI ADCPs; black dots denote Aanderaa RCM8 velocity, conductivity, and temperature recorders; red dots denote Aanderaa RCM8 velocity and temperature recorders; and orange dots denote ULSs. Inset image shows a close-up of the Baffin Island shelf instruments. Spatial coverage varies from year to year throughout the program.

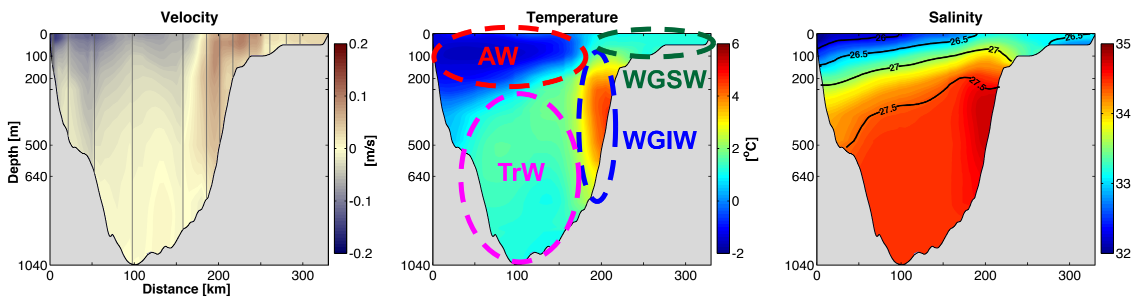

Figure 4.3: Objectively analyzed annual averages (2004-10) from daily estimates of along-strait velocity, temperature and salinity. Gray lines indicate mooring locations in the velocity panel. Potential density lines (black lines) are noted in the salinity panel. The boundaries of the four dominant water masses (AW: Arctic Water, WGIW: West Greenland Irminger Water, WGSW: West Greenland Shelf Water, TrW: Transitional Water) are shown in the temperature panel.

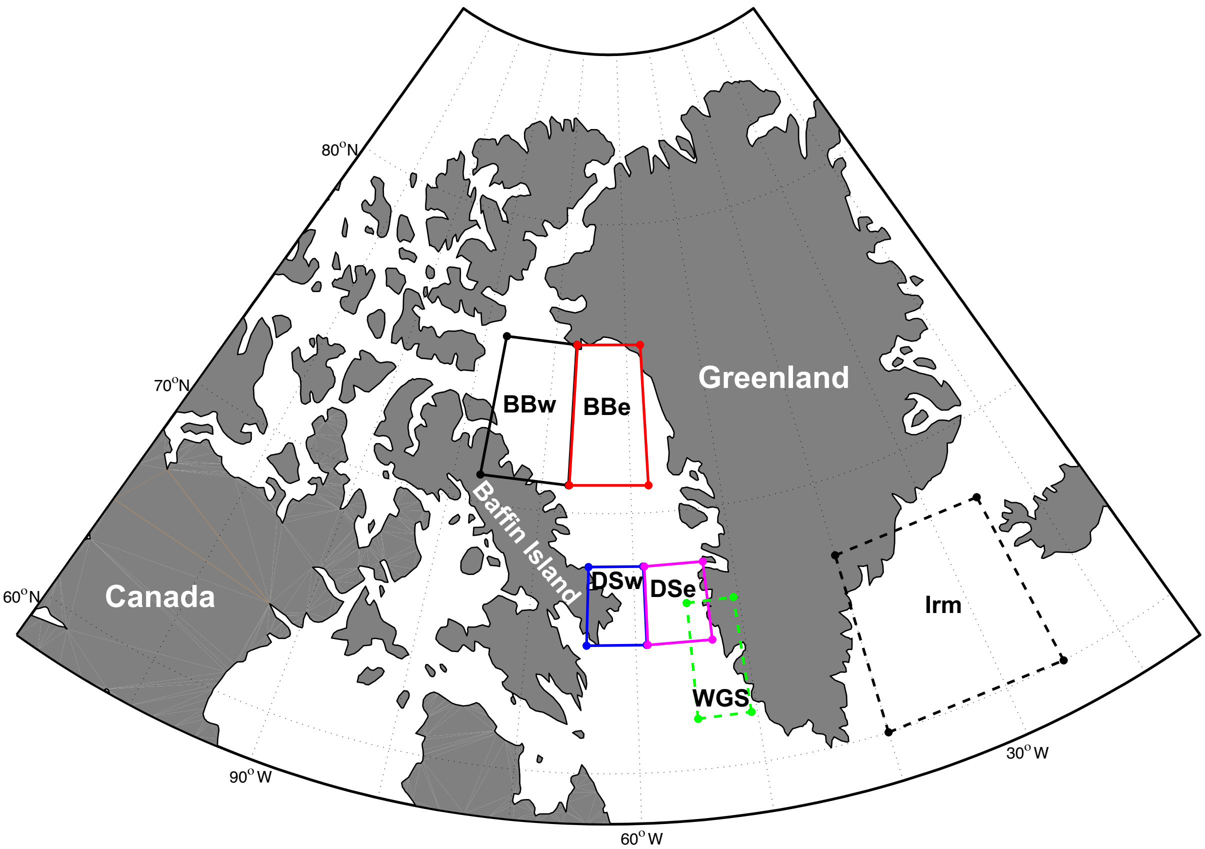

Figure 4.4: Regions within Baffin Bay, Davis Strait and the North Atlantic (averaged within) used in the lag correlation analysis between Davis Strait transports and NARR atmospheric variables. Regions discussed in this analysis: western Baffin Bay (BBw, black box), eastern Baffin Bay (BBe, red box), western Davis Strait (DSw, blue box), eastern Davis Strait (DSe, magenta box), off the southern coast of West Greenland (WGS, dashed green box) and the Irminger Sea (Irm, dashed black box).

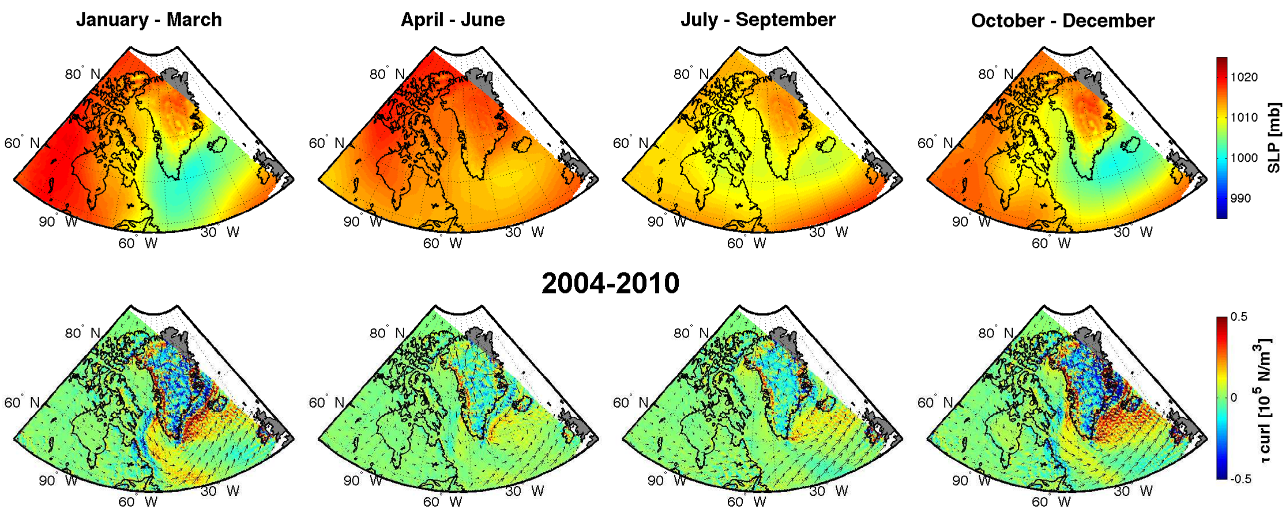

Figure 4.5: Seasonal SLP, winds and wind stress curl in and around Baffin Bay for October 2004- August 2010.

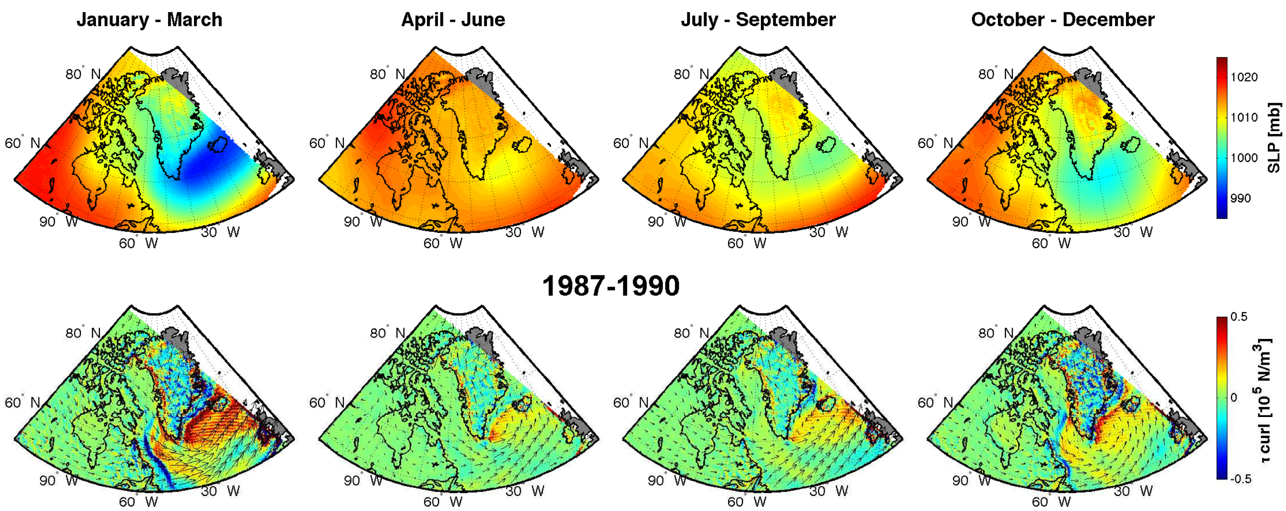

Figure 4.6: Seasonal SLP (top row), winds and wind stress curl (bottom row) in and around Baffin Bay for September 1987- September 1990.

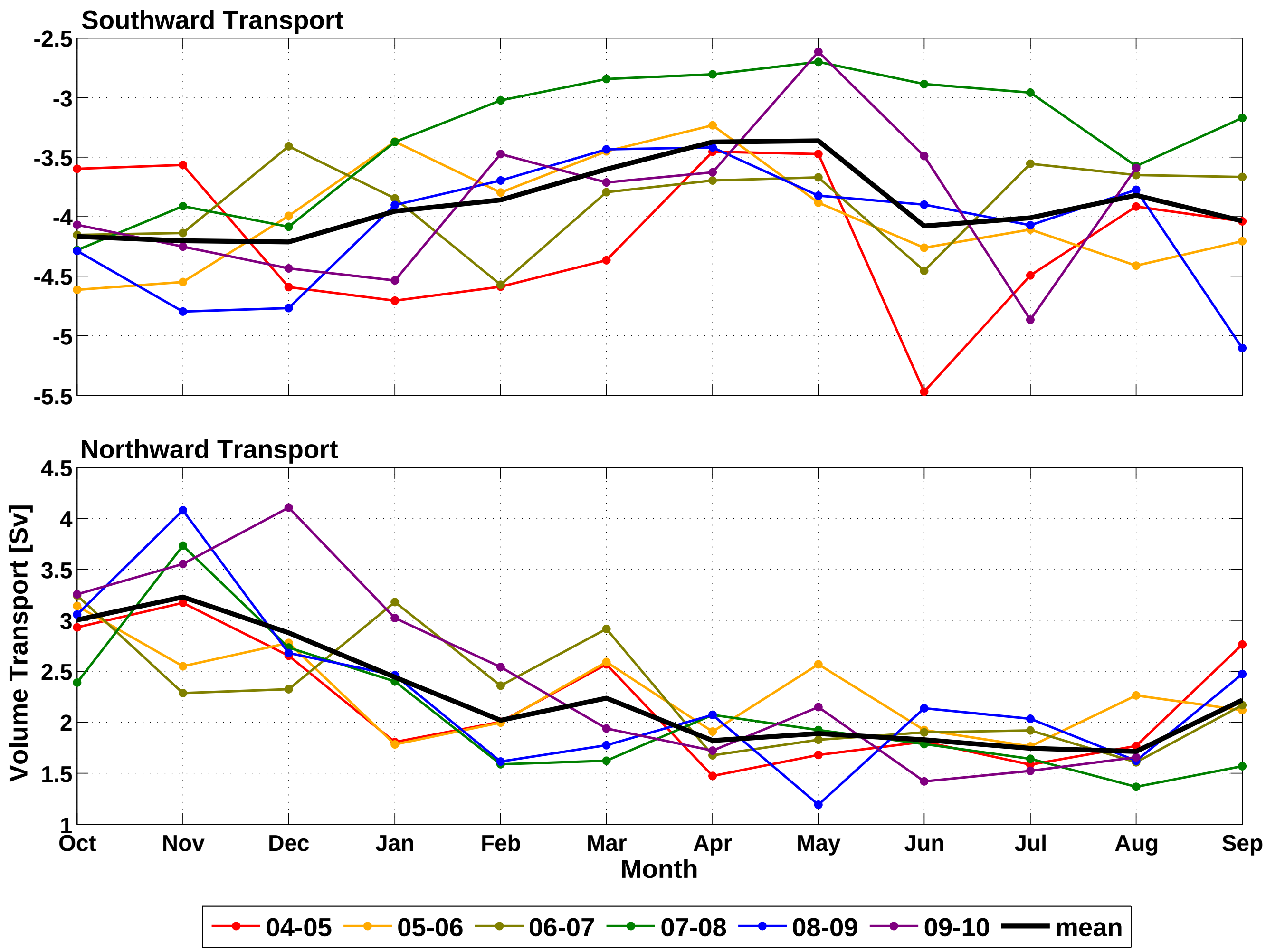

Figure 4.7: Objectively analyzed monthly average northward and southward components of Davis Strait volume transport for each year (negative = southward transport) with the 2004-10 averages (annual cycles) noted by the black lines. All transports are estimated from the surface to the sill depth, 640 m.

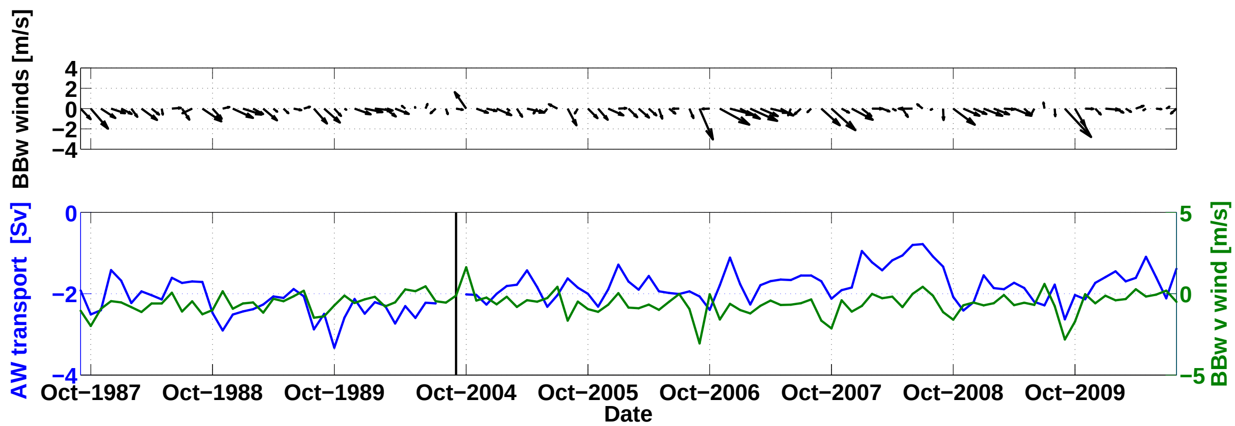

Figure 4.8: Monthly vector winds over western Baffin Bay (top panel) and the v component of the winds plotted against monthly AW transport (bottom panel) for the period between September 1987- September 1990 and October 2004- August 2010. Winds are averaged over the region labeled BBw in Figure 4.4.

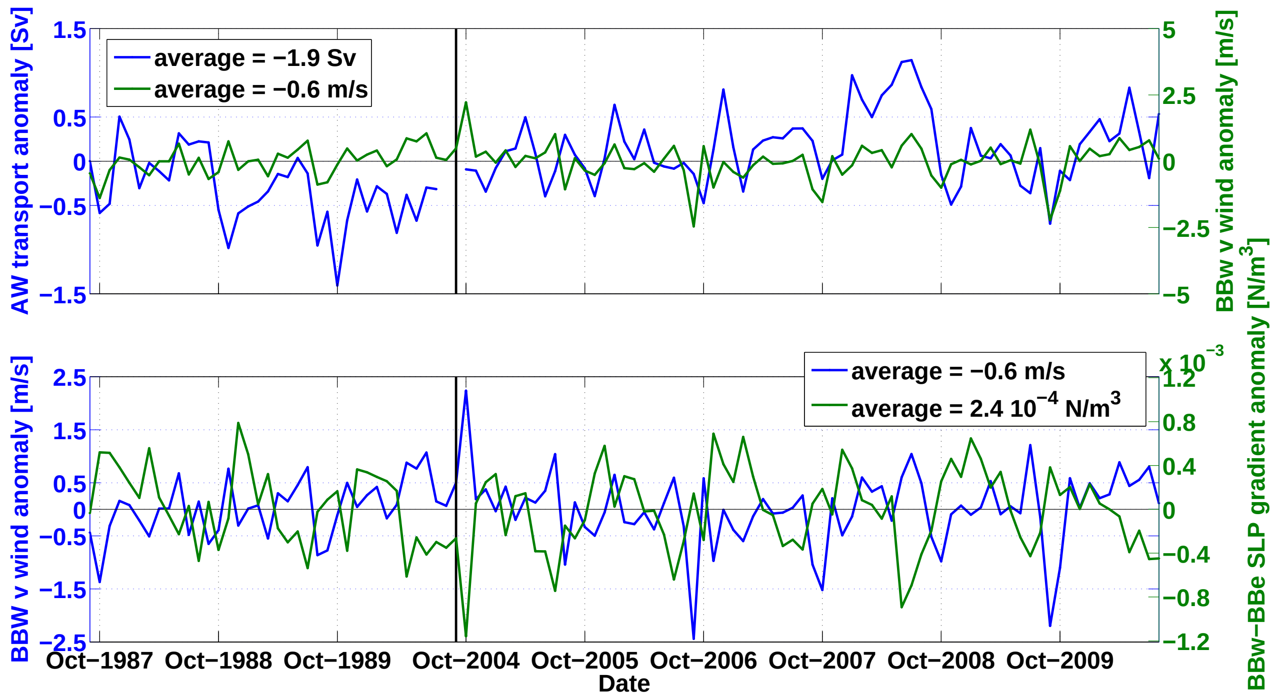

Figure 4.9: Monthly AW transport anomalies plotted against the v component wind anomalies over western Baffin Bay (top panel). The monthly v component winds over western Baffin Bay plotted against the SLP gradient between western Baffin Bay and eastern Baffin Bay is shown in the bottom panel. Monthly September 1987-September 1990 and October 2004- August 2010 values are plotted in both panels. Winds and SLP are averaged over the regions labeled BBw and BBe in Figure 4.4.

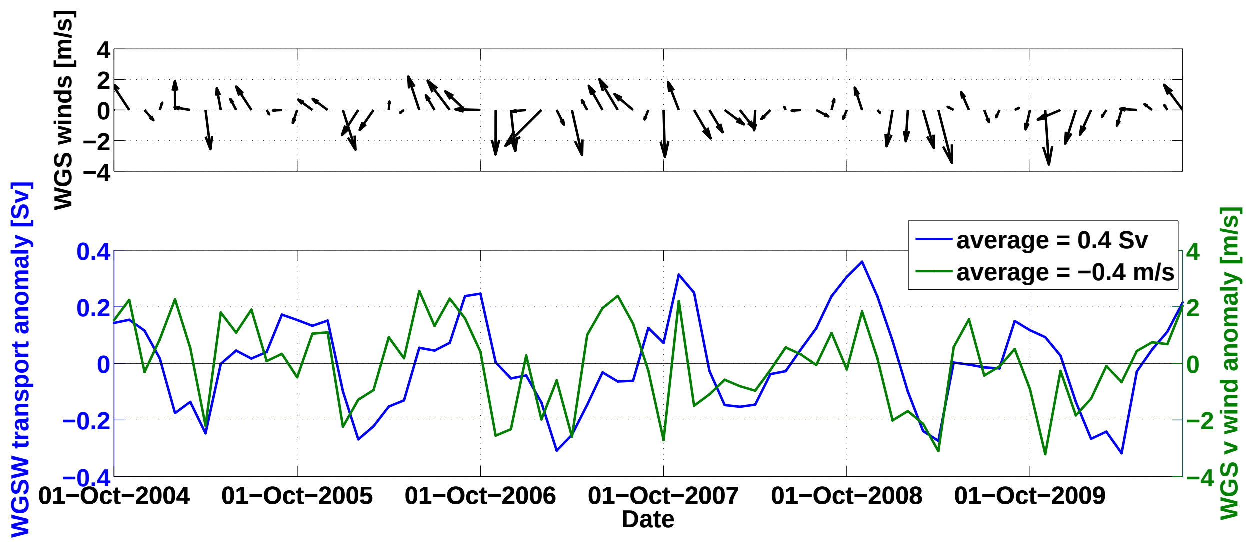

Figure 4.10: Monthly vector winds off the southern coast of West Greenland (top panel) and the v component of the wind anomalies plotted against monthly WGSW transport anomalies (bottom panel). Monthly October 2004- August 2010 values are plotted in both panels. Winds are averaged over the regions labeled WGS in Figure 4.4.

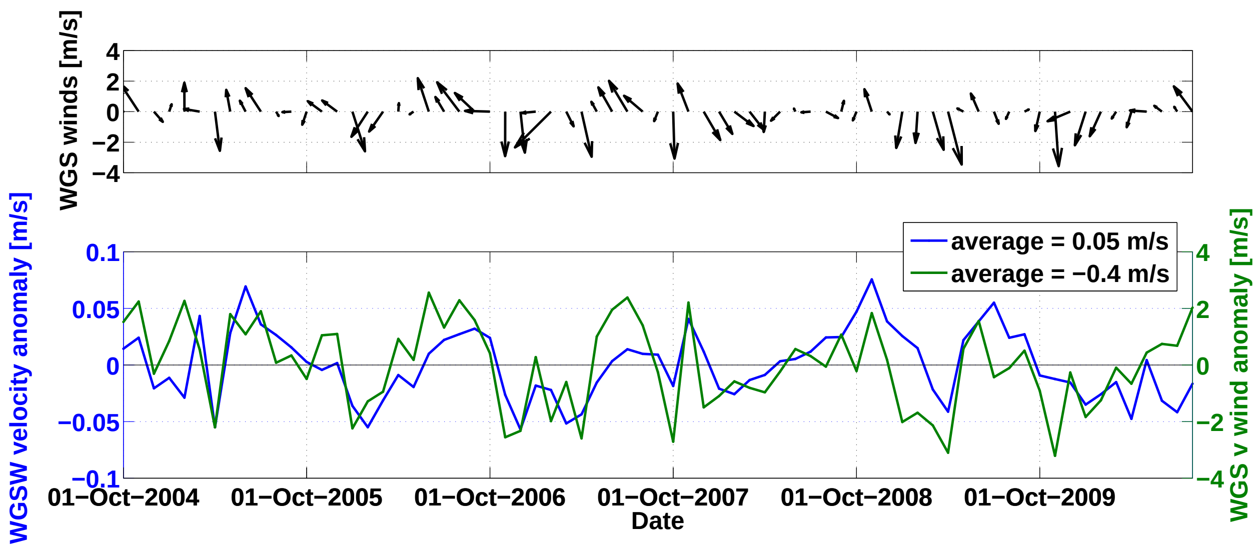

Figure 4.11: Monthly vector winds off the southern coast of West Greenland (top panel) and the v component of the wind, with the annual cycle removed, plotted against monthly WGSW velocity anomalies, with the annual cycle removed, (bottom panel). Monthly October 2004- August 2010 values are plotted in both panels. Winds are averaged over the regions labeled WGS in Figure 4.4.

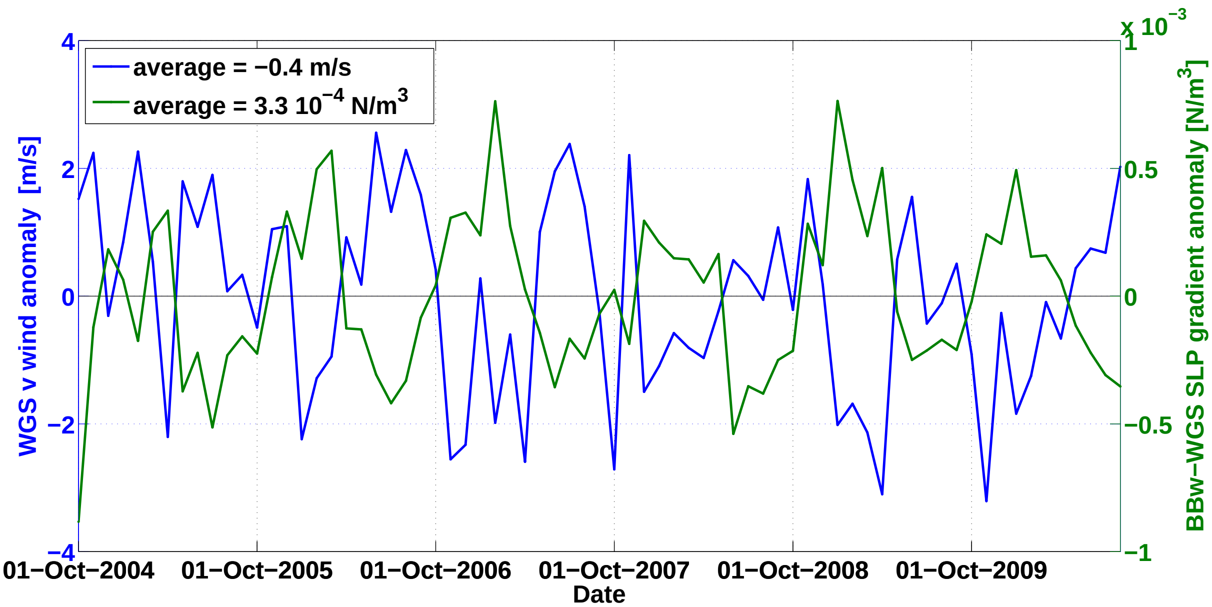

Figure 4.12: Monthly WGS v wind anomalies plotted against the monthly SLP gradient anomalies between western Baffin Bay and off the southern coast of West Greenland for the period between October 2004- August 2010. Winds and SLP are averaged over the regions labeled BBw (Baffin Bay winds) and WGS (off of southern West Greenland) in Figure 4.4.

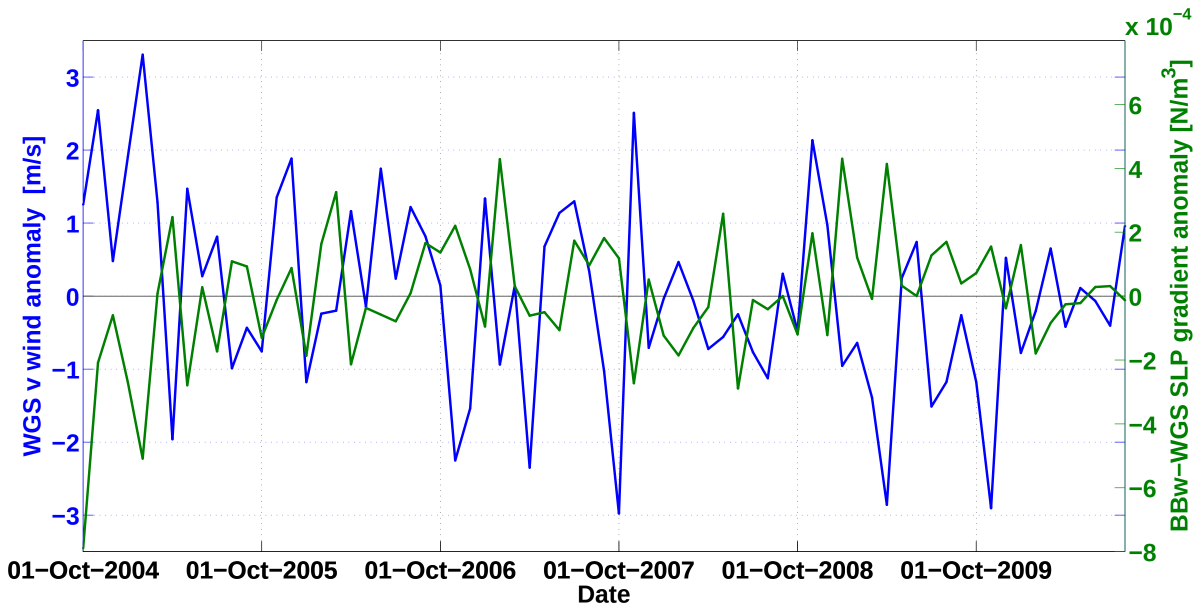

Figure 4.13: Monthly WGS v wind, with the annual cycle removed, plotted against the monthly SLP gradient between western Baffin Bay and off the southern coast of West Greenland, with the annual cycle removed, for the period between October 2004-August 2010. Winds and SLP are averaged over the regions labeled BBw (Baffin Bay winds) and WGS (off of southern West Greenland) in Figure 4.4.

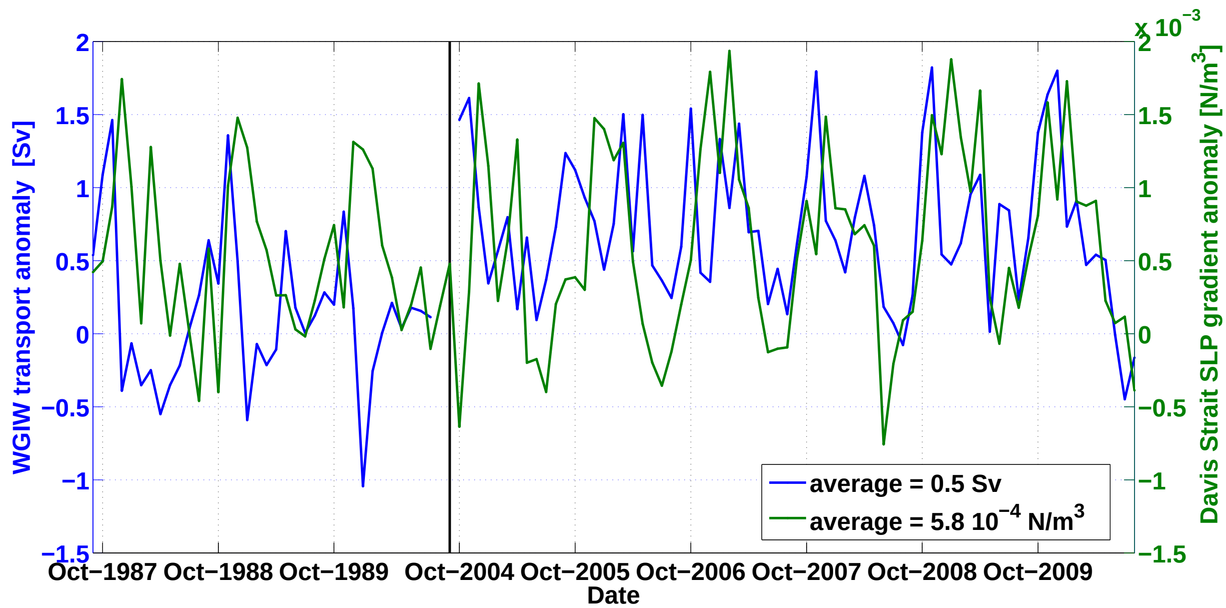

Figure 4.14: Monthly WGIW transport anomalies plotted against the SLP gradient anomalies across Davis Strait for the period between September 1987- September 1990 and October 2004- August 2010. The gradient of SLP across Davis Strait is estimated between the regions labeled DSw (Davis Strait west) and DSe (Davis Strait east) in Figure 4.4.

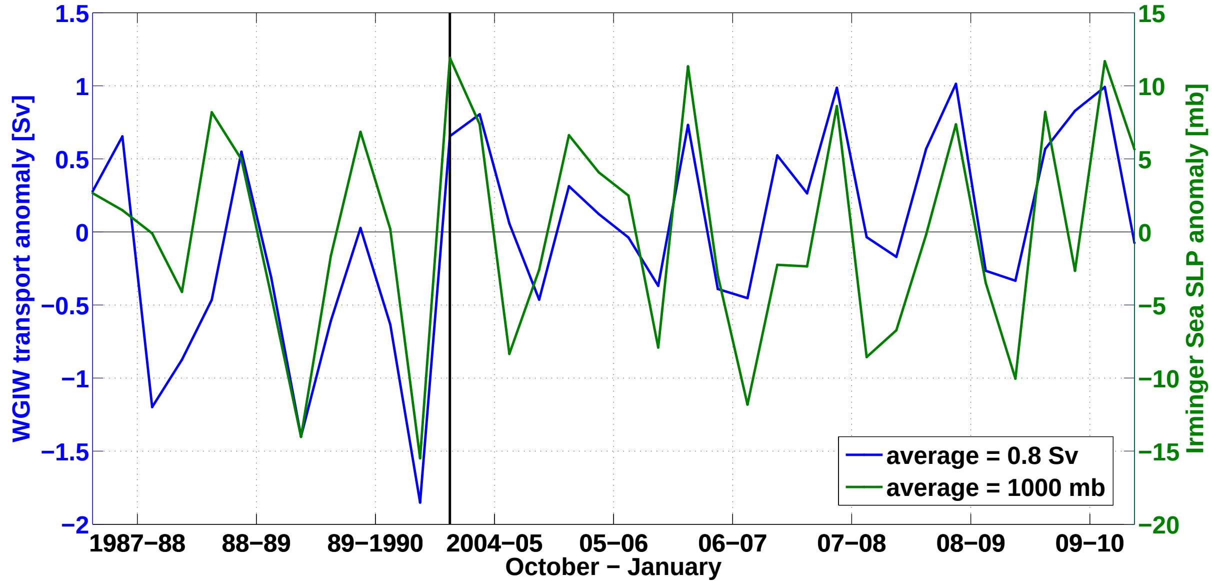

Figure 4.15: Seasonal, October-January average WGIW transport anomalies plotted against Irminger Sea SLP anomalies for the period between September 1987- September 1990 and October 2004- August 2010. Irminger Sea SLP is averaged over the region labeled Irm in Figure 4.4.

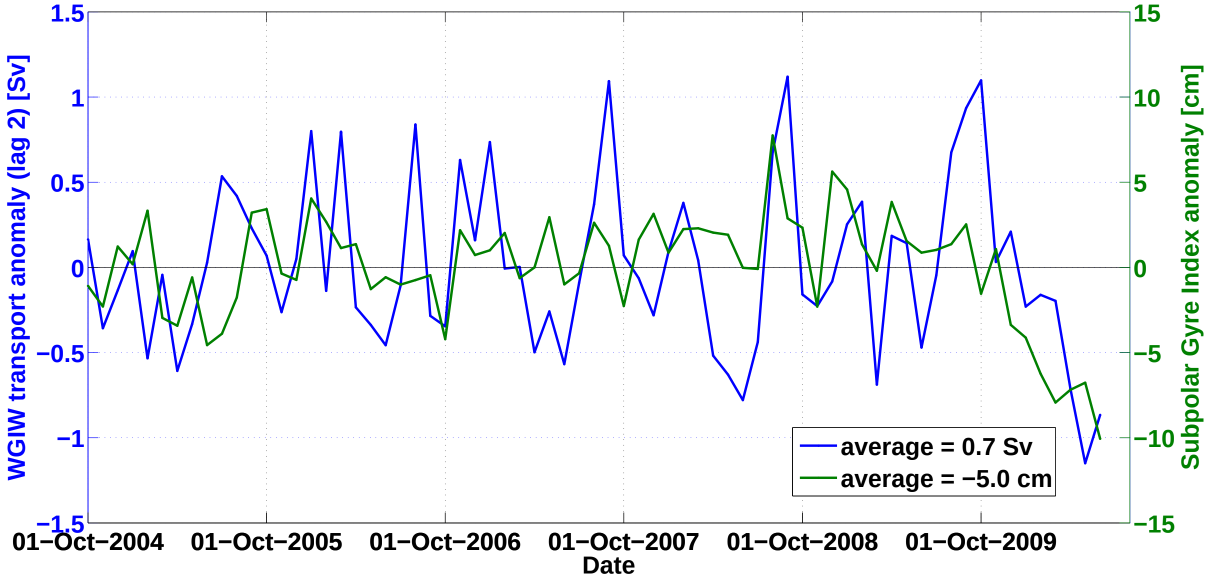

Figure 4.16: Monthly WGIW transport anomalies, lagged at 2 months, relative to the Subpolar Gyre Index (first principal component of satellite based SSH) anomalies for the period between October 2004- August 2010. Monthly indices courtesy of Häkkinen and Rhines (2004).

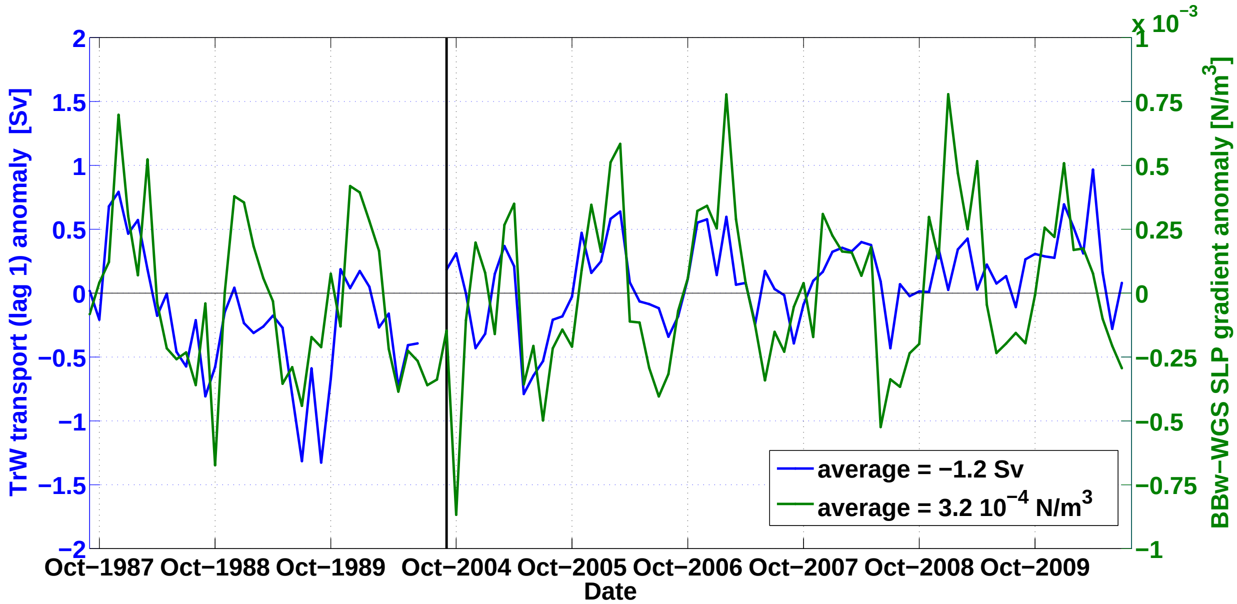

Figure 4.17: Monthly TrW transport (lagged at one month) anomalies against the SLP gradient anomalies between western Baffin Bay and off the southern coast of West Greenland for the period between September 1987- September 1990 and October 2004- August 2010. SLP is averaged over the regions labeled BBw (Baffin Bay winds) and WGS (off of southern West Greenland) in Figure 4.4.

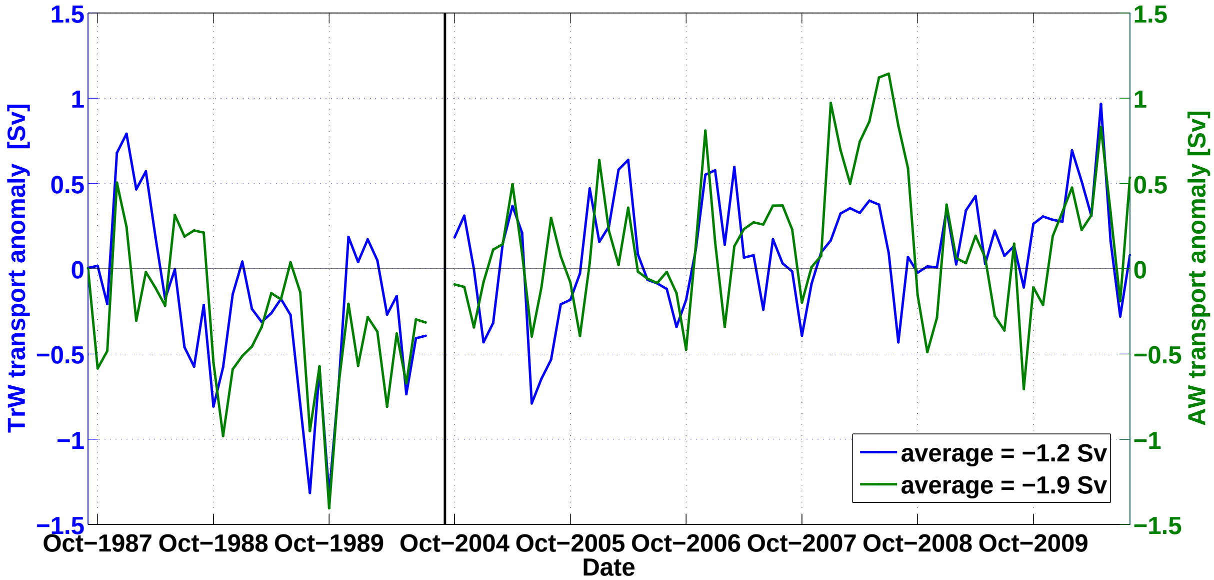

Figure 4.18: Monthly TrW transport anomalies plotted against AW transport anomalies for the period between September 1987- September 1990 and October 2004- August 2010.

Chapter 5

CONCLUSION

Six years of volume, liquid freshwater and heat transports in Davis Strait (2004-10) show significant interannual variability, weak annual cycles and no clear trends with average transports of of -1.6 ± 0.5 Sv, -93 ± 6 mSv and 23 ± 2 TW, respectively. Sea ice export contributes additional 10 mSv of freshwater transport. Interannual and annual variability of the net transports are large, with average annual volume, freshwater and heat transport standard deviations of 0.7 Sv, 17 mSv and 12 TW and interannual standard deviations of 0.3 Sv, 15 mSv and 2 TW. Annual cycles of net volume and freshwater transports are weak due to phase shifts in seasonal cycles. These cycles are more apparent, particularly over the West Greenland shelf and slope, when transports are decomposed into water mass classes. Though interannual variability is large, Davis Strait outflow was significantly fresher in 2009-10, likely caused by freshwater release from the Beaufort Gyre. This event was not clearly evident in the net or water mass freshwater transports due to a reduction in southward volume transport and the choice of reference salinity. Reanalysis of the 1987-90 mooring data indicate that there is currently less outflow and more inflow through Davis Strait, reflective of variations upstream in the Arctic Ocean and downstream in the subpolar gyre between the two periods.

The current monitoring program, combining the temporal resolution of the full strait moored array and spatial resolution of the Seaglider sections, resolves transport variability and detects variations in temperature and salinity properties likely linked to changes in the Arctic. Seaglider sections across the central strait provide important high resolution knowledge about annual variations in stratification that were unknown prior to this measurement program. Net volume and freshwater transports through Davis Strait are similar in magnitude to those estimated for Fram Strait, the other major pathway connecting the Arctic and North Atlantic. Davis Strait net volume and freshwater fluxes are within the uncertainty of the Fram Strait estimates (-2.3 $\pm$ 4.3 Sv, Rudels et al. (2008); Schauer et al. (2008); Curry et al. (2011) and -120 $\pm$ 30 mSv, Kwok et al. (2004); de Steur et al. (2009)). It is unclear how freshwater export will vary between these two gateways due to changes in the Arctic. Mechanisms driving Davis Strait transports are a complex and poorly understood combination of local Arctic and subarctic interactions. Continued measurements are needed in Davis Strait to isolate interannual variability from long term trends and to attribute observed changes to driving mechanisms in the Arctic and North Atlantic Oceans.

Lagged correlation analysis between Davis Strait water mass volume transports and and sea level pressure (SLP) and winds reveals that atmospheric variability within Baffin Bay significantly influences circulation and transport through Davis Strait. A seasonal SLP trough establishes in Baffin Bay beginning around October and weakening rapidly around March and April and is related to high SLP over the Arctic and low SLP over the subpoar North Atlantic around Greenland and Iceland. The SLP trough that forms in response to seasonal temperature changes, seasonal ice variability, the rough ice covered topography of Greenland, and the presence of strong low pressure systems that move across the subpolar seas, is an important mechanism driving Davis Strait transport.

Variations in winds and SLP in Baffin Bay are associated with variations observed in the Arctic and North Atlantic but they are modified and altered due to the inflows and adjustment caused by the presence of Greenland. Atmospheric variability, both locally within Baffin Bay as well as regionally, are important, but density variations in Baffin Bay can also affect CAA and Davis Strait transports. Rudels (2011) emphasized variations in Baffin Bay density are important to monitor because additional freshwater from the WGC and glacial runoff could reduce CAA outflow by reducing the density in Baffin Bay and thus impacting the baroclinic exchanges between the Arctic and Baffin Bay. Baffin Bay is not a passive pathway for freshwater enroute to the North Atlantic. Continued monitoring of transports through Davis Strait as well as observations regarding the modification of water masses in Baffin Bay is needed. This work can hopefully aid modelers in identifying areas that are not adequately resolved when trying to model the Baffin Bay region.

BIBLIOGRAPHY

Aagaard, K. and E. Carmack, 1989: The role of sea ice and other fresh water in the Arctic circulation. *Journal of Geophysical Research*, **94 (C10)**, 14,485–14,498.

Agnew, T., A. Lambe, and D. Long, 2008: Estimating sea ice area flux across the Canadian Arctic Archipelago using enhanced AMSR-E. *Journal of Geophysical Research*, **113**, C10011, doi:10.1029/2007JC004582.

Bacon, S., G. Reverdin, I. Rigor, and H. Snaith, 2002: A freshwater jet on the east Greenland shelf. *Journal of Geophysical Research*, **107 (C7)**, doi:10.1029/2001JC000935.

Barber, D., J. Hanesiak, W. Chan, and J. Piwowar, 2001: Sea-ice and meteorological conditions in Northern Baffin Bay and the North Water Polynya between 1979 and 1996. *Atmosphere-Ocean*, **39 (3)**, 343–359, doi:10.1080/07055900.2001.9649685.

Bretherton, F., R. Davis, and C. Fandry, 1976: A technique for objective analysis and design of oceanographic experiments applied to MODE-73. *Deep-Sea Research*, **23 (7)**, 559–582, doi:10.1016/0011-7471(76)90001-2.

Cavalieri, D., T. Markus, and J. Comiso, 2004a: *AMSR-E/Aqua Daily L3 12.5 km Brightness Temperature, Sea Ice Concentration, and Snow Depth Polar Grids V002 [2004-2010]*. Boulder, Colorado USA, National Snow and Ice Data Center.

Cavalieri, D., T. Markus, and J. Comiso, 2004b: *AMSR-E/Aqua Daily L3 6.25 km 89 GHz Brightness Temperature Polar Grids V002 [2004-2010]*. Boulder, Colorado USA, National Snow and Ice Data Center.

Chen, J., C. Wilson, and B. Tapley, 2011: Interannual variability of Greenland ice losses from satellite gravimetry. *Journal of Geophysical Research*, **116**, B07406, doi:doi:10.1029/2010JB007789.

Cuny, J., P. Rhines, and R. Kwok, 2005: Davis Strait volume, freshwater and heat fluxes. *Deep-Sea Research I*, **52 (3)**, 519–542, doi:10.1016/j.dsr.2004.10.006.

Cuny, J., P. Rhines, P. Niiler, and S. Bacon, 2002: Labrador Sea Boundary Currents and the Fate of the Irminger Sea Water. *Journal of Physical Oceanography*, **32 (2)**, 627–647, doi:10.1175/1520-0485(2002)032⟨0627:LSBCAT⟩2.0.CO;2.

Curry, B., C. Lee, and B. Petrie, 2011: Volume, Freshwater and Heat Fluxes through Davis Strait, 2004-05. *Journal of Physical Oceanography*, **41**, 429–436, doi:10.1175/2010JPO4536.1.

de Jong, M., H. van Aken, K. Våge, and P. Pickart, 2012: Convective mixing in the central Irminger Sea: 2002-2010. *Deep-Sea Research I*, **63**, 36–51, doi:10.1016/j.dsr.2012.01.003.

de Steur, L., E. Hansen, R. Gerdes, M. Karcher, E. Fahrbach, and J. Holfort, 2009: Freshwater fluxes in the East Greenland Current: A decade of observations. *Geophysical Research Letters*, **36**, L23611, doi:10.1029/2009GL041278.

Déry, S., M. Hernández-Hernríquez, J. Buford, and E. Wood, 2009: Observational evidence of an intensifying hydrological cycle in northern Canada. *Geophys. Res. Lett.*, **36**, L13402, doi:10.1029/2009GL038852.

Dickson, R., B. Rudels, S. Dye, M. Karcher, J. Meincke, and I. Yashayaev, 2007: Current estimates of freshwater flux through Arctic and Subarctic seas. *Progress in Oceanography*, **73 (3-4)**, 210–230, doi:10.1016/j.pocean.2006.12.003.

Drucker, R., S. Martin, and R. Moritz, 2003: Observations of ice thickness and frazil ice in the St. Lawrence Island Polynya from satellite imagery, upward looking sonar, and salinity/temperature moorings. *Journal of Geophysical Research*, **108 (C5)**, doi:10.1029/2001JC001213.

Dunlap, E. and C. Tang, 2006: Modelling the Mean Circulation of Baffin Bay. *Atmosphere-Ocean*, **44 (1)**, 99–110, doi:10.3137/ao.440107.

Eriksen, C., T. Osse, R. Light, T. Wen, T. Lehman, P. Sabin, J. Ballard, and A. Chiodi, 2001: Seaglider: A long-range autonomous underwater vehicle for oceanographic research. *IEEE J. Oceanic Eng.*, **26 (4)**, 424–436, doi:10.1109/48.972073.

Gardner, A., et al., 2011: Sharply increased mass loss from glaciers and ice caps in the Canadian Arctic Archipelago. *Nature*, **473**, 357–360, doi:doi:10.1038/nature10089.

Goosse, H., T. Fichefet, and J.-M. Campin, 1997: The effects of the water flow through the Canadian Archipelago in a global ice-ocean model. *Geophysical Research Letters*, **24 (12)**, 1507–1510.

Greene, C., A. Pershing, T. Cronin, and N. Ceci, 2008: Arctic climate change and its impacts on the ecology of the North Atlantic. *Ecology*, **89 (11sp)**, S24–S38, doi:10.1890/07-0550.1.

Häkkinen, S. and P. Rhines, 2004: Decline of Subpolar North Atlantic Circulation During the 1990s. *Science*, **304 (5670)**, 555–559, doi:10.1126/science.1094917.

Häkkinen, S., P. Rhines, and D. Worthen, 2011: Warm and saline events embedded in the meridional circulation of the northern North Atlantic. *Journal of Geophysical Research*, **116 (C3)**, doi:10.1029/2010JC006275.

Holland, D., R. Thomas, B. De Young, M. Ribergaard, and B. Lyberth, 2008: Acceleration of Jakobshavn Isbræ triggered by warm subsurface ocean waters. *Nature Geoscience*, **1**, 659–664, doi:doi:10.1038/ngeo316.

Holland, M., C. Bitz, M. Eby, and A. Weaver, 2001: The role of ice-ocean interactions in the variability of the North Atlantic thermohaline circulation. *Journal of Climate*, **14 (5)**, 656–675, doi:10.1175/1520-0442(2001)014⟨0656:TROIOI⟩2.0.CO;2.

Houssais, M. and C. Herbaut, 2011: Atmospheric forcing on the Canadian Arctic Archipelago freshwater outflow and implications for the Labrador Sea variability. *Journal of Geophysical Research*, **116**, C00D02, doi:10.1029/2010JC006323.

Ingvaldsen, R., L. Asplin, and H. Loeng, 2004: The seasonal cycle in the Atlantic transport to the Barents Sea during the years 1997-2001. *Continental Shelf Research*, **24 (9)**, 1015–1032, doi:10.1016/j.csr.2004.02.011.

Jackson, J., C. Lique, M. Alkire, M. Steele, C. Lee, W. Smethie, and P. Schlosser, 2013: On the waters upstream of Nares Strait, Arctic Ocean, from 1991-2012. *Continental Shelf Research*, **submitted**.

Jahn, A., B. Tremblay, L. Mysak, and R. Newton, 2010: Effect of the large-scale atmospheric circulation on the variability of the Arctic Ocean freshwater export. *Climate Dynamics*, **34 (2-3)**, 201–222, doi:10.1007/s00382-009-0558-z.

Jakobsson, M., R. Macnab, M. Mayer, R. Anderson, M. Edwards, J. Hatzky, H. Schenke, and P. Johnson, 2008: An improved bathymetric portrayal of the Arctic Ocean: Implications for ocean modeling and geological, geophysical and oceanographic analyses. *Geophysical Research Letters*, **35**, L07602, doi:10.1029/2008GL033520.

Jensen, L. and M. Rasch, 2008: Nuuk ecological research operations. 1^{st} annual report, 2007, Danish Polar Centre, Danish Agency for Science, Technology and Innovation, Copenhagen.

Jordan, F. and H. Neu, 1982: Ice drift in southern Baffin Bay and Davis Strait. *Atmosphere-Ocean*, **20 (3)**, 268–275, doi:10.3137/ao.200306.

Kållberg, P., P. Berrisford, B. Hoskins, A. Simmons, S. Uppala, S. Lamy-Thépaut, and R. Hine, 2005: ERA-40 atlas. ERA-40 Project Report Series 19, ECMWF.

Kovacs, K., C. Lydersen, J. Overland, and S. Moore, 2010: Impacts of changing sea-ice conditions on Arctic marine mammals. *Marine Biodiversity*, **41 (1)**, 181–194, doi:10.1007/s12526-010-0061-0.

Kreiss, J. and E. Paparoditis, 2011: Bootstrap methods for dependent data: A review. *Journal of the Korean Statistical Society*, **40 (4)**, 357–378, doi:10.1016/j.jkss.2011.08.009.

Kwok, R., 2005: Variability of Nares Strait ice flux. *Geophysical Research Letters*, **32**, L24502, doi:10.1029/2005GL024768.

Kwok, R., 2007: Baffin Bay ice drift and export: 2002-2007. *Geophyical Research Letters*, **34**, L19501, doi:10.1029/2007GL031204.

Kwok, R., G. Cunningham, and S. Pang, 2004: Fram Strait sea ice outflow. *Journal of Geophysical Research*, **109**, C01009, doi:10.1029/2003JC001785.

Kwok, R. and N. Untersteiner, 2011: The thinning of Arctic sea ice. *Physics Today*, **64 (4)**, 36–41, doi:10.1063/1.3580491.

Lilly, J., P. Rhines, F. Schott, K. Lavender, J. Lazier, U. Send, and E. D'Asaro, 2003: Observations of the Labrador Sea eddy field. *Progress in Oceanography*, **59 (1)**, 75–176, doi:10.1016/j.pocean.2003.08.013.

Loder, J., B. Petrie, and G. Gawarkiewicz, 1998: The coastal ocean off northeastern North America: A large-scale view. *The Global Coastal Ocean: Regional Studies and Syntheses*, A. Robinson and K. Brink, Eds., Harvard University Press, The Sea, Vol. 11, chap. 5, 105–133.

McGeehan, T. and W. Maslowski, 2012: Evaluation and control mechanisms of volume and freshwater export through the Canadian Arctic Archipelago in a high-resolution pan-Arctic ice-ocean model. *Journal of Geophysical Research*, **117**, C00D14, doi:10.1029/2011JC007261.

Melling, H., et al., 2008: Fresh-water fluxes via Pacific and Arctic outflows across the Canadian polar shelf. *Arctic-Subarctic Ocean Fluxes: Defining the Role of the Northern Seas in Climate*, R. Dickson, J. Meincke, and P. Rhines, Eds., Springer Verlag, chap. 9, 193–247.

Mernild, S., G. Liston, C. Hiemstra, K. Steffen, E. Hanna, and J. Christensen, 2009: Greenland ice sheet surface mass-balance modelling and freshwater flux for 2007, and in a 1995-2007 perspective. *Hydrological Processes*, **23 (17)**, 2470–2484, doi:10.1002/hyp.7354.

Moritz, R., 2013: Variability of sea-ice draft in Davis Strait estimated from upward-looking sonar measurements., unpublished.

Moritz, R. and A. Ivakin, (Eds.), 2012: *Retrieving sea-ice thickness from ULS echoes: methods and data analysis*, Institute of Acoustics, Edinburgh, UK, Proc. 11th Euro. Conf. Underwater Acoustics.

Mote, T., 2007: Greenland surface melt trends 1973-2007: Evidence of a large increase in 2007. *Geophyical Research Letters*, **34**, L22507, doi:10.1029/2007GL031976.

Münchow, A. and H. Melling, 2008: Ocean current observations from Nares Strait to the west of Greenland: Interannual to tidal variability and forcing. *Journal of Marine Research*, **66 (6)**, 801–833.

Myers, P., 2005: Impact of freshwater from the Canadian Arctic Archipelago on Labrador Sea Water formation. *Geophysical Research Letters*, **32**, L06605, doi:10.1029/2004GL022082.

Myers, P., C. Donnelly, and M. Ribergaard, 2009: Structure and variability of the West Greenland Current in Summer derived from 6 repeat standard sections. *Progress in Oceanography*, **80**, 93–112, doi:10.1016/j.pocean.2008.12.003.

Myers, P., N. Kulan, and M. Ribergaard, 2007: Irminger Water variability in the West Greenland Current. *Geophyical Research Letters*, **34**, L1760, doi:doi:10.1029/2007GL030419.

Overland, J., M. Wang, and S. Salo, 2008: The recent Arctic warm period. *Tellus*, **60 (4)**, 589–597, doi:10.1111/j.1600-0870.2008.00327.x.

Perkin, R. and E. Lewis, 1980: The Practical Salinity Scale 1978: Fitting the Data. *IEEE J. Oceanic Eng.*, **OE-5 (1)**, 9–16.

Peterson, I., J. Hamilton, S. Prinsenberg, and R. Pettipas, 2012: Wind-forcing of volume transport through Lancaster Sound. *Journal of Geophysical Research*, **117 (C11)**, doi:10.1029/2012JC008140.

Politis, D. and H. White, 2004: Automatic block-length selection for the dependent bootstrap. *Econometric Reviews*, **23 (1)**, 53–70, doi:10.1081/ETC-120028836.

Post, E., et al., 2009: Ecological Dynamics Across the Arctic Associated with Recent Climate Change. *Science*, **325 (5946)**, 1355–1358, doi:10.1126/science.1173113.

Prater, M., 2002: Eddies in the Labrador Sea as observed by profiling RAFOS floats and remote sensing. *Journal of Physical Oceanography*, **32 (2)**, 411–427, doi:10.1175/1520-0485(2002)032⟨0411:EITLSA⟩2.0.CO;2.

Prinsenberg, S., J. Hamilton, I. Peterson, and R. Pettipas, 2009: Observing and interpreting the seasonal variability of the oceanographic fluxes passing through Lancaster Sound of the Canadian Arctic Archipelago. *Influence of Climate Change on* *the Changing Arctic and Sub-Arctic Conditions*, C. Jacques, J. Nihoul, and A. Kostianoy, Eds., Springer Netherlands, 10.1007/978-1-4020-9460-6, NATO Science for Peace and Security Series C: Environmental Security, 125–143.

Proshutinsky, A. and M. Johnson, 1997: Two circulation regimes of the wind-driven Arctic Ocean. *Journal of Geophysical Research*, **102 (C6)**, doi:10.1029/97JC00738.

Proshutinsky, A. and M. Johnson, 2010: Decadal variability of Arctic climate: Cyclonic and anticyclonic circulation regimes. *Abstract GC12B-09*, San Francisco, California, AGU Fall Meeting.

Proshutinsky, A., et al., 2009: Beaufort Gyre freshwater reservoir: State and variability from observations. *Journal of Geophysical Research*, **114 (C1)**, doi: 10.1029/2008JC005104.

Rabe, B., H. Johnson, A. Münchow, and H. Melling, 2012: Geostrophic Ocean Currents and Freshwater Fluxes across the Canadian Polar Shelf via Nares Strait. *Journal of Marine Research*, **70 (4)**, 603–640, doi:10.1357/002224012805262725, unpublished.

Rabe, B., A. Münchow, H. Johnson, and H. Melling, 2009: Nares Strait hydrography and salinity field from a three-year moored array. *Journal of Physical Oceanography*.

Rignot, E., M. Koppes, and I. Velicogna, 2010: Rapid submarine melting of the calving faces of West Greenland glaciers. *Nature Geoscience*, **3**, 187–191, doi:DOI: 10.1038/NGEO765.

Ross, C., 1992: Moored current meter measurements across the Davis Strait. Tech. Rep. 92/70, NAFO Research Document.

Rossby, T., D. Dorson, and J. Fontaine, 1986: The RAFOS System. *Journal of Atmospheric and Oceanic Technology*, **3**, 672–679, doi:http://dx.doi.org/10.1175/1520-0426(1986)003⟨0672:TRS⟩2.0.CO;2.

Rothrock, D. and M. Wensnahan, 2007: The accuracy of sea-ice drafts measured from U.S. Navy submarines. *Journal of Atmospheric and Oceanic Technology*, **24**, 1936–1949, doi:10.1175/JTECH2097.1.

Rudels, B., 2011: Volume and freshwater transports through the Canadian Arctic Archipelago-Baffin Bay system. *Journal of Geophysical Research*, **116 (C11)**, doi: 10.1029/2011JC007019.

Rudels, B., M. Marnela, and P. Eriksson, 2008: Constraints on estimating mass, heat and freshwater transports in the Arctic Ocean: An exercise. *Arctic-Subarctic Ocean Fluxes: Defining the Role of the Northern Seas in Climate*, R. Dickson, J. Meincke, and P. Rhines, Eds., Springer Verlag, chap. 13, 315–341.

Samelson, R. and P. Barbour, 2008: Low-Level Jets, Orographic Effects, and Extreme Events in Nares Strait: A Model-Based Mesoscale Climatology. *Monthly Weather Review*, **136**, 4746–4759, doi:10.1175/2007MWR2326.1.

Schauer, U., A. Beszczynska-Möller, W. Walczowski, E. Fahrbach, J. Piechura, and E. Hansen, 2008: Variation of measured heat flow through the Fram Strait between 1997 and 2006. *Arctic-Subarctic Ocean Fluxes: Defining the Role of the Northern Seas in Climate*, R. Dickson, J. Meincke, and P. Rhines, Eds., Springer Verlag, chap. 3, 65–85.

Schmidt, S. and U. Send, 2007: Origin and Composition of Seasonal Labrador Sea Freshwater. *Journal of Physical Oceanography*, **37**, 1445–1454, doi:DOI:10.1175/JPO3065.1.

Serreze, M., A. Barrett, and A. Slater, 2008: Variability and change in the atmospheric branch of the Arctic hydrological cycle. *Arctic-Subarctic Ocean Fluxes: Defining the Role of the Northern Seas in Climate*, R. Dickson, J. Meincke, and P. Rhines, Eds., Springer Verlag, chap. 14, 343–362.

Skagseth, O., T. Furevik, R. Ingvaldsen, H. Loeng, K. Mork, K. Orvik, and V. Ozhigin, 2008: Volume and heat transports to the Arctic Ocean via the Norwegian and Barents Seas. *Arctic-Subarctic Ocean Fluxes: Defining the Role of the Northern Seas in Climate*, R. Dickson, J. Meincke, and P. Rhines, Eds., Springer Verlag, chap. 2, 45–64.

Spall, M. and R. Pickart, 2003: Wiind-Driven Recirculations and Exchange in the Labrador and Irminger Seas. *Journal of Physical Oceanography*, **33 (8)**, 1829–1845, doi:10.1175/2384.1.

Steffen, K., 1985: Warm water cells in the North Water, Northern Baffin Bay during winter. *Journal of Geophysical Research*, **90 (C5)**, 9129–9136, doi:10.1029/JC090iC05p09129.

Straneo, F., G. Hamilton, D. Sutherland, L. Stearns, F. Davidson, M. Hammill, G. Stenson, and A. Rosing Asvid, 2010: Rapid circulation of warm subtropical waters in a major glacial fjord off East Greenland. *Nature Geoscience*, **3**, 182–186, doi:10.1038/NGEO764.

Straneo, F. and F. Saucier, 2008: The Arctic-Subarctic exchange through Hudson Strait. *Arctic-Subarctic Ocean Fluxes: Defining the Role of the Northern Seas in Climate*, R. Dickson, J. Meincke, and P. Rhines, Eds., Springer Verlag, chap. 10, 249–261.

Stroeve, J., M. Serreze, M. Holland, J. Kay, J. Malanik, and A. Barrett, 2012: The Arctic's rapidly shrinking sea ice cover: a research synthesis. *Climate Change*, **110**, 1005–1027, doi:10.1007/s10584-011-0101-1.

Sutherland, D. and R. Pickart, 2008: The East Greenland Coastal Current: Structure, variability, and forcing. *Progress in Oceanography*, **78**, 58–77, doi:doi:10.1016/j.pocean.2007.09.006.

Tang, C., C. Ross, T. Yao, B. Petrie, B. DeTracey, and E. Dunlap, 2004: The circulation, water masses and sea-ice of Baffin Bay. *Progress in Oceanography*, **63 (4)**, 183–228, doi:10.1016/j.pocean.2004.09.005.

Timmermans, M., A. Proshutinsky, R. Krishfield, D. Perovich, J. Richter-Menge, T. Stanton, and J. Toole, 2011: Surface freshening in the Arctic Ocean's Eurasian Basin: An apparent consequence of recent change in the wind-driven circulation. *Journal of Geophysical Research*, **116**, C00D03, doi:10.1029/2011JC006975.

Våge, K., et al., 2009: Surprising return of deep convection to the subpolar North Atlantic Ocean in winter 2007-2008. *Nature Geoscience*, **2**, 67–72, doi:10.1038/ngeo382.

Vinje, T., N. Nordlund, and A. Kvambekk, 1998: Monitoring ice thickness in Fram Strait. *Journal of Geophysical Research*, **103 (C5)**, 10 437–10 449, doi:10.1029/97JC03360.

Wang, M. and J. Overland, 2009: A sea ice free summer Arctic within 30 years? *Geophysical Research Letters*, **36**, L07502, doi:10.1029/2009GL037820.

Chapter 6

APPENDIX A

Data Processing

6.0.1 Data Losses

The 2004-05 program suffered data losses. All six Upward Looking Sonars, deployed at 90 m on moorings C1-C6, stopped recording before the start of the ice season due to battery failure and no data were recovered from the 200 m RCM at C6 due to a casing leak. The ADCP record on the inner West Greenland shelf (WG3) ended in early February 2005 due to firmware problems. The missing shelf data at WG3 (February 2005-August 2005) were estimated using the ratio of the depth averaged flows (WG3/WG1, February 2006 -August 2006) times WG1 (February 2005-August 2005).

Conductivity data from the bottom-mounted sensors on both shelves were unreliable due to sediment contamination. Data from the 2005-06 deployment (10-day low pass filtered to remove both the tidal and meteorological variability), including an additional 20 m IceCAT at WG2, were substituted as a proxy to capture the low frequency salinity variability on the shelves. IceCAT temperature and salinity records at BI2 for both years have strong (r = 0.98 and 0.86 respectively) and significant correlations at the 99% confidence level. Temperature and salinity data during 2005-06 at BI2 is on average 0.38 fresher and 0.3°C warmer than in 2004-05. An additional uncertainty of 7 mSv was assessed for the freshwater flux estimate using the mean 2005-06 salinity and historical salinity standard deviations (Bedford Institute of Oceanography (BIO) data archive, `http://www.mar.dfo-mpo.gc.ca/science/ocean/`) for both shelves.

6.0.2 Estimation of full depth profiles

Archived Baffin Bay and Davis Strait data (BIO archives) and the 2004-05 autumn CTD observations were used to obtain monthly mean temperature and salinity profiles every 4 m from the surface to the shallowest MicroCAT at each mooring. Profiles were smoothed using a 20 m running boxcar filter and offset to match the shallowest array observations. Linear interpolation filled vertical measurement gaps, with temperature and salinity held constant between the deepest (500m) measurement and the ocean bottom, consistent with archived data. Bottom velocities at C3 and C4 were set to zero. On the western side of the Strait, velocities over the 250 m and 500 m isobaths were set to C1 (250 m) and C2 (500 m) values. On the eastern side of the Strait, the 500 m isobath flow was set to the C5 (500 m) value. WG1 provided bottom currents at the Greenland shelf break. Bottom velocities elsewhere were estimated using linear interpolation along the bathymetry.

Estimated profiles were constrained using the IceCAT data and daily ice coverage maps provided by the Canadian Ice Service. If ice were present over mooring sites the surface temperature was set to -1.8°C, the freezing point of seawater with a salinity of 35, and the temperature profile between the surface and 20 m was filled by linear interpolation for a smoother transition. The maximum surface temperature in the central Strait was constrained to be less than the maximum temperature at 20 m at WG2, assuming that the predominantly ice free, well mixed shallow shelf would experience the greatest solar heating. If the gradient from the archived data in combination with the temperature at 100 m yielded a surface temperature greater than the 20 m temperature at WG2, the surface temperature of the central Strait profile was set equal to the 20 m value and the remaining archived profile was scaled accordingly to the temperature at 100 m. The minimum salinity in the central Strait was constrained to be greater than the salinity at 25 m at BI2 assuming that the freshest water would be along the Baffin Island shelf and slope, at the core of the BIC. The same procedure that was used to constrain the surface temperature was also used for the surface salinity.

Sensitivity tests were performed to assess the uncertainty in the freshwater and heat flux estimates due to a lack of temperature and salinity measurements above 100 m in the central Strait. Flux estimates made assuming no stratification in the upper 100 m (temperature and salinity are held constant) changed the net freshwater and heat fluxes by 7 mSv and 0.2 TW, respectively. Flux calculations using a variety of reasonable profile shapes added an additional 10 mSv and 2 TW to the uncertainty. To test how sensitive the liquid freshwater flux estimate is to salinity variations, the flux was computed setting the salinity in the upper 52 m constant at the minimum salinity recorded from the 25 m IceCAT at station BI2, 30.6, between the Baffin Island coast and station C4 (162 km from the Baffin Island coast), resulting in 43 mSv of increased southward freshwater transport.

Chapter 7

APPENDIX B

Objective Analysis

Observations were decomposed into mean and variable V, T, and S fields. The mean was removed from the observations prior to performing objectively analysis.

7.0.3 Convariance Function

Daily objectively analyzed maps of the variable V, T, and S fields were made using a Gaussian covariance function:

$$C(x) = \sigma^2 \exp\left[-\left(\frac{\Delta x}{L_x}\right)^2\right],$$

based on horizontal separation (Δx), decorrelation length scale (L_x), and data anomaly variance (σ^2). Correlations calculated from hydrographic sections and mooring time series yielded horizontal decorrelation length scales of 20 km (V) and 40 km (T and S).

7.0.4 Formulation of the objective analysis expected mean fields

General Approach

Daily two-dimensional mean fields were estimated from the mooring data, which had been low-passed filtered using a 10-day cutoff to reduce both tidal and meteorological variability. The data were divided into three groups based on depth: the surface to 100 m (150 m for the slope stations BI4 and WG1), 200 to 250 m, and 500 m to the sea floor. Each group was further divided into sections based on cross-strait location to account for: the shelves; the frontal zone between the warm, salty northward flowing West Greenland Slope Current (WGSC) and the cold, fresh southward flowing Baffin Island Current (BIC); and variability with property (Figure 7.1b). The data in each section were spatially averaged to obtain one value per section by giving each mooring site a weight based on the sum of half its distance to adjacent moorings or the coast. The section averages were used at three depth levels (100, 200, and 500 m) to obtain full horizontal sections across the strait at each level (Figure 7.1b). The areas between sections were filled using linear interpolation and values were held constant to the edges to obtain a full horizontal section for each depth level. Full two-dimensional gridded fields were obtained by linearly interpolating vertically between the sections at 100, 200, and 500 m (Figure 7.1c). Different spatial sections and methods for estimating the upper 100 m and below 500 m were used for each property.

Formulation of the along-strait velocity mean field

The ADCP data at each mooring (BI3, C1-C6, WG1, and WG3) were depth averaged to obtain one estimate for the upper 100 m for each mooring before being spatially averaged. The velocity in the mean field is constant in the upper 100 m; the horizontal profile at 100 m was used as the mean velocity from the surface to 100 m. A number of schemes for splitting the observations into horizontal spatial averages were tried before settling on the following scheme.

The mean horizontal profile at 100 m consisted of three sections: 1) from the Baffin Island coast to last mooring west of the front (data from BI3, and C1 to the west front station); 2) from the first mooring east of front to WG1 (data from east front station to C6 and WG1); and, 3) from WG2 to the West Greenland coast (data from WG3). The front was defined as the steepest positive velocity gradient between

C3 and C6. Three sections were used at 100 m because the mean velocity for the eastern front section is much larger than the inner West Greenland shelf velocity. The mean horizontal profile at 200 m consisted of two sections to account for the frontal zone: 1) from the Baffin Island slope to C4 (data from C1-C4); and, 2) from C5 to the West Greenland slope (data from C5).

The mean horizontal profile at 500 m consisted of three sections: 1) from the Baffin Island slope to C2 (data from C2); 2) from C3 to C4 (data from C3-C4); and, 3) from C5 to the West Greenland slope (data from C5). Three sections were used at 500 m to account for the frontal zone and because the velocity along the Baffin Island slope is on average much larger than at C3 and C4.

Velocity below 500 m was filled by linearly interpolating between 500 m and 1040 m (maximum strait depth) where the latter was set to have zero velocity. Bottom velocities elsewhere were estimated using linear interpolation along the bathymetry.

Formulation of the temperature and salinity mean field

Profiles of temperature and salinity at each mooring from the surface to the shallowest MicroCAT (at 100 m except for the shelves and slopes) were estimated in the same manner as described in Appendix A and then horizontally interpolated across to obtain the full mean fields from the Baffin Island coast to the West Greenland coast.

The mean horizontal profile at 200 m consisted of two sections to account for the frontal zone: 1) from the Baffin Island slope to C3 (data from C1-C3); and, 2) from C4 to the West Greenland slope (data from C4-C5) for salinity but only from C5 to the West Greenland slope for temperature (data from C5). C4 was omitted from the temperature section east of the front because the temperature at C4 is often in the front as opposed to being on either side of the front. The mean horizontal temperature profile at 500 m consisted of three sections to account for the frontal zone and the transition region in between: 1) from the Baffin Island slope to C3 (data from C2-C3); 2) C4; and, 3) from C5 to the West Greenland slope (data from C5). The mean horizontal salinity profile at 500 m consisted of two sections to account for the frontal zone: 1) from the Baffin Island slope to C4 (data from C2-C4) and, 2) from C5 to the West Greenland slope (data from C5).

Below 500 m the temperature and salinity were held constant at the 500 m value.

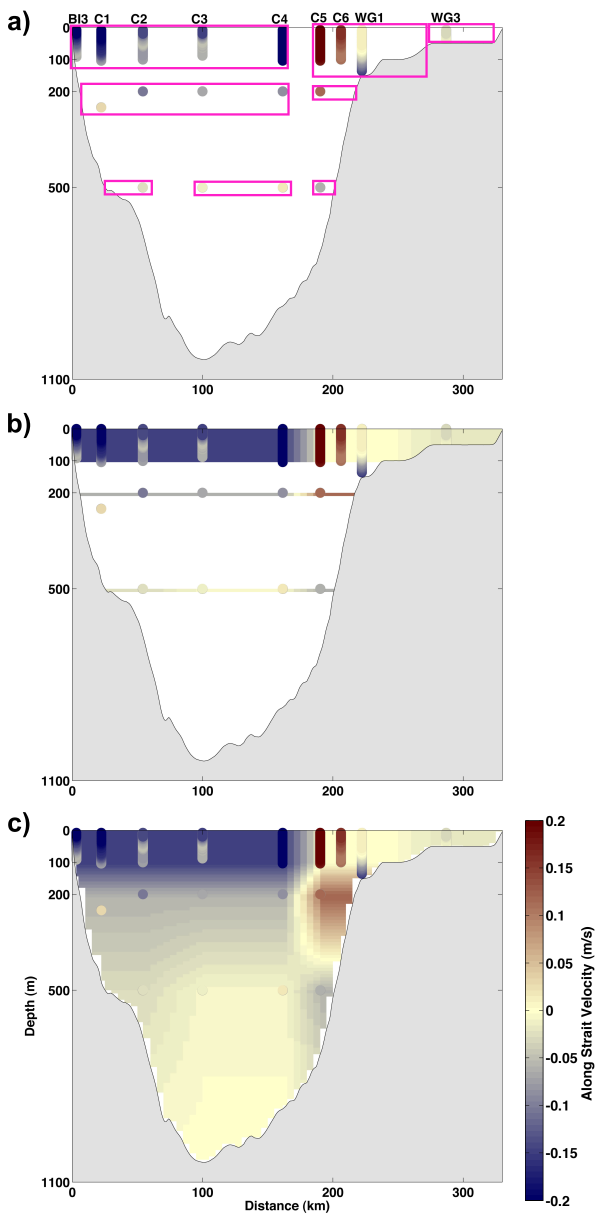

Figure 7.1: Formulation of the mean along-strait velocity field for December 9, 2004. (a) First, data are divided into groups based on location and depth. (b) Then data are spatially averaged in each group to obtain one value per group. Group averages are used at three depth levels (100, 200, and 500 m) to obtain full horizontal sections for each level. Areas between sections were filled using linear interpolation and the values are held constant to the edges. (c) The full two-dimensional gridded field is filled by linearly interpolating vertically between horizontal sections, keeping the upper 100 m constant, and filling the velocity below 500 m by linearly interpolating between 500 m and 1040 m (maximum strait depth) where the latter is set to have zero velocity.

Chapter 8

APPENDIX C

Estimation of fluxes and uncertainties used for the Baffin Bay budgets

If not noted below, estimates and uncertainties presented in Table 1 come directly from the referenced text. Budget estimates were converted from $km^3\ yr^{-1}$ to Sv when necessary using the conversion, 1 Sv = 31 536 $km^3\ yr^{-1}$. Freshwater export via sea ice for all budget pathways was calculated as:

$$FW_{iceflux} = V_{ice}\frac{S_0 - S_{ice}}{S_0} \cdot \frac{\rho_{ice}}{\rho_{water}},$$

where V_{ice} is the annual sea ice volume flux, S_{ice} its salinity [5], ρ_{ice} its density [900 kg m^{-3}], ρ_{water} the density of water [1000 kg m^{-3}], and S_0 the reference salinity [34.8].

1. **Nares Strait -** Münchow and Melling (2008) note a southward volume flux of 0.57 ± 0.09 Sv, excluding the upper 30 m and bottom 30 m between 2003-06. A rough volume estimate for the full strait, assuming the vertically averaged current represents the depth average current, of 0.72 ± 0.11 Sv southward is also given but with the warning that the vertical shear is likely quite large. Rabe et al. (2012) estimated the geostrophic freshwater flux, 20 ± 3 mSv southward, and volume flux, 0.47 ± 0.05 Sv southward, excluding the upper 30 m, below 200 m, and a fraction towards both coasts. They also made a rough estimate of the freshwater flux including the upper 30 m, 28 mSv southward, noting that it is a conservative estimate covering 56% of the total cross-sectional area.

Additional uncertainty associated with the freshwater flux in the upper 30 m was not assessed.

2. **Lancaster Sound -** Annual uncertainties (standard deviations) of the volume and freshwater fluxes, 0.2 Sv and 15 mSv respectively, were calculated using data generously supplied by Simon Prinsenberg and James Hamilton at BIO. Prinsenberg et al. (2009) note the annual standard deviation for the freshwater flux and the monthly standard deviation for the volume flux.

3. **Jones Sound -** The freshwater flux was calculated from the volume flux presented in Melling et al. (2008) using an average salinity of 33.44 to obtain a southward freshwater flux of 12 mSv. The average salinity is the depth average of the April, August, and September historical data profiles from the Jones Sound region from BIOs database, `www.mar.dfompo.gc.ca/science/ocean/database/data_query.html`. The same percent of uncertainty as the Lancaster Sound volume, 26%, and freshwater flux estimates, 31%, were used to calculate the uncertainty of volume and freshwater fluxes.

4. **CAA Ice Flux -** The mean area ice flux for Nares Strait between 1996-2002 was 33x10^3 km^2 yr^{-1} with a thickness of 4 $\pm$ 0.5 m (Kwok, 2005) yielding a southward freshwater flux of 3.2 $\pm$ 0.4 mSv. The mean area ice flux for Lancaster Sound between 2002-07 is 68x10^3 km^2 yr^{-1} with a thickness of 1.5 $\pm$ 0.5 m (Agnew et al., 2008) yielding a southward freshwater flux of 2.5 $\pm$ 0.8 mSv; Jones Sound had an mean area flux of zero between 2002-07. Ice flux uncertainties were estimated using the range of ice thicknesses noted in the references.

5. **Greenland Ice Sheet -** Mernild et al. (2009) estimated 786 km^3 yr^{-1} of freshwater enters the ocean from Greenland, including contributions (45%) from ice-

berg calving and geothermal bottom melting. Approximately 42% drains from the east Greenland Ice Sheet leaving 58% to draining from the West Greenland Ice Sheet. Freshwater drains both north and south of the Davis Strait moored array line. Half of the western drainage, 29%, is roughly estimated to pass the moored array line. The expected model uncertainty is 7% but does not include uncertainty from bottom melting or calving. The freshwater flux uncertainty was very roughly estimated as 10% or 1 mSv.

6. **Baffin Bay P-E -** Evaporation (33 mm yr^{-1}) was estimated as the average difference between the annual mean (between 1979-2001) total precipitation and evaporation minus precipitation maps in the ERA-40 Atlas (Kållberg et al., 2005). Precipitation (355 mm yr^{-1}) was estimated as the mean annual precipitation from four precipitation stations on Baffin Island and four on Greenland: Pond Inlet, Clyde River, Cape Dyer, and Cape Hooper on Baffin Island (between 1971-2000) from the Canadian Climate and Data Information Archive (`www.climate.weatheroffice.ec.gc.ca`); and Nuuk (between 1961-90, Jensen and Rasch (2008)), Pituffik (between 1982-2006) from the National Climate Data Center (`www.ncdc.noaa.gov/oa/ncdc.html`), Sisimuit, and Ilulissat (between 1961-1990) from the Danish Meteorological Institute (`www.dmi.dk/dmi/index/gronland/klimanormaler-gl.htm`) on Greenland. The area of Baffin Bay used in the calculation was 690 000 km^2. Estimates of P-E and evaporation are consistent with ranges presented in Serreze et al. (2008) and Kållberg et al. (2005). Uncertainty was estimated using NCEP Reanalysis precipitation model results indicating small gradients across Baffin Bay at decadal scales (2000-09 long-term mean) and larger gradients if shorter times scales are considered (2004-05). The distribution suggests that using coastal stations could underestimate the direct precipitation by as much as 0.5 mm/day (annual case, an upper bound) corresponding to 4000 m^{3}s^{-1}.

7. **Baffin Island Runoff -** Precipitation (327 mm yr^{-1}) was estimated as the mean annual precipitation (between 1971-2000) from four precipitation stations on Baffin Island: Pond Inlet, Clyde River, Cape Dyer and Cape Hooper (Canadian Climate and Data Information Archive). The drainage area into Baffin Bay from Baffin, Ellesmere and Devon islands unaccounted for in the inflows (271 652 km^3) was estimated using drainage area maps from the Water Survey of Canada (`http://geogratis.cgdi.gc.ca/geogratis/en/index.html`). Uncertainty was estimated as the average standard deviation of the Pond Inlet, Clyde River and Cape Dyer precipitation records.

Estimation of fluxes and uncertainties for Fram Strait

The mean volume flux between 1997-2002 is 2 Sv southward with a standard deviation of 5.9 Sv when 14 moorings (1997-2002) were deployed and 2.7 Sv when 16 moorings (2003-06) were deployed (Schauer et al., 2008). A mean standard deviation between the two sampling periods was used to obtain a volume flux of 2 ± 4.3 Sv, excluding the East Greenland Coastal Current. Rudels et al. (2008) estimate the volume and liquid freshwater flux, including the east Greenland Coastal Current, using hydrographic sections from Fram Strait between 1980-2005, yielding 2.8 Sv and 65 mSv southward, respectively. The freshwater flux was calculated using a reference of 34.92. Rudels et al. (2008) increased the outflow from 2.5 Sv to 2.8 Sv to account for the transport along the east Greenland shelf; an additional 0.3 Sv southward is added to the volume flux estimate by Schauer et al. (2008) yielding a net southward transport of 2.3 Sv. No additional uncertainty was added to account for the shelf transport. Uncertainty for the liquid freshwater flux is roughly estimated as 28 mSv using the standard deviation of the estimates of liquid freshwater fluxes presented in Dickson et al. (2007). The ice flux and standard deviation from Kwok et al. (2004), 2218 $\pm$ 497 km^3 yr^{-1}, is converted to a freshwater flux using the ice flux equation given in the main body of this text, 54 $\pm$ 12 mSv.

Chapter 9

APPENDIX D

Moored Array Data Return

A summary of the locations, depths, record lengths and type of instruments, measuring velocity, temperature and conductivity, deployed between September 2004-September 2010 is presented in Table D19.1. Details about the upward-looking sonar data and processing are presented in Moritz (2013).

Seaglider Data Details

A summary of the Seaglider sections used in this analysis are presented in Table D2 9.2. For each section, the Seaglider identification number, start and end dates and number of dives are noted.

Table 9.1: Davis Strait 2004-10 mooring data return

Instrument Type	Station	Nominal Depth (m)	2004-05	2005-06	2006-07	2007-08	2008-09	2009-10
MicroCat	BI1	52	Sep 27 - Sep 8[1]	Sep 17 - Oct 3	Oct 10 - Oct 5			
	BI2	20	Sep 27- Sep 10	Sep 17 - Apr 7	Oct 10 - Jan 28	Oct 17 - Jan 6		
	BI2	32						Oct 16 - Sep 10
	BI2	40				Oct 17 - Jan 16	Sep 18 - Oct 10	
	BI2	76	Sep 27 - Sep 10[1]		Oct 10 - Oct 5	Oct 17 - Sep 6		Oct 16 - Sep 10
	BI3	96	Sep 28 - Nov 24[1]	Sep 18 - Oct 3	Oct 10 - Oct 5			
	BI4	20			Oct 10 - Aug 22		Sep 18 - Jan 16	
	BI4	32						Oct 16 - Sep 10
	BI4	40					Sep 18 - Jan 16	
	BI4	52						Oct 16 - Sep 10
	BI4	96					Sep 18 - Oct 10	Oct 16 - Sep 10
	BI4	148	Sep 28 - Sep 8[1]	Sep 18 - Oct 3	Oct 10 - Oct 5		Sep 18 - Oct 10	Oct 16 - Sep 10
	C1	104	Sep 27 - Sep 8	Sep 17 - Oct 4	Oct 16 - Oct 5	Oct 17 - Sep 5	Sep 17 - Oct 10	Oct 16 - Sep 9
	C1	252	Sep 27 - Sep 8	Sep 17 - Oct 4	Oct 16 - Oct 5[2]	Oct 17 - Sep 5	Sep 17 - Oct 10[2]	
	C2	104	Sep 27 - Sep 8	Sep 17 - Oct 4	Oct 16 - Oct 4	Oct 17 - Sep 5	Sep 17 - Oct 10	Oct 17 - Sep 9
	C2	500	Sep 27 - Sep 8	Sep 17 - Oct 4	Oct 16 - Oct 4	Oct 17 - Sep 5	Sep 17 - Oct 10[2]	Oct 17 - Sep 9
	C3	104	Sep 23 - Sep 7	Sep 17 - Oct 4		Oct 16 - Sep 5	Sep 17 - Oct 10	Oct 17 - Sep 9
	C3	500	Sep 23 - Sep 7	Sep 17 - Oct 4		Oct 16 - Sep 5	Sep 17 - Oct 10	Oct 17 - Sep 9
	C4	104	Sep 26 - Sep 7	Sep 16 - Oct 5	Oct 18 - Oct 6	Oct 16 - Sep 3[2]	Sep 17 - Oct 11	Oct 18 - Sep 9
	C4	500	Sep 26 - Sep 7	Sep 16 - Oct 5[2]	Oct 18 - Oct 6[2]	Oct 16 - Sep 3	Sep 17 - Oct 11[2]	Oct 18 - Sep 9
	C5	104	Sep 24 - Sep 7	Sep 16 - Oct 5	Oct 18 - Oct 6	Oct 16 - Sep 3	Sep 16 - Oct 8	Oct 18 - Sep 8
	C5	500	Sep 24 - Sep 7	Sep 16 - Oct 5	Oct 18 - Oct 6[2]	Oct 16 - Sep 3	Sep 16 - Oct 8[1]	Oct 18 - Sep 8
	C6	104	Sep 24 - Sep 7		Oct 17 - Oct 6	Oct 15 - Sep 3	Sep 16 - Oct 8	Oct 18 - Sep 8
	C6	252						Oct 18 - Sep 8
	C6	390					Sep 16 - Oct 8[1]	
	WG1	104					Sep 16 - Oct 7	Oct 18 - Sep 8
	WG1	144	Sep 25 - Sep 7[1]	Sep 15 - Oct 5	Oct 17 - Oct 7	Oct 15 - Sep 4	Sep 16 - Oct 7[1]	Oct 18 - Sep 8
	WG1.5	20				Oct 15 - Aug 27	Sep 16 - Oct 7	Oct 19 - Sep 8
	WG1.5	108				Oct 15 - Sep 4		Oct 19 - Sep 8
	WG2	20		Sep 15 - Oct 7	Oct 17 - Aug 30	Oct 15 - Sep 2	Sep 16 - Oct 7	Oct 19 - Sep 8
	WG2	76	Sep 25 - Sep 6[1]	Sep 15 - Oct 7	Oct 17 - Oct 7	Oct 15 - Sep 2		Oct 19 - Sep 8
	WG3	52	Sep 25 - Sep 6[1]	Sep 14 - Oct 7	Oct 17 - Oct 7	Oct 15 - Sep 2		
	WG4	20			Oct 17 - Oct 7	Oct 15 - Aug 26	Sep 16 - Oct 7	Oct 19 - Sep 8
	WG4	52	Sep 25 - Sep 5[1]	Sep 14 - Oct 7	Oct 17 - Oct 7	Oct 15 - Sep 2	Sep 16 - Oct 7	Oct 19 - Sep 8
ADCP	BI3	105	Sep 28 - Nov 24		Oct 10 - Oct 5			
	BI4	92					Sep 18 - Oct 10	Oct 16 - Sep 6
	BI4	150		Sep 24 - Oct 3				
	C1	104	Sep 27 - Sep 8	Sep 19 - Oct 4	Oct 16 - Oct 5	Oct 17 - Sep 5	Sep 17 - Oct 10	Oct 16 - Jun 19
	C2	104	Sep 27 - Sep 8	Sep 17 - Oct 4	Oct 16 - Oct 4	Oct 17 - Sep 5	Sep 17 - Oct 10	Oct 17 - Sep 9
	C3	104	Sep 23 - Sep 7	Sep 17 - Oct 4		Oct 16 - Sep 5	Sep 17 - Oct 10	Oct 17 - Sep 9
	C4	104	Sep 26 - Sep 7		Oct 18 - Oct 6	Oct 16 - Sep 3	Sep 17 - Oct 11	Oct 18 - Sep 9
	C5	104	Sep 24 - Sep 7	Sep 16 - Oct 5		Oct 16 - Sep 3	Sep 16 - Oct 8	Oct 18 - Sep 8
	C6	104	Sep 24 - Sep 7		Oct 17 - Oct 6	Oct 15 - Sep 3		Oct 20 - Sep 10
	C6	390					Sep 16 - Oct 8	
	WG1	144	Sep 25 - Sep 7	Sep 15 - Oct 5	Oct 17 - Oct 7	Oct 15 - Sep 4	Sep 16 - Oct 7	Oct 18 - May 26
	WG3	56	Sep 25 - Feb 6	Sep 14 - Jun 23	Oct 17 - Oct 7	Oct 15 - Sep 2		
	WG4	56					Sep 16 - Jun 3	Oct 19 - Sep 8[2]
RCM	C1	252	Sep 27 - Sep 8	Sep 17 - Oct 4		Oct 17 - Sep 5	Sep 17 - Oct 10	Oct 16 - Sep 9
	C2	200	Sep 27 - Sep 8	Sep 17 - Oct 4	Oct 16 - Oct 4	Oct 17 - Sep 5	Sep 17 - Oct 10[1]	Oct 17 - Sep 9
	C2	352						Oct 17 - Sep 9
	C2	500	Sep 27 - Sep 8	Sep 17 - Oct 4	Oct 16 - Oct 4	Oct 17 - Sep 5	Sep 17 - Oct 10	Oct 17 - Sep 9
	C3	200	Sep 23 - Sep 7	Sep 17 - Oct 4		Oct 16 - Sep 5	Sep 17 - Oct 10	Oct 17 - Sep 9
	C3	500	Sep 23 - Sep 7	Sep 17 - Oct 4		Oct 16 - Sep 5	Sep 17 - Oct 10	Oct 17 - Sep 9
	C4	200	Sep 26 - Sep 7	Sep 16 - Oct 5	Oct 18 - Oct 6	Oct 16 - Sep 3	Sep 17 - Oct 11	Oct 18 - Sep 9
	C4	500	Sep 26 - Sep 7	Sep 16 - Oct 5	Oct 18 - Oct 6	Oct 16 - Sep 3[3]	Sep 17 - Oct 11	Oct 18 - Sep 9
	C5	200	Sep 24 - Sep 7	Sep 16 - Oct 5[1]	Oct 18 - Oct 6	Oct 16 - Sep 3	Sep 16 - Oct 8	Oct 18 - Sep 8
	C5	500	Sep 24 - Sep 7	Sep 16 - Oct 5	Oct 18 - Oct 6	Oct 16 - Sep 3[3]	Sep 16 - Oct 8	Oct 18 - Sep 8
	C6	252			Oct 17 - Oct 6	Oct 15 - Sep 3	Sep 16 - Oct 8	

[1] Bad salinity for the entire record

[2] Bad salinity periods > 5 hours

[3] Bad velocity > 50% of the record

Table 9.2: Davis Strait 2004-10 Seaglider sections

Seaglider ID	Start Date	End Date	Number of Dives
SG018	9/17/2005	9/28/2005	143
SG018	9/28/2005	10/06/2005	83
SG018	10/06/2005	10/19/2005	107
SG109	10/11/2006	10/22/2006	98
SG109	10/22/2006	11/01/2006	83
SG109	11/01/2006	11/10/2006	80
SG113	9/08/2008	9/19/2008	98
SG113	9/19/2008	9/29/2008	85
SG113	9/30/2008	10/12/2008	95
SG113	10/12/2008	10/23/2008	84
SG113	10/23/2008	11/05/2008	106
SG113	12/18/2008	12/29/2008	89
SG108	9/07/2008	9/17/2008	88
SG108	9/17/2008	9/30/2008	103
SG108	9/30/2008	10/12/2008	99
SG108	10/12/2008	10/24/2008	92
SG108	10/25/2008	11/06/2008	101
SG108	11/7/2008	11/17/2008	80
SG143	11/07/2009	11/21/2009	122
SG143	11/24/2009	12/01/2009	67
SG108	6/19/2010	6/28/2010	81
SG108	6/28/2010	7/07/2010	77
SG108	7/27/2010	8/06/2010	87
SG108	8/06/2010	8/14/2010	67
SG108	8/14/2010	8/23/2010	85
SG108	8/23/2010	9/2/2010	83
SG108	9/2/2010	9/13/2010	90
SG183	9/10/2010	9/22/2010	143
SG183	10/08/2010	10/19/2010	108
SG183	10/19/2010	10/28/2010	87
SG183	10/28/2010	11/08/2010	107
SG183	11/08/2010	11/16/2010	78
SG183	11/16/2010	11/24/2010	73
SG183	11/26/2010	12/01/2010	57
SG183	12/02/2010	12/11/2010	100
SG183	12/11/2010	12/18/2010	81
SG183	12/19/2010	12/28/2010	139
SG183	12/29/2010	1/07/2011	174
SG183	1/15/2011	1/22/2011	71
SG183	1/22/2011	1/31/2011	131
SG141	3/19/2011	3/29/2011	39
SG141	3/31/2011	4/14/2011	34
SG141	5/06/2011	5/13/2011	84
SG141	5/15/2011	5/24/2011	94
SG141	5/24/2011	6/2/2011	91

Chapter 10

APPENDIX E

Objective Analysis (OA)

10.0.5 Background Fields

Daily mooring along-strait velocity, temperature and salinity (VTS) data are broken down into mean and variable (anomaly) components; only the variable fields are objectively mapped. Mean in this case refers to the best estimates of the large-scale background fields for V, T and S. The background fields vary daily over a year and the same annual background fields are used for each year. Annual transports from the background fields are -1.63 Sv, -113 mSv and 29 TW for volume, freshwater and heat. The annual background fields used for the 2004-10 data set differs from the ones used for the 1987-90 dataset. Background fields and the daily VTS mooring data are used to estimate daily full depth VTS profiles. Background fields are then subtracted from the estimated daily full depth VTS profiles and the remaining variable (daily background) fields are objectively mapped. Mooring data and Seaglider TS sections are used to calculate the OA large-scale background VTS fields.

Both the 2004-10 and 1987-90 data sets are objectively mapped twice, to improve the background fields, before obtaining the final background VTS fields used to estimate the transports. For the 2004-10 data set, the first OA run (OA1) uses monthly average full strait Seaglider sections (described in Section 4.2) as background fields. The monthly averaged TS Seaglider fields are used to compute the monthly geostrophic V fields, referenced to the monthly average depth averaged moored observations that have been linearly interpolated to extend across the OA grid. The monthly average VTS sections are linearly interpolated in time, setting the sections at the 15th of each month, to create daily background VTS fields. The OA is performed a second time (OA2) to improve the background fields since the Seaglider sections are temporally sparse, biased towards the autumn months and have a harder time resolving the edge of the West Greenland Slope Current when ice is present due to a reduction in position accuracy with acoustic navigation. The OA2 is performed using the smoothed (15-day moving Hanning window) annual average OA1 results as the OA2 background TS fields. The OA2 geostrophic background V fields are created using the OA2 T and S fields, referenced to the depth averaged smoothed annual average OA1 V fields.

For the 1987-90 data set, the monthly average 2004-10 OA2 TS background fields are modified to create the 1987-90 background TS fields for the first run of the OA (OA1b) by shifting them 40 km to the east. Temperature sections are also stretched vertically between 52 m 120 m, linearly interpolating in between, to align with the 1987-90 moored observations. The TS sections are linearly interpolated and extrapolated to fully span the central strait; the shelves are not objectively mapped. The modified TS fields are used to compute the monthly geostrophic V fields, referenced to the monthly average depth averaged moored observations that have been linearly interpolated to extend across the OA grid. The monthly average VTS sections are linearly interpolated in time, setting the sections at the 15th of each month, to create the OA1b daily background VTS fields. The OA is run a second time (OA2b) using the smoothed (15-day running Hanning window) annual average OA1b results for the OA2b background fields. The OA2b geostrophic background V field is created using the OA2b TS fields, referenced to the depth averaged smoothed annual average OA1b V fields. Monthly background fields for both data sets for the OA1/OA1b and OA2/OA2b runs are presented in Figure 10.1 - Figure 10.4.

10.0.6 Full Depth VTS Profiles

Monthly OA2 and OA2b background VTS fields are used in combination with the daily moored observations to create daily full depth geostrophic V, T and S profiles for both the 2004-10 and 1987-90 datasets, respectively. Full depth geostrophic velocity profile shapes, obtained from the OA2 background fields at each mooring location for each month, are used to fill in the vertical gaps in the VTS daily mooring data. Profiles are smoothed using a 20 m running boxcar filter. Offsetting the top part of the profile to match the shallowest observation fills the surface to the shallowest observation and offsetting the bottom part of the profile to match the deepest observation fills the profile from the deepest observation to the bottom. Vertical gaps between observations are either filled using linear interpolation (for gaps $\leq$ 200 m) or the profile shape is constrained between the two observations.

Estimated daily profiles between 2004-10 in the central strait are constrained using the shelf data and daily ice coverage maps provided by the Canadian Ice Service. If ice is present over mooring sites the surface temperature is set to -1.8°C, the freezing point of seawater with a salinity of 35, and the temperature profile between the surface and 20 m is filled by linear interpolation. The maximum surface temperature in the central strait is constrained to be less than the maximum temperature on the West Greenland shelf, assuming that the predominantly ice free, well mixed shallow shelf would experience the greatest solar heating. If the estimated profiles yield a surface temperature greater than the shelf temperature, the surface temperature of the central Strait profile is set equal to the shelf value and the upper portion of the temperature profile is refit. The minimum salinity in the central strait is constrained to be greater than the salinity on the Baffin Island shelf assuming that the freshest water would be along the Baffin Island shelf and slope, at the core of the BIC. The same procedure used to constrain the maximum surface temperature is also used to constrain the minimum surface salinity in the central strait.

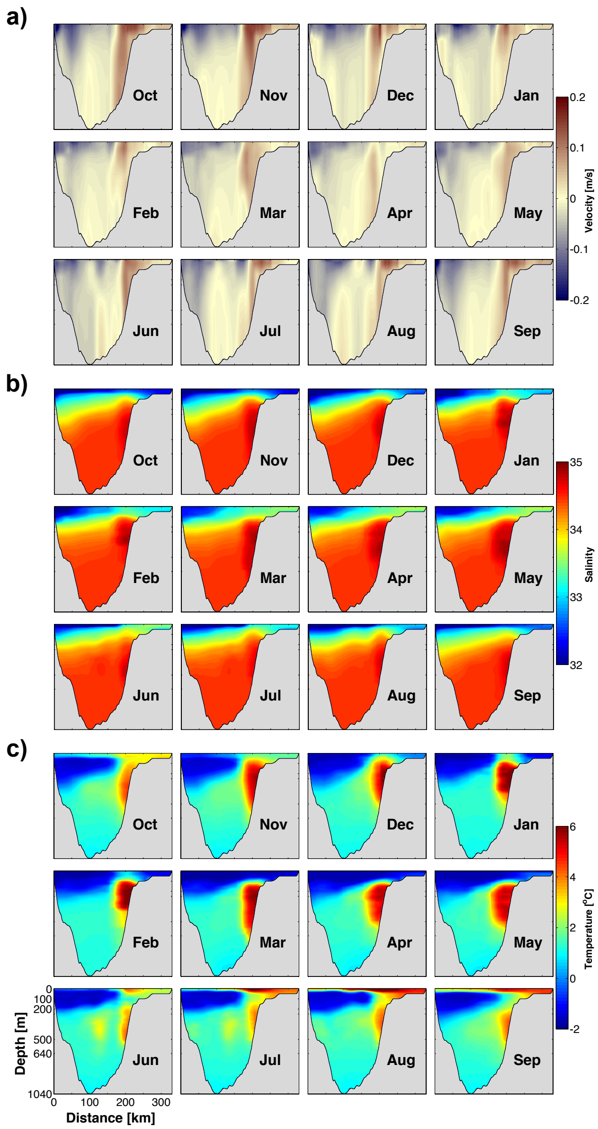

Figure 10.1: Monthly average background fields used for the first run of the objective analysis routine (OA1) for the 2004-10 data set of (a) along-Strait velocity, (b) salinity and (c) temperature. Estimated OA1 fields are composed of Seaglider data in the central strait and mooring data along the slopes and shelves.

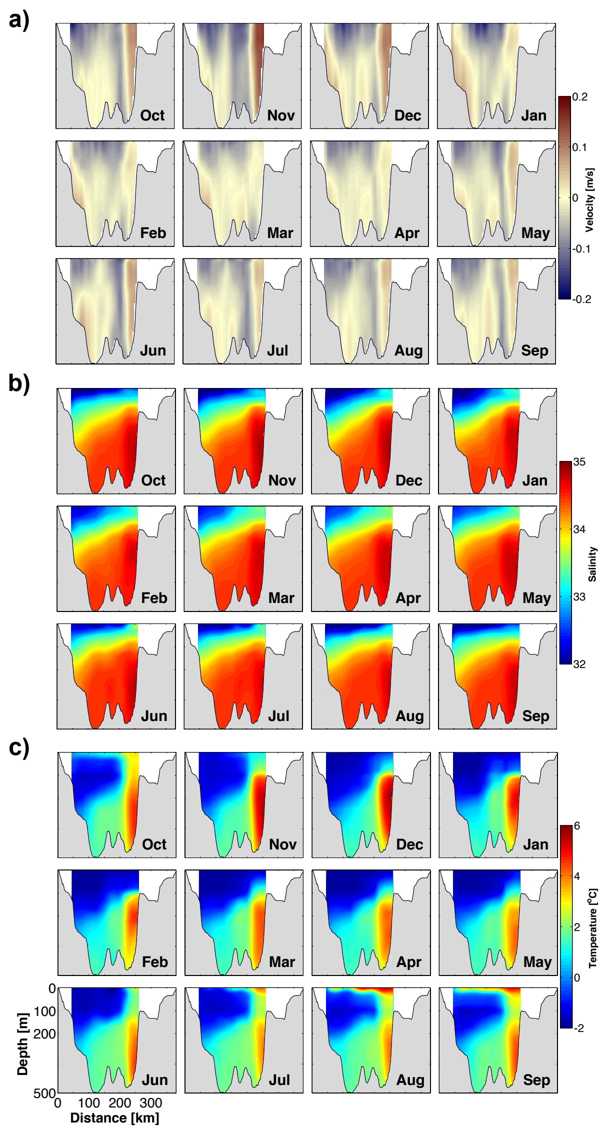

Figure 10.2: Monthly average background fields used for the first run of the objective analysis routine (OA1b) for the 1987-90 data set of (a) along-Strait velocity, (b) salinity and (c) temperature. Estimated OA1b fields are modified OA1 fields, adjusted to align with the 1987-90 mooring data.

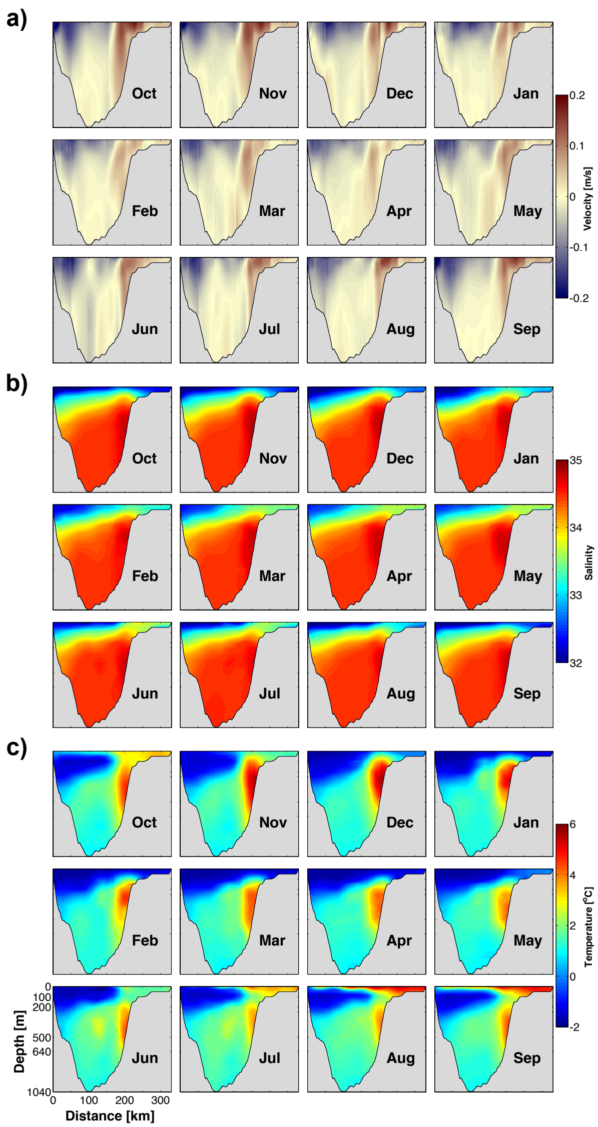

Figure 10.3: Monthly average background fields used for the second run of the objective analysis routine (OA2) for the 2004-10 data set of (a) along-Strait velocity, (b) salinity and (c) temperature. Estimated OA2 fields are the annual averages of the OA1 results.

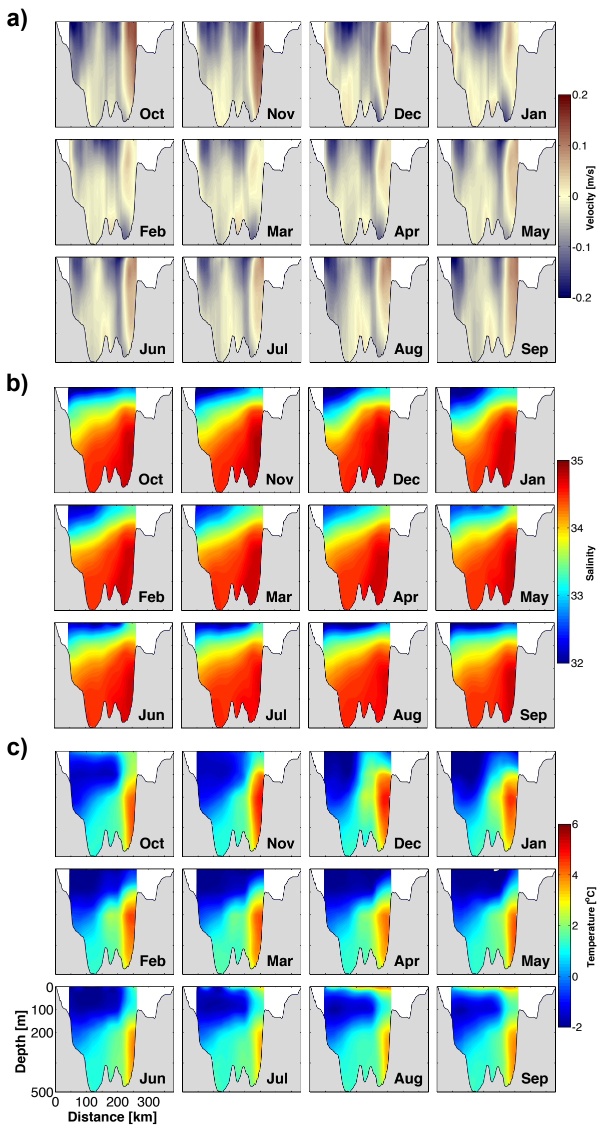

Figure 10.4: Monthly average background fields used for the second run of the objective analysis routine (OA2b) for the 1987-90 data set of (a) along-Strait velocity, (b) salinity and (c) temperature. Estimated OA2b fields are the annual averages of the OA1b results.

Chapter 11

APPENDIX F

Transport Uncertainties

Total transport uncertainties for the 2004-10 and 1987-90 data sets are estimated by summing in quadrature three types of errors, those due to: the method of objective mapping, biases due to spatial gaps in the moored array and assumptions regarding the choice of large-scale background fields. Each type of error is discussed below. The 1987-90 transports and uncertainties only pertain to the central strait.

11.0.7 Spatial Bias Errors

Estimating VTS properties between the gaps of the moored arrays creates biases in the transport estimates. Monthly transport bias errors are assumed Gaussian and calculated using the OA covariance function and daily estimated full depth VTS profiles at each mooring location. The Gaussian covariance function used in the OA is:

$$C(x) = \sigma^2 \exp\left[-\left(\frac{\Delta x}{L_x}\right)^2\right]$$

and is based on horizontal separation (Δx), decorrelation length scale (L_x), and data anomaly variance (σ^2). Using the two-dimensional grid from the OA, the strait is divided up into sections based on mooring pairs and errors between pairs are assumed independent. For cases with a boundary on one side, the nearest mooring data is used instead of a pair of moorings. Unresolved variance at each grid point is expressed as:

$$\sigma_x^2 = \left(\frac{x_2 - x}{x_2 - x_1}\right)\left(1 - \sigma_1^2 \exp\left[-\left(\frac{x_1 - x}{L_x}\right)^2\right]\right) + \left(\frac{x - x_1}{x_2 - x_1}\right)\left(1 - \sigma_2^2 \exp\left[-\left(\frac{x_2 - x}{L_x}\right)^2\right]\right),$$

where L_x is the decorrelation length scale = 20 km, x is the horizontal distance of the grid point, x_1, x_2 and σ_1, σ_2 are the horizontal distances and data variances at the two nearest moorings. The fraction of unresolved variances are weighted linearly so that the unresolved variance is zero at the mooring locations. Variances expressed in the equation above are the monthly data variances at each grid cell, estimated from the daily V, T and S mooring data. Since transport uncertainties are desired, velocity (V) variance is used for volume transport, the variance of velocity multiplied by the salinity fraction ($V\frac{S_0-S}{S_0}$) where $S_0 = 34.8$ is used for freshwater transport and the variance of velocity multiplied by temperature (VT) is used for heat transport. Both freshwater and heat transport are dominated by velocity so the OA velocity decorrelation length scale (L_x) is also used for freshwater and heat transport. The square root of the unresolved variance is multiplied by the grid cell area to obtain the bias errors in volume and freshwater transports. Bias errors in heat transport are calculated by multiplying the square root of the unresolved variance with the grid cell area, specific heat and density. Errors for each section (between moorings) are summed and the sections are added in quadrature to obtain monthly transport errors; mooring pairs are assumed uncorrelated. Monthly transport bias errors are averaged and divided by the square root of the number of monthly estimates (N) minus one ($N-1 = 11$, except for 2009-10 where $N-1 = 10$) to obtain yearly bias error estimates. Similarly, yearly bias error estimates are averaged and divided by the square root of the number of years minus one ($N-1 = 5$ or 2) to obtain the six and three year average bias errors.

11.0.8 OA Errors

The error estimates from the OA are based on the misfit between the mooring data anomalies (mooring data minus the background fields) and the objectively mapped results. Transport equations are expanded out to include uncertainties in VTS and error is propagated to determine total OA transport errors. Velocity errors are assumed independent with temperature and salinity errors. Using the OA results, errors and grid area the transport equations are expanded and error is propagated to obtain total transport errors. Volume transport errors are determined at each grid cell. Starting with the volume transport equation,

$$V_{transport} = VA$$

and expanding to include the errors yields

$$V_{transport} + \delta V_{transport} = V + \delta VA.$$

Treating A as a constant, volume transport error is expressed as

$$\delta V_{transport} = \delta VA,$$

where V, δV and A are the grid cell mapped velocity, velocity error and area respectively. Volume transport and corresponding error are expressed as $V_{transport}$ and $\delta V_{transport}$ respectively. Freshwater transport errors are determined at each grid cell. Starting with the freshwater transport equation,

$$FW_{transport} = V\frac{S_0 - S}{S_0}A.$$

Substituting in

$$Y = \frac{S_0 - S}{S_0}$$

where

$$\delta Y = \frac{\delta S}{S_o}.$$

Treating A as a constant and expanding the equation to include the errors yields,

$$FW_{transport} + \delta FW_{transport} = (V + \delta V)(Y + \delta Y)A,$$

$$FW_{transport} + \delta FW_{transport} = VYA + V\delta YA + Y\delta VA + \delta V\delta YA,$$

$$\delta FW_{transport} = VYA + Y\delta VA + \delta V\delta YA.$$

Substituting back in for Y and recalling that δV and δS are uncorrelated, freshwater transport error is expressed as

$$\delta FW_{transport} = \frac{V\delta S}{S_o}A + \frac{S_o - S}{S_o}\delta VA + FW_{transport}\sqrt{\left(\frac{\delta V}{|V|}\right)^2 + \left(\frac{\delta S}{S_o}\left|\frac{S_o}{S_o - S}\right|\right)^2}$$

where S, δS and $FW_{transport}$ are the mapped grid cell salinity, salinity error and freshwater transport. S_o is the reference salinity (34.8) and freshwater transport error is expressed as $\delta FW_{transport}$. Heat transport errors are determined at each grid cell. Starting with the heat transport equation,

$$H_{transport} = \rho V(T - T_0)C_pA.$$

Substituting in

$$Y = T - T_o,$$

where

$$\delta Y = \delta T.$$

Treating A, ρ, and C_p as constants, expanding the equation to include errors yields,

$$H_{transport} + \delta H_{transport} = (V + \delta V)(Y + \delta Y)\rho C_pA,$$

$$H_{transport} + \delta H_{transport} = VY\rho C_pA + Y\delta V\rho C_pA + V\delta Y\rho C_pA + \delta V\delta Y\rho C_pA.$$

Substituting back in for Y and recalling that δV and δT are uncorrelated, heat transport error is expressed as

$$\delta H_{transport} = (T - T_o)\delta V\rho C_pA + V\delta T\rho C_pA + H_{transport}\sqrt{\left(\frac{\delta V}{|V|}\right)^2 + \left(\frac{\delta T}{|T - T_o|}\right)^2}$$

where T, δT and $H_{transport}$ are the mapped grid cell temperature, temperature error and heat transport respectively and $\delta H_{transport}$ is the estimated heat transport error. T_o is the reference temperature (0°C) and grid cell water density and specific heat are expressed as ρ and C_p.

The strait is divided up into sections based on mooring pairs and errors between sections are assumed independent. Each day errors for each section (between moorings) are summed and the sections are added in quadrature to obtain daily transport errors; mooring pairs are assumed uncorrelated. Daily errors are averaged to obtain monthly transport errors. Monthly errors are averaged and divided by the square root of the number of monthly estimates (N) minus one ($N - 1 = 11$, except for 2009-10 where $N - 1 = 10$) to obtain yearly OA error estimates. Similarly, yearly OA error estimates are averaged and divided by the square root of the number of years minus one ($N - 1 = 5$ or 2) to obtain the six and three year average OA errors.

11.0.9 OA Background Errors

Errors due to the creations of the background fields are determined by varying the background fields used for the OA2 runs and computing the transport differences between the OA2 and OA test cases.

For each month and each instrument, for VTS, the standard deviations of the data are computed. Test case background fields for VTS are created using ± 2 standard deviations from the monthly VTS averages. Two sets of monthly full depth VTS test profiles are created using the OA2 background field profile shapes and ± 2 standard deviations from the average VTS data. Most instruments have a Gaussian distribution, but in a few cases (ex: near surface temperature) the distribution is skewed and the standard deviations go outside the range of the observations; in these cases the maximum or minimum is used instead. The OA is run twice to create test background fields for VTS. The first run of the OA (OA1t), for both the + 2 standard deviations and -2 standard deviations test cases, uses the monthly average Seaglider sections and the monthly VTS test profiles. Monthly OA1t results are interpolated to obtain daily background fields for the OA2t runs. The daily OA2t geostrophic background V fields are created using the interpolated OA1t T and S fields, referenced to the depth averaged OA1t V fields. The OA2t cases are run using the OA2t background fields and the OA2 daily profiles. All pairings of the OA2t cases (two velocity cases, four salinity cases and four temperature cases) are used to compute daily transports. The maximum differences between the OAt cases and OA2 results are used to compute monthly uncertainties arising from the assumed background fields. Monthly transport background errors are averaged and divided by the square root of the number of monthly estimates (N) minus one ($N-1=11$, except for 2009-10 where $N-1=10$) to obtain yearly bias error estimates. Similarly, yearly background error estimates are averaged and divided by the square root of the number of years minus one ($N-1=5$ or 2) to obtain the six and three year average bias errors.

Mary Beth Curry earned a bachelors of science in Civil Engineering at Georgia Institute of Technology in 2002. She received a Master of Sciences in Physical Oceanography in 2009 and a PhD in 2013 at the University of Washington.